GENE REGULATORY ANALYSIS OF THE DEVELOPING ENTERIC NERVOUS SYSTEM OF ZEBRAFISH (DANIO RERIO)

Thesis by

Can Li

In Partial Fulfillment of the Requirements for

the Degree of

Doctor of Philosophy

CALIFORNIA INSTITUTE OF TECHNOLOGY

Pasadena, California

2025

(Defended August 29, 2024)

Can Li
ORCID: 0000-0002-5352-6212

ACKNOWLEDGEMENTS

I would like to express my deep and sincere thanks to my advisor Dr. Marianne Bronner for the great mentorship, brilliant guidance, constant support, and genuine encouragement to me. Her insightful perspectives in science always guide my project to keep going in the correct direction. I always remember that when I first presented her the single cell RNA-seq data of zebrafish ENS, she immediately pointed out *Satb2*, *Ebf1a*, and *Gata3* as critical transcription factors to control the differentiation of serotonergic neurons, inhibitory and excitatory motor neurons, and the experimental results proved her keen instinct. During my PhD studies, my advisor gave me full freedom and support to try many new techniques, like establishing the CRISPR/Cas9-mediated knock-in fish line, developing the single cell ATAC-seq project, optimizing the condition of CUT&RUN experiment in the zebrafish system, which are risky and require substantial financial investment. Her constant support made me feel fearless and confident to overcome many technical obstacles. When I experienced frustration and stressful periods in this long run to complete the PhD study, my advisor accompanied me, worked with me together, and always encouraged me, so I could walk out from the difficult times. I always feel fortunate, grateful, and privileged to have had Dr. Marianne Bronner as my PhD advisor.

I am profoundly thankful to Dr. Lior Pachter for the collaboration and substantial inputs on the first project of discovering the spatiotemporal dynamics of the developing ENS and for his professional guidance as one of my committee members. I feel deeply grateful to Dr. Angelike Stathopoulos and Dr. David Prober for their instructive advice and tremendous support. I wish to thank Dr. Kai Zinn and Dr. Katalin Fejes Tóth for providing me with precious opportunities to do research in their labs and for supporting me to enter graduate school in Caltech.

I would like to thank my collaborator Dr. Jase Gehring for his enormous dedication to the first project. I remember that when I first talked with Jase, he showed great love for this project. As a collaborator, he contributed to many aspects, performed one of the most important experiments—scRNA-seq—and provided many thoughtful suggestions for this project. As a teacher, he generously tutored me in computational analysis. I would like to thank Xun Wang, Dr. Yapeng Su, and Dr. Guideng Li for the collaboration on the scATAC-seq and CUT&RUN experiments. I highly appreciate the massive energy, time, and intellectual inputs they gave to push the project forward.

I sincerely thank my two post-doc mentors—Dr. Rosa Uribe and Dr. Megan Martik—for their invaluable suggestions on the development of my first project and for their kind support. I would like to express great gratitude to my colleagues in Bronner lab for helpful discussions, constant support, and nice accompaniment. Special thanks to David Mayorga, Ryan Fraser, and Justin Yip for the professional management of the zebrafish facility and to Johanna Tan-Cabugao and Constanza Gonzalez for their support of reagent ordering and maintenance of lab resources.

To complete my PhD projects, Caltech facilities provide professional and immense support. I want to thank Dr. Andres Collazo and Dr. Giada Spigolon from the Biological Imaging facility, Dr. Sisi Chen and Mr. Jeff Park from the Single-Cell Profiling and Engineering Center, Rochelle Diamond, Patrick Cannon, Diana Perez, and Jamie Tijerina from the Flow Cytometry facility, Grace Shin from the Molecular Technologies facility, and Dr. Igor Antoshechkin from the Genomics facility. Special thanks to Patrick Cannon, who invested much time and energy to help us optimize the sorting conditions in the single cell ATAC-seq experiment. Here I also would like to thank the administrations at Caltech for the important academic support.

I feel grateful to my friends during the PhD periods. Thanks so much for your warm support and sweet accompaniment.

My progress tightly relies on the dedication of my family. My grandparents and my parents brought me up and taught me valuable life lessons. My parents-in-law gave me huge support when I struggled to enter graduate school. My husband Xun Wang is an excellent teacher, a reliable collaborator, and a dependable companion to me. I want to thank you and other family members for all your unconditional love and ever-present support.

ABSTRACT

Neural crest cells give rise to the neurons of the enteric nervous system (ENS) that innervate the gastrointestinal tract to regulate gut motility. The immense size and distinct subregions of the gut present a challenge to understanding the spatial organization and sequential differentiation of different neuronal subtypes. To tackle this, we profile enteric neurons and progenitors at single cell resolution during zebrafish embryonic and larval development to provide a near complete picture of transcriptional changes that accompany emergence of ENS neurons throughout the gastrointestinal tract. Multiplex spatial RNA transcript analysis was then used to reveal the temporal order and distinct localization patterns of neuronal subtypes along the length of the gut. Next, we show that functional perturbation of select transcription factors *Ebf1a, Gata3* and *Satb2* alters the cell fate choice, respectively, of inhibitory, excitatory and serotonergic neuronal subtypes in the developing ENS. To decipher the molecular mechanism underlying the development of ENS, we further performed single cell ATAC-seq to profile the epigenetic landscape of the developing ENS. Together with CUT&RUN results, we found the master regulator *Phox2bb* harbors extensive binding sites throughout the genome and plays versatile roles in neuronal differentiation, including regulating progenitor gene *Sox10*, activating transcription factors *Phox2a* and *Insm1b* for early neural development and regulating genes *Etv1* and *Hmx3a* for neuronal differentiation. Integrated with single cell RNA-seq analysis, we further reconstruct a putative gene regulatory circuit involving in the specification and maturation of ENS neurons.

PUBLISHED CONTENT AND CONTRIBUTIONS

Li, C., Gehring, J., and Bronner, M.E. (2024). Spatiotemporal dynamics of the developing zebrafish enteric nervous system at the whole-organ level. Developmental Cell, S1534580724006713. https://doi.org/10.1016/j.devcel.2024.11.006.

Personal Contribution Statement: As the first author of this publication, I played a leading role in conceptualization, methodology development, investigation, and data analysis. I collaborated closely with co-authors and the corresponding author, Dr. Bronner, in writing the manuscript and revising the publication.

TABLE OF CONTENTS

Acknowledgements……iii
Abstract ……v
Published Content and Contributions……vi
Table of Contents……vii
List of Illustrations and/or Tables……ix
Nomenclature……xi
Chapter I: Introduction……1
Structure and Functions of the Enteric Nervous System (ENS)……1
Innervation of the Intestine by the Enteric Neurons……2
Origin and Development of the ENS……3
Diseases and Developmental Disorders of the ENS……5
Signaling Molecules Play Important Roles in the Developing ENS……6
Transcription Factors in the Developing ENS……7
Bibliography……10
Chapter II: Identifying Different Cell Types and Key Genes in the Developing Zebrafish ENS……16
Background……16
Results……16
Single-cell (sc) RNA-seq Reveals Heterogeneity of ENS Cells……16
Identification of ENS Progenitors and Neuroblasts……18
Identification of Enteric Neuron Subtypes by the Combinatorial Expression of Neurotransmission Genes……19
Multiplex Spatiotemporal Analysis Reveals the Distribution of Enteric Neuronal Subtypes in the Developing Gut……20
Developmental Trajectories Provide Clues to Lineage Specification……22
Cell-type Specific Transcription Factors Shape the Maturation of ENS Neurons ……23
Methods……95
Fish Husbandry……95
Generation of CRISPR-Cas9 Mediated Knock-in Line Tg(*Phox2bb:mNeonGreen*) ……95
Embryo Collection and Tissue Dissection……97
Cell Dissociation……97
Cell Barcoding, Library Preparation, and Sequencing……98
Single-cell RNA-seq Analysis: Cell Clustering and Differential Gene Expression (DGE) Analysis……98
Single-cell RNA-seq Analysis: RNA Velocity Analysis with UniTVelo Package ……99
Single-cell RNA-seq Analysis: Developmental Trajectory and Bifurcation Analysis with scFates Package……99

Hybridization Chain Reaction (HCR).....100
Analysis of Sequential HCR Results……..……102
Double Fluorescent in situ Hybridization.....102
CRISPR/Cas9-mediated Perturbation Experiments.....103
Analysis of Perturbation Efficiency by qPCR.....104
Bibliography.....106
Chapter III: Single Cell Epigenomic Analysis Uncovers Gene Regulatory Circuits in Neuronal Differentiation of the ENS.....113
Background.....113
Results.....114
Bulk ATAC-seq Identifies Extensive Open Chromatic Regions Across the Genome.....114
CUT&RUN Profiles Phox2bb Binding Sites.....115
scATAC-seq Reveals Heterogeneity of ENS Cells.....116
Integrative Analysis of scRNA-seq and scATAC-seq.....117
Methods.....118
Bulk ATAC-seq Experiment and Analysis.....118
CUT&RUN Experiment and Analysis.....118
scATAC-seq Experiment and analysis.....118
Bibliography.....130
Chapter IV: Conclusion.....134
Bibliography.....139

LIST OF ILLUSTRATIONS AND/OR TABLES

Number *Page*
Figure 1. Single-cell transcriptome analysis reveals cell-type heterogeneity in zebrafish enteric nervous system during embryogenesis ….....27
Figure 2. Single cell RNA-seq analysis reveals major subtypes of mature enteric neurons 29
Figure 3. Spatial localization of specific ENS neuronal subtypes throughout the gut.....30
Figure 4. Developmental trajectory analysis reveals emergence of subtypes of ENS neurons.....32
Figure 5. Expression and function of *Ebf1a* in the developing ENS.....34
Figure 6. Expression and function of *Gata3* in the developing ENS.....36
Figure 7. Expression and function of *Satb2* in the developing ENS.....38
Figure 8. Validation of Tg(*Phox2bb:mNeonGreen*) line and experimental procedure for scRNA-seq of the developing ENS.....40
Figure 9. Validation of ENS versus non-ENS cells.....42
Figure 10. Violin plot displaying the expression of genes involved in neurotransmission and membrane trafficking; genes encoding ion channels, signaling molecules, and transcription factors; and genes marking ENS progenitors, neuroblasts, and neurons……..….44
Figure 11. Spatiotemporal expression of multiple marker genes in one sample revealed by sequential HCR.....51
Figure 12. Merged images of 9 neurotransmitter-related genes.....55
Figure 13. Lineage trajectories and bifurcation analysis.....57
Figure 14. Expression and functions of transcription factors *Ebf1a, Satb2,* and *Gata3* in the ENS.....60
Figure 15. Bulk ATAC-seq and CUT&RUN experiment.....120
Figure 16. Bulk ATAC-seq and CUT&RUN results demonstrate extensive regulatory activity across the genome in zebrafish ENS at 3 dpf.....122
Figure 17. Flow cytometry records and quality examination of scATAC-seq experiments 124
Figure 18. scATAC-seq data manifest heterogeneity and the regulatory activity of ENS cells during embryonic development.....126
Figure 19. Integration of scRNA and scATAC-seq data unravels the gene regulatory circuit underlying ENS development.....128
Figure 20: UMAP plots displaying the expression of genes encoding signaling molecules and transcription factors.....138

Table 1. Marker genes identified in each cluster.....62
Table 2. Spatial Expression of multiple marker genes in the zebrafish ENS at 6 dpf revealed by sequential HCR.....74
Table 3. crRNA sequence.....89

Table 4. Primer sequences used in qPCR experiment.....90
Table 5. Cq value in qPCR experiment.....91
Table 6. Primer sequences used in the detection of Indels generated by CRISPR/Cas9 system.....92
Table 7. Indel sequences detected in each embryo.....93

NOMENCLATURE

Neural crest cells. Transient embryonic stem cells that delaminate from the neural tube and migrate into the periphery to differentiate into multiple derivatives, such as bones and cartilage in the head, cardiac septum and outflow tract, neurons and glia in the peripheral nervous system and melanocytes.

Vagal neural crest cells. Vagal neural crest cells typically originate within the hindbrain adjacent to somites 1 through 7. They differentiate into numerous derivatives, including melanocytes, neurons and glia of the superior cervical ganglion, smooth muscle cells of the vascular system and conotruncal region of the heart and neurons and glia of the enteric nervous system

Sacral neural crest cells. Sacral neural crest cells delaminate from neural tube at the axial level adjacent to somites 28 and beyond. They contribute to melanocytes, as well as neurons and glia in both the enteric and sympathetic nervous system.

Enteric nervous system. A network of interconnected ganglia that innervate the digestive tract to insure efficient nutrient absorption and waste excretion. In amniotes, such as chicken, mouse, and human, there are two typical layers of neurons and glia—submucosal plexus and myenteric plexus distributed in the inner and outer areas of the gastrointestinal wall, respectively.

Submucosal plexus. A network of interconnected ganglia that populate the submucosal layer to control the gastrointestinal secretion, adjust blood flow, maintain water and electrolyte balance, and transmit signals to the myenteric plexus to coordinate gut movement.

Myenteric plexus. A network consisting of inhibitory, excitatory and motor neurons and that resides between the circular and longitudinal muscle layer to regulate the gut movement.

Intrinsic primary afferent neuron (IPANs). Multipolar neurons that play a pivotal role in mediating responses to mechanical, chemical, and thermal stimuli, thus influencing gastrointestinal motility, secretion, and blood flow. They branch extensively within the enteric plexuses, allowing them to integrate and relay sensory information from the gut's mucosal layer, smooth muscle, and vascular structures.

Interneuron. Neurons that are intermediaries within neural circuits to interconnect sensory or motor neurons. They are crucial for processing incoming signals from sensory neurons and for transmitting these signals to motor neurons or other interneurons.

Excitatory motor neuron. These neurons reside in the myenteric plexus and control contraction of smooth muscle primarily through release of neurotransmitters, such as acetylcholine (ACh) and substance P (SP).

Inhibitory motor neuron. These neurons are situated in the myenteric plexus and regulate relaxation of the smooth muscles. Nitric Oxide, vasoactive intestinal peptide (VIP), purine beta-nicotinamide adenine dinucleotide (bNAD) and pituitary adenylate cyclase-activating peptide (PACAP) are important neurotransmitters of inhibitory motor neurons.

Nerve of Remak. A unique structure in avian species, the Nerve of Remak consists of a series of ganglia arranged in a chain along the mesentery, adjacent to the distal midgut and hindgut. During embryogenesis, neurons in the Nerve of Remak project their axons to the hindgut, forming a conduit for sacral neural crest to migrate into and colonize the posterior half of the digestive tract.

Chapter 1

INTRODUCTION

Structure and the Functions of the Enteric Nervous System (ENS)

Replenishing necessary nutrients and energy is critical for survival. Through the digestive tract, large chunks of food are broken down into small pieces, and complex compounds are chemically digested by appropriate enzymes into simple molecules for easy absorption. Water and electrolytes are balanced to maintain intestinal homeostasis. Hostile organisms, toxic substances and food debris are removed from the digestive tract. To fulfill this sophisticated and elaborate task, the enteric nervous system forms a pivotal hub, orchestrating interactions between epithelial layer, enteroendocrine cells, blood vessel, muscle, and interstitial cells of Cajal (ICC), for food digestion and absorption[1–5]. There is also active cooperation with immune cells and microorganisms for defending intestinal health in a hostile environment[6,7]. The ENS also communicates with the central nervous system (CNS), sympathetic nervous system and parasympathetic nervous system for information transmission and rapid responses to environmental change[8].

The ENS is a portion of the peripheral nervous system (PNS), comprised of neurons located outside the brain and spinal cord. Due to the huge size, complexity and physiological importance, the ENS is often referred to as a "second brain". In the mid-1700s, it was discovered that a segment of vertebrate intestine can respond to stimuli even when disconnected from the brain and spinal cord[8]. As the largest division in the PNS, the human ENS is composed of about 600 million neurons, a number greater than or equal to that of the spinal cord[9]. These neurons and glia cells form interconnected ganglia of the submucosal (Meissner) and myenteric (Auerbach) plexuses, with the former residing in the submucosal layer and the latter lying in between the longitudinal and circular smooth muscle layers[10,11]. Recent studies revealed that this two-layered structure is a simplified model and the organization and cellular composition of the ENS along the gut wall showed significant regional differences[12].

Innervation of the Intestine by Enteric Neurons

There are a variety of neuronal subtypes in the ENS. The intrinsic primary afferent neurons (IPANs) are responsible for sensing environmental changes and transmitting signals to interneurons and motor neurons[13]. The cell bodies of the IPANs are situated in the submucosal or myenteric plexuses for rapid response to different scenarios. Introduction of luminal contents (food or liquid) trigger the IPANs to elicit responses to secretomotor neurons located in the submucosal layer to activate the gastrointestinal gland for secretion and control the permeability of the intestinal mucosa to ions for maintenance of water and electrolyte balance[14]. Another type of secretomotor neurons, also known as secretomotor/vasodilator neurons release acetylcholine (ACh) to the neuroepithelium and neurovascular junctions, which stimulates the endothelium to discharge nitric oxide (NO) for vasodiation[15]. The main neurotransmitters/neuropeptides in the secretomotor neurons are vasoactive intestinal peptide (VIP) or ACh[10].

IPANs in the myenteric plexus establish extensive linkages with excitatory and inhibitory motor neurons and interneurons[13]. The ascending interneurons primarily connect with excitatory motor neurons for gut contraction, and descending interneurons mainly stimulate the inhibitory motor neurons for relaxation[10]. Regular contraction and relaxation along the gut propel the luminal contents from the oral to the anal terminus. Previous findings revealed ACh and substance P (SP) as key neurotransmitters in excitatory motor neurons and NO, VIP, purine beta-nicotinamide adenine dinucleotide (bNAD) and pituitary adenylate cyclase-activating peptide (PACAP) as important neurotransmitters in inhibitory motor neurons[10,11]. Ascending interneurons release enkephalin (Enk) and descending interneurons employ ACh and serotonin (5-HT)[10]. Recent single cell RNA-sequencing analysis displayed a more complicated composition of neurons in the myenteric plexuses. Twelve different types of enteric neurons were uncovered, containing a combination of neurotransmitter or neuropeptide *Calb2*, *Ndufa4l2*, *Gda*, *Penk*, *Fut9*, *Nos1*, *Npy*, *Rprml*, *Gad2*, *Neurod6*, *Sst*, *Calcb*, *Nmu*, *Ucn3*, *Cck*, *vGlut2*, *Nxph2*, *Ntng1*, *Calb1*, *Th*, and *Dbh*[16]. This discovery further demonstrates the complexity of the ENS.

Although the ENS can function independent of the CNS, there are extensive neural linkages between the two. The ENS communicates with the brain primarily through the nodose ganglia and dorsal motor vagal nucleus in the upper part of the body[8]. At lower axial levels, ENS-spinal cord connections through dorsal root ganglia and sympathetic and parasympathetic nervous systems predominate[8].

Origin and Development of the ENS

The ENS mainly arises from a group of embryonic multipotent cells called neural crest cells (NCCs), that emerge at the border between the neural plate and the non-neural ectoderm[17,18]. During neurulation, this border region elevates to form the neural folds, which ultimately converge at the dorsal midline, transforming the flat neural plate into a cylindrical neural tube. Presumptive NCCs within the neural folds then undergo an epithelial to mesenchymal transition to migrate away from the neural tube into the periphery as bona fide neural crest cells. They subsequently differentiate into a multitude of derivatives cell types, including melanocytes in the skin, bone and cartilage in the head, neurons and glia, the cardiac valves, and cells in the adrenal medulla and thyroid gland, among others[19].

Along the anterior-posterior axis, NCCs are typically classified into four subdivisions: cranial, vagal, trunk, and sacral[20,21]. In amniotes, the cranial NCCs extend from the forebrain to the anterior hindbrain; vagal NCCs reside within the neural tube adjacent to somite s1-7; trunk NCCs arise from the neural tube adjacent to somites 8-27; finally, the sacral NCCs comprise cells originating from the posterior to the somite 28 axial level. In addition to the vagal and sacral NCCs, Schwann cell precursors play an important role in enteric neurogenesis, and thus are considered as the third source of the ENS[22–24]. For example, the zebrafish ENS is mainly derived from the vagal NCCs, with a secondary contribution to ENS neurogenesis from Schwann cell precursors[25,26]. In sea lamprey, the ENS primarily stems from Schwann cell precursors[27]. The evolutionary progress from the sea lamprey to the amniotes is also reflected by the mounting sources and the complicating structure of the ENS.

In birds and mammals, vagal NCCs invade the foregut, migrate caudally along and eventually colonize the whole gut, while the sacral NCCs migrate rostrally and contribute to the neurons and glia in the post-umbilical region[28]. Vagal NCCs arising adjacent to somites 1 and 2 migrate along the descending fibers of the vagus nerves into the esophagus and differentiate into neurons and glia in the esophagus and the anterior foregut, while the posterior vagal NCCs from somite level 3-7 colonize the digestive tract from the foregut to the anus[22]. In mice, vagal NCCs invade the foregut at approximately embryonic day (E) 9, migrate caudally and colonize the whole gut by E14. The sacral NCCs emigrate from the neural tube at E9.5, and aggregate to form the prospective pelvic ganglia flanking the hindgut bilaterally at E11.5[28]. From there, the sacral NCCs enter the distal hindgut at around E13.5 and migrate rostrally until reaching the umbilicus[29]. Besides migration along the gut wall, a trans-mesentery migration has also been observed from the mouse ileum to the closely juxtaposed post-cecal bowel[10]. This demonstrates the potent invasive capability of the NCCs. In chick embryos, the vagal NCCs reach the foregut at E3-3.5 and complete colonization at approximately E8[28]. The sacral NCCs first reach the nerve of Remak, structure unique to birds, and then invade the hindgut. At E10, both vagal NCCs and sacral NCCs are present in the colorectal region. The amniote ENS is distributed into two layers - the inner submucosal and outer myenteric plexuses. In mouse, formation of the myenteric ganglia precedes their submucosal counterpart, and some progenitors migrate from the myenteric to the submucosal plexus, suggesting an "outside-in" hypothesis during ENS development[10]. However, in chick, the submucosal region is colonized prior to the myenteric region[28].

Although the zebrafish is a relatively new organisms for ENS study, the favorable genetic and developmental features make this model system increasingly popular in this field[25]. Zebrafish have a simplified ENS composed of myenteric neurons while lacking the submucosal layer. This architecture is reminiscent of the esophagus and stomach regions in small mammals. Genetically, humans and zebrafish share 70% of the same orthologs and 84% of human genes identified as involved in diseases have zebrafish counterparts[30]. The zebrafish genome is amenable to gene-editing techniques, like transposable-induced gene insertion and CRISPR/Cas9-mediated gene knockout. Zebrafish embryos are transparent in

the presence of 1-phenyl-2-thiourea (PTU) and develop externally to the maternal body, which facilitates the long-term observation of tissue development during embryogenesis.

In zebrafish, enteric progenitors invade the digestive tract at around 31 hours post-fertilization (hpf) and migrate caudally in streams on the left and right side of the gut[25,31]. Neuronal differentiation is observed by 2 dpf, characterized by the expression of the pan-neuronal marker Elavl3/4 (HuC/D)[32,33]. Later, the progenitors move circumferentially to populate the medial area[25]. By 3 days post-fertilization (dpf), when they reach the most distal portion of the gut, ENS cells are distributed uniformly in the foregut. In a rostral to caudal wave, they progressively differentiate into neurons that are peptidergic, nitrergic, serotonergic or cholinergic in character and become functional by 5 dpf[34].

Diseases and Developmental Disorders of the ENS

Abnormal development of ENS can lead to severe gastrointestinal disorders. One life-threatening disease is Hirschsprung's disease (HSCR), occurring in 1:5000 live human births[35]. This disorder is characterized by aganglionosis or hypoganglionosis of the colon, resulting in obstruction of the digestive tract. Patients with this disorder suffer from constipation, malnutrition, vomiting, and inflammation in the abdomen. HSCR requires surgery intervention for partial relief.

Another gastrointestinal disease is chronic intestinal pseudo-obstruction syndrome (CIPO), caused by significantly reduced or absent gut movement[11]. Thus, luminal substances—food, fluid, and air—fail to pass down the digestive tract, causing obstruction. Symptoms of CIPO include abdominal bloating and pain, nausea, vomiting, and weight loss. Different from HSCR, ENS neurons and glia seem to be present and well-ordered throughout the gut. Possible reasons include scarcity of secreted neurotransmitters by ENS neurons, accelerated degradation of neurotransmitters by surrounding enzymes and malfunctions of receptors of the muscles. A series of prokinetic medicines, like pyridostigmine for prevention of ACh degradation, octreotide for activation of somatostatin receptors and erythromycin for activation of motilin receptors, have some albeit minimal effectiveness in treatment.

Irritable bowel syndrome (IBS) is also a common bowel disorder[36]. Symptoms of IBS include abdominal distention and pain, cramping, and diarrhea or constipation, or even the combination of both. The cause of IBS is still not clear, but several factors can lead to IBS, including dysfunction of muscles and nervous system, stress, severe infection or alterations in gut microbes. As to involvement of ENS in IBS, one possibility is that perturbed signals between the neural network and the bowel may trigger IBS. Some studies have shown that disruption of the interaction of neurons and glia in the ENS can lead to IBS. There can also be an indirect effect via the brain-gut axis. Malfunction of ENS can result in dramatic emotional change in the CNS, and stress and anxiety are known factors for causing IBS.

Recent research also demonstrated an association between ENS malfunction and an array of neurodegenerative diseases of the brain, like Parkinson's disease (PD)[37,38]. The development of PD often occurs concomitant with the deterioration of ENS neurons. Some studies observed early aggregation of a-synuclein (aS) in specific neuronal subtypes of the ENS, and the retrograde transport brought the aS to the CNS through preganglionic vagal fibers. This discovery emphasizes the pivotal role of the ENS in growth and health.

Signaling Molecules Play Important Roles in the Developing ENS

As an elaborate and sophisticated nervous system, development of the ENS relies on the precise orchestration and orderly coordination of numerous intracellular and extracellular molecules to ensure proper formation. After decades of studies, a large number of genes that influence ENS development have been identified.

Among the genes associated with developmental disorders of the ENS, one of the centerpieces is the RET/GFRa/GDNF pathway[39,40], which plays a crucial role in survival, growth, proliferation, and differentiation of the ENS progenitors. *RET* encodes a transmembrane tyrosine kinase receptor and usually interacts with the glycosylphosphtidylinositol-linked GDNF family of receptors (GFRa1, GFRa2, GFRa3 and GFRa4), forming a heterodimer on the membrane of ENS progenitors to respond to the environmental GDNF (glial cell line-derived neurotrophic factor) signal. Cells failing to

receive GDNF signal usually undergo apoptosis. *RET* mutation has been detected in 50% of familial cases as well as ~15% of sporadic cases of HSCR. Complete loss of functional RET results in intestinal aganglionsis in humans and mice. Similar phenotypes also have been observed in mice with *Gfra1* and *Gdnf* deficiency.

EDNRB/ET-3 pathway is another pathway identified in HSCR[39,41]. Endothelin receptor type B gene (EDNRB) belongs to G protein-coupled receptor family expressed in the developing ENS, and the ligand ET-3 (Endothelin 3) is encoded by *EDN3* gene. EDNRB/ET-3 pathway also influences cell proliferation, migration and differentiation. *EDNRB*/*EDN3* mutations were found in ~5% of patients diagnosed with HSCR. Mouse and rat models carrying *EDNRB* and *EDN3* mutations also displayed megacolon[42,43]. Inhibition of EDNRB/ET-3 pathway in avian embryos brought about severe hypoganglionosis[44]. Interestingly, the presence of ET-3 counteracts the chemoattraction of NCC to GDNF, indicating that there is crosstalk between EDNRB/ET-3 and RET/GFRa/GDNF pathway[44].

In addition to these two pathways, some canonical developmental-related pathways also play important roles in the ENS development. Notch signaling pathway has been demonstrated to maintain the progenitor pool and prevent the premature maturation of the ENS progenitors[45]. BMP signaling pathway was hypothesized to be involves in multiple events of ENS development, including progenitor migration, ganglion formation and neurite expansion. In particular, BMP2 expression is decreased in HSCR patients[46]. In vivo experiment in mice suggested that *BMP2b* is important in regulating the expression of *GDNF*. Hedgehog molecules—*Sonic hedgehog* (*Shh*) and *Indian hedgehog* (*Ihh*)—display specific expression patterns in the gut wall and affect migration of ENS cells[47,48]. Zebrafish harboring *shha* mutation completely lose neurons in the gut, likely due to the adverse impact on *GDNF*[49].

Transcription Factors in the Developing ENS

Many transcription factors expressed in NCCs, most notably *Sox10*, *Foxd3*, *Zeb2* and *Pax3,* also have significant impact on the developing ENS[50]. *Sox10* belongs to the Sox (SRY-

related HMG-box) family of transcription factors. This gene was observed to continuously express in the ENS progenitors[51]. Perturbation of *Sox10* eliminates ENS neurons and even its heterozygous mutations can lead to severe aganglionosis in the colon, which is the HSCR-like symptom, partially because *Sox10* participates in the regulation of *Ret* and *Ednrb* expression.

Phox2b is a homeodomain transcription factor expressing in the ENS progenitor[10]. Previous studies hypothesized that *Phox2b* and *Sox10* were mutually exclusive during progenitor differentiation: *Phox2b* expression is maintained in ENS neurons, while *Sox10* expression is downregulated as neurons differentiate but remains in ENS glia, which in turn suppresses *Phox2b*. However, some studies with mouse have detected low levels of *Phox2b* expression in ENS glia[52]. Moreover, ENS neurons derived from Schwann cell precursors in zebrafish also turned on *Phox2bb* (zebrafish *Phox2b* homolog) when they migrate into the gut[26]. Mutations in *Phox2b* genes causes dramatic loss of ENS neurons, likely because *Phox2b* controls the receptor *RET*, which is essential for cell survival and proliferation[52]. Biallelic mutation of transcription factor *Tlx2*, the downstream target of *Phox2b* causes pseudo-obstruction or megacolon symptoms in the intestine[53].

Transcription factors *Hand2* (*Heart- and Neural Crest Derivatives-Expressed 2*) was also demonstrated to regulate ENS development. Deletion of *Hand2* in both mouse and zebrafish models caused a dramatic loss of ENS neurons[49,54]. Gain of function of *Hand2* detected increased number of Vip (vasoactive intestinal polypeptide)-positive neurons[54]. Loss of function of Homeobox gene *Hoxb5b* also resulted in reduction of ENS neurons, while overexpression of *Hoxb5b* led to rising number of ENS progenitors in zebrafish[55]. Recently, *Pbx3* (*PBX homeobox 3*) has been to be expressed in myenteric neurons by single cell RNA-sequencing[16]. This gene may function as a cell fate switch. Upon depletion of *Pbx3*, Calb+ neurons decrease, but Vip+/Nos1+/Gal+ neurons expand. CRISPR/Cas9 screening experiment identified *Etv1*(*ETS variant transcription factor 1*) and *Tbx2a/b* (*T-box transcription factor 2a/b*) as important effectors of zebrafish ENS development[56,57]. With the

advent of new techniques, more ENS development-related genes will be discovered, and the underlying molecular mechanism will be unraveled.

BIBLIOGRAPHY

1. Vanner, S., and Surprenant, A. (1991). Cholinergic and noncholinergic submucosal neurons dilate arterioles in guinea pig colon. American Journal of Physiology-Gastrointestinal and Liver Physiology *261*, G136–G144. https://doi.org/10.1152/ajpgi.1991.261.1.G136.

2. Ye, L., Bae, M., Cassilly, C.D., Jabba, S.V., Thorpe, D.W., Martin, A.M., Lu, H.-Y., Wang, J., Thompson, J.D., Lickwar, C.R., et al. (2021). Enteroendocrine cells sense bacterial tryptophan catabolites to activate enteric and vagal neuronal pathways. Cell Host & Microbe *29*, 179-196.e9. https://doi.org/10.1016/j.chom.2020.11.011.

3. Klein, S., Seidler, B., Kettenberger, A., Sibaev, A., Rohn, M., Feil, R., Allescher, H.-D., Vanderwinden, J.-M., Hofmann, F., Schemann, M., et al. (2013). Interstitial cells of Cajal integrate excitatory and inhibitory neurotransmission with intestinal slow-wave activity. Nat Commun *4*, 1630. https://doi.org/10.1038/ncomms2626.

4. Vergnolle, N., and Cirillo, C. (2018). Neurons and Glia in the Enteric Nervous System and Epithelial Barrier Function. Physiology *33*, 269–280. https://doi.org/10.1152/physiol.00009.2018.

5. Gershon, M.D. (1981). The Enteric Nervous System. Annu. Rev. Neurosci. *4*, 227–272. https://doi.org/10.1146/annurev.ne.04.030181.001303.

6. Yoo, B.B., and Mazmanian, S.K. (2017). The Enteric Network: Interactions between the Immune and Nervous Systems of the Gut. Immunity *46*, 910–926. https://doi.org/10.1016/j.immuni.2017.05.011.

7. Geng, Z.-H., Zhu, Y., Li, Q.-L., Zhao, C., and Zhou, P.-H. (2022). Enteric Nervous System: The Bridge Between the Gut Microbiota and Neurological Disorders. Front. Aging Neurosci. *14*, 810483. https://doi.org/10.3389/fnagi.2022.810483.

8. Spencer, N.J., and Hu, H. (2020). Enteric nervous system: sensory transduction, neural circuits and gastrointestinal motility. Nat Rev Gastroenterol Hepatol *17*, 338–351. https://doi.org/10.1038/s41575-020-0271-2.

9. Furness, J.B., Callaghan, B.P., Rivera, L.R., and Cho, H.-J. (2014). The Enteric Nervous System and Gastrointestinal Innervation: Integrated Local and Central Control. In Microbial Endocrinology: The Microbiota-Gut-Brain Axis in Health and Disease Advances in Experimental Medicine and Biology., M. Lyte and J. F. Cryan, eds. (Springer New York), pp. 39–71. https://doi.org/10.1007/978-1-4939-0897-4_3.

10. Rao, M., and Gershon, M.D. (2018). Enteric nervous system development: What could possibly go wrong? Nat Rev Neurosci *19*, 552–565. https://doi.org/10.1038/s41583-018-0041-0.

11. Schneider, S., Wright, C.M., and Heuckeroth, R.O. (2019). Unexpected Roles for the Second Brain: Enteric Nervous System as Master Regulator of Bowel Function. Annu. Rev. Physiol. *81*, 235–259. https://doi.org/10.1146/annurev-physiol-021317-121515.

12. Hamnett, R., Dershowitz, L.B., Sampathkumar, V., Wang, Z., Gomez-Frittelli, J., De Andrade, V., Kasthuri, N., Druckmann, S., and Kaltschmidt, J.A. (2022). Regional cytoarchitecture of the adult and developing mouse enteric nervous system. Current Biology *32*, 4483-4492.e5. https://doi.org/10.1016/j.cub.2022.08.030.

13. Clerc, N. (2002). Controlling the excitability of IPANs: a possible route to therapeutics. Current Opinion in Pharmacology *2*, 657–664. https://doi.org/10.1016/S1471-4892(02)00222-9.

14. Hansen, M.B. (2003). The Enteric Nervous System I: Organisation and Classification. Pharmacology & Toxicology *92*, 105–113. https://doi.org/10.1034/j.1600-0773.2003.t01-1-920301.x.

15. Fung, C., and Vanden Berghe, P. (2020). Functional circuits and signal processing in the enteric nervous system. Cell. Mol. Life Sci. *77*, 4505–4522. https://doi.org/10.1007/s00018-020-03543-6.

16. Morarach, K., Mikhailova, A., Knoflach, V., Memic, F., Kumar, R., Li, W., Ernfors, P., and Marklund, U. (2021). Diversification of molecularly defined myenteric neuron classes revealed by single-cell RNA sequencing. Nat Neurosci *24*, 34–46. https://doi.org/10.1038/s41593-020-00736-x.

17. Sauka-Spengler, T., and Bronner-Fraser, M. (2008). A gene regulatory network orchestrates neural crest formation. Nat Rev Mol Cell Biol *9*, 557–568. https://doi.org/10.1038/nrm2428.

18. Gammill, L.S., and Bronner-Fraser, M. (2003). Neural crest specification: migrating into genomics. Nat Rev Neurosci *4*, 795–805. https://doi.org/10.1038/nrn1219.

19. Green, S.A., Simoes-Costa, M., and Bronner, M.E. (2015). Evolution of vertebrates as viewed from the crest. Nature *520*, 474–482. https://doi.org/10.1038/nature14436.

20. Hutchins, E.J., Kunttas, E., Piacentino, M.L., Howard, A.G.A., Bronner, M.E., and Uribe, R.A. (2018). Migration and diversification of the vagal neural crest. Developmental Biology *444*, S98–S109. https://doi.org/10.1016/j.ydbio.2018.07.004.

21. Martik, M.L., and Bronner, M.E. (2017). Regulatory Logic Underlying Diversification of the Neural Crest. Trends in Genetics *33*, 715–727. https://doi.org/10.1016/j.tig.2017.07.015.

22. Espinosa-Medina, I., Jevans, B., Boismoreau, F., Chettouh, Z., Enomoto, H., Müller, T., Birchmeier, C., Burns, A.J., and Brunet, J.-F. (2017). Dual origin of enteric neurons in vagal Schwann cell precursors and the sympathetic neural crest. Proc. Natl. Acad. Sci. U.S.A. *114*, 11980–11985. https://doi.org/10.1073/pnas.1710308114.

23. Uesaka, T., Okamoto, M., Nagashimada, M., Tsuda, Y., Kihara, M., Kiyonari, H., and Enomoto, H. (2021). Enhanced enteric neurogenesis by Schwann cell precursors in mouse models of Hirschsprung disease. Glia *69*, 2575–2590. https://doi.org/10.1002/glia.24059.

24. Kastriti, M.E., Faure, L., Von Ahsen, D., Bouderlique, T.G., Boström, J., Solovieva, T., Jackson, C., Bronner, M., Meijer, D., Hadjab, S., et al. (2022). Schwann cell precursors represent a neural crest-like state with biased multipotency. The EMBO Journal *41*, e108780. https://doi.org/10.15252/embj.2021108780.

25. Shepherd, I., and Eisen, J. (2011). Development of the Zebrafish Enteric Nervous System. In Methods in Cell Biology (Elsevier), pp. 143–160. https://doi.org/10.1016/B978-0-12-387036-0.00006-2.

26. El-Nachef, W.N., and Bronner, M.E. (2020). De novo enteric neurogenesis in post-embryonic zebrafish from Schwann cell precursors rather than resident cell types. Development, dev.186619. https://doi.org/10.1242/dev.186619.

27. Green, S.A., Uy, B.R., and Bronner, M.E. (2017). Ancient evolutionary origin of vertebrate enteric neurons from trunk-derived neural crest. Nature *544*, 88–91. https://doi.org/10.1038/nature21679.

28. Heanue, T.A., Shepherd, I.T., and Burns, A.J. (2016). Enteric nervous system development in avian and zebrafish models. Developmental Biology *417*, 129–138. https://doi.org/10.1016/j.ydbio.2016.05.017.

29. Wang, X., Chan, A.K.K., Sham, M.H., Burns, A.J., and Chan, W.Y. (2011). Analysis of the Sacral Neural Crest Cell Contribution to the Hindgut Enteric Nervous System in the Mouse Embryo. Gastroenterology *141*, 992-1002.e6. https://doi.org/10.1053/j.gastro.2011.06.002.

30. Kalueff, A.V., Stewart, A.M., and Gerlai, R. (2014). Zebrafish as an emerging model for studying complex brain disorders. Trends in Pharmacological Sciences *35*, 63–75. https://doi.org/10.1016/j.tips.2013.12.002.

31. Uribe, R.A., and Bronner, M.E. (2015). Meis3 is required for neural crest invasion of the gut during zebrafish enteric nervous system development. MBoC *26*, 3728–3740. https://doi.org/10.1091/mbc.E15-02-0112.

32. Kelsh, R.N., and Eisen, J.S. (2000). The zebrafish *colourless* gene regulates development of non-ectomesenchymal neural crest derivatives. Development *127*, 515–525. https://doi.org/10.1242/dev.127.3.515.

33. Holmberg, A., Schwerte, T., Fritsche, R., Pelster, B., and Holmgren, S. (2003). Ontogeny of intestinal motility in correlation to neuronal development in zebrafish embryos and larvae. Journal of Fish Biology *63*, 318–331. https://doi.org/10.1046/j.1095-8649.2003.00149.x.

34. Uyttebroek, L., Shepherd, I.T., Harrisson, F., Hubens, G., Blust, R., Timmermans, J.-P., and Van Nassauw, L. (2010). Neurochemical coding of enteric neurons in adult and embryonic zebrafish (Danio rerio). J. Comp. Neurol. *518*, 4419–4438. https://doi.org/10.1002/cne.22464.

35. Heuckeroth, R.O. (2018). Hirschsprung disease — integrating basic science and clinical medicine to improve outcomes. Nat Rev Gastroenterol Hepatol *15*, 152–167. https://doi.org/10.1038/nrgastro.2017.149.

36. Jahng, J., and Kim, Y.S. (2016). Irritable Bowel Syndrome: Is It Really a Functional Disorder? A New Perspective on Alteration of Enteric Nervous System. J Neurogastroenterol Motil *22*, 163–165. https://doi.org/10.5056/jnm16043.

37. Braak, H., Rüb, U., Gai, W.P., and Del Tredici, K. (2003). Idiopathic Parkinson's disease: possible routes by which vulnerable neuronal types may be subject to neuroinvasion by an unknown pathogen. Journal of Neural Transmission *110*, 517–536. https://doi.org/10.1007/s00702-002-0808-2.

38. Kim, S., Kwon, S.-H., Kam, T.-I., Panicker, N., Karuppagounder, S.S., Lee, S., Lee, J.H., Kim, W.R., Kook, M., Foss, C.A., et al. (2019). Transneuronal Propagation of Pathologic α-Synuclein from the Gut to the Brain Models Parkinson's Disease. Neuron *103*, 627-641.e7. https://doi.org/10.1016/j.neuron.2019.05.035.

39. Lake, J.I., and Heuckeroth, R.O. (2013). Enteric nervous system development: migration, differentiation, and disease. American Journal of Physiology-Gastrointestinal and Liver Physiology *305*, G1–G24. https://doi.org/10.1152/ajpgi.00452.2012.

40. Baloh, R.H., Enomoto, H., Johnson, E.M., and Milbrandt, J. (2000). The GDNF family ligands and receptors — implications for neural development. Current Opinion in Neurobiology *10*, 103–110. https://doi.org/10.1016/S0959-4388(99)00048-3.

41. Bondurand, N., Dufour, S., and Pingault, V. (2018). News from the endothelin-3/EDNRB signaling pathway: Role during enteric nervous system development and involvement in neural crest-associated disorders. Developmental Biology *444*, S156–S169. https://doi.org/10.1016/j.ydbio.2018.08.014.

42. Cheng, Z., Dhall, D., Zhao, L., Wang, H.L., Doherty, T.M., Bresee, C., and Frykman, P.K. (2010). Murine model of Hirschsprung-associated enterocolitis. I: Phenotypic characterization with development of a histopathologic grading system. Journal of Pediatric Surgery *45*, 475–482. https://doi.org/10.1016/j.jpedsurg.2009.06.009.

43. Gariepy, C.E., Cass, D.T., and Yanagisawa, M. (1996). Null mutation of endothelin receptor type B gene in spotting lethal rats causes aganglionic megacolon and white coat color. Proc. Natl. Acad. Sci. U.S.A. *93*, 867–872. https://doi.org/10.1073/pnas.93.2.867.

44. Nagy, N., and Goldstein, A.M. (2006). Endothelin-3 regulates neural crest cell proliferation and differentiation in the hindgut enteric nervous system. Developmental Biology *293*, 203–217. https://doi.org/10.1016/j.ydbio.2006.01.032.

45. Okamura, Y., and Saga, Y. (2008). Notch signaling is required for the maintenance of enteric neural crest progenitors. Development *135*, 3555–3565. https://doi.org/10.1242/dev.022319.

46. Huang, S., Wang, Y., Luo, L., Li, X., Jin, X., Li, S., Yu, X., Yang, M., and Guo, Z. (2019). BMP2 Is Related to Hirschsprung's Disease and Required for Enteric Nervous System Development. Front. Cell. Neurosci. *13*, 523. https://doi.org/10.3389/fncel.2019.00523.

47. Walton, K.D., and Gumucio, D.L. (2021). Hedgehog Signaling in Intestinal Development and Homeostasis. Annu. Rev. Physiol. *83*, 359–380. https://doi.org/10.1146/annurev-physiol-031620-094324.

48. Nagy, N., Barad, C., Graham, H., Hotta, R., Cheng, L., Fejszak, N., and Goldstein, A.M. (2015). Sonic hedgehog controls enteric nervous system development by patterning the extracellular matrix. Development, dev.128132. https://doi.org/10.1242/dev.128132.

49. Reichenbach, B., Delalande, J.-M., Kolmogorova, E., Prier, A., Nguyen, T., Smith, C.M., Holzschuh, J., and Shepherd, I.T. (2008). Endoderm-derived Sonic hedgehog and mesoderm Hand2 expression are required for enteric nervous system development in zebrafish. Developmental Biology *318*, 52–64. https://doi.org/10.1016/j.ydbio.2008.02.061.

50. Uribe, R.A. (2024). Genetic regulation of enteric nervous system development in zebrafish. Biochemical Society Transactions *52*, 177–190. https://doi.org/10.1042/BST20230343.

51. Bondurand, N., and Sham, M.H. (2013). The role of SOX10 during enteric nervous system development. Developmental Biology *382*, 330–343. https://doi.org/10.1016/j.ydbio.2013.04.024.

52. Cossais, F., Lange, C., Barrenschee, M., Möding, M., Ebsen, M., Vogel, I., Böttner, M., and Wedel, T. (2019). Altered enteric expression of the homeobox transcription factor Phox2b in patients with diverticular disease. UEG Journal *7*, 349–357. https://doi.org/10.1177/2050640618824913.

53. Borghini, S., Di Duca, M., Santamaria, G., Vargiolu, M., Bachetti, T., Cargnin, F., Pini Prato, A., De Giorgio, R., Lerone, M., Stanghellini, V., et al. (2007). Transcriptional regulation of TLX2 and impaired intestinal innervation: possible role of the PHOX2A and PHOX2B genes. Eur J Hum Genet *15*, 848–855. https://doi.org/10.1038/sj.ejhg.5201852.

54. Hendershot, T.J., Liu, H., Sarkar, A.A., Giovannucci, D.R., Clouthier, D.E., Abe, M., and Howard, M.J. (2007). Expression of Hand2 is sufficient for neurogenesis and cell type–specific gene expression in the enteric nervous system. Developmental Dynamics *236*, 93–105. https://doi.org/10.1002/dvdy.20989.

55. Howard, A.G.A., Nguyen, A.C., Tworig, J., Ravisankar, P., Singleton, E.W., Li, C., Kotzur, G., Waxman, J.S., and Uribe, R.A. (2022). Elevated Hoxb5b Expands Vagal Neural Crest Pool and Blocks Enteric Neuronal Development in Zebrafish. Front. Cell Dev. Biol. *9*, 803370. https://doi.org/10.3389/fcell.2021.803370.

56. Moreno-Campos, R., Singleton, E.W., and Uribe, R.A. (2024). A targeted CRISPR-Cas9 mediated F0 screen identifies genes involved in establishment of the enteric nervous system. PLoS ONE *19*, e0303914. https://doi.org/10.1371/journal.pone.0303914.

57. Kuil, L.E., MacKenzie, K.C., Tang, C.S., Windster, J.D., Le, T.L., Karim, A., De Graaf, B.M., Van Der Helm, R., Van Bever, Y., Sloots, C.E.J., et al. (2021). Size matters: Large copy number losses in Hirschsprung disease patients reveal genes involved in enteric nervous system development. PLoS Genet *17*, e1009698. http://doi.org/10.1371/journal.pgen.1009698

Chapter 2

IDENTIFYING DIFFERENT CELL TYPES AND KEY GENES IN THE DEVELOPING ZEBRAFISH ENS

Background

Zebrafish studies have identified more than 60 genes that affect enteric development to different extents[1] with mutation of genes like *Mapk10*, *BMP2* and *ATP5PO*[2–4] resulting in hypoganglionosis or aganglionosis in the colon, a characteristic of Hirschsprung's disease. While studies utilizing single cell RNA sequencing have generated transcriptomic profiles of ENS progenitors and differentiated neurons in zebrafish at 2dpf, 3pf[5] and 5dpf[6], the relatively low numbers of neurons warrant a more complete analysis of ENS development in zebrafish.

Here, we investigate cell lineage decisions and gene regulatory events underlying ENS differentiation by isolating and analyzing the transcriptome of pure populations of individual enteric neural crest-derived cells ranging from progenitors to differentiated cell types at progressive stages. This enables reconstruction of the developmental trajectories of each subtype of neurons in relationship to transcript expression at different developmental stages. Importantly, the relatively small size of the zebrafish intestinal tract at embryonic and larval stages makes it tractable to visualize the entire gut by multiplex analysis of spatial transcript expression, thus revealing neuronal subtype distribution *in toto* throughout the ENS. Finally, we identify key transcription factors in major neuronal differentiation trajectories and explore their functions by CRISPR-mediated perturbations. Taken together, our study provides a holistic developmental atlas of the developing zebrafish ENS and insights into transcriptional inputs that influence neuronal differentiation.

Results

Single-cell (sc) RNA-seq reveals heterogeneity of ENS cells

To investigate the developmental trajectory and cellular composition of the zebrafish ENS, we first generated a transgenic line which endogenously labels *paired like*

homeobox 2bb, the zebrafish homolog of the human *Phox2b* gene, a key transcription factor that plays a critical role in ENS development and is expressed in all enteric progenitors and mature neurons[7–11]. The reporter line was generated by inserting a monomeric green fluorescent protein *mNeonGreen*[12] after the *Phox2bb* coding sequence exploiting the microhomology-mediated end joining (MMEJ) mechanism triggered by genomic cleavage using the CRISPR/Cas9 system[13] (Figure 1A). Genomic sequences of the Tg(*Phox2bb: mNeonGreen*) were validated in F1 fish for accurate integration (Figure 8A). Because *mNeonGreen* and *Phox2bb* are present in the same transcript, this reporter faithfully recapitulates endogenous *Phox2bb* expression as revealed by colocalization of anti-Phox2b immunoreactivity with mNeonGreen fluorescent signals in the gut (Figure 1B). Thus, this line avoids ectopic expression that can plague reporter lines. These fish are healthy in both the heterozygous and homozygous state and have been bred for seven generations (Figure 8B). We observed that some cells from adjacent gut tissues exhibited strong autofluorescence. The spindle-shaped morphology and hollow nuclei seen in the staining can help distinguish these cells from genuine signals (Figure 8C).

The vagal neural crest cells in zebrafish first migrate ventrally and reach the post-otic regions on left and right sides (Figure 8D), migrate toward the midline and invade the gut at around 31 hpf[14,15] (Figures 1C and 1D). Thus, we performed scRNA-seq of sorted *Phox2bb*+ ENS cells at 2-, 3-, 4-, 5- and 6-days post-fertilization (dpf), profiling >22,000 cells. (Figures 1E, 1F and 8E-8H). This range of time points was chosen since ENS neurons are first detected at 2 dpf and the ENS is fully functional at 5-6 dpf[16]. Prior to sorting, the head was removed to minimize inclusion of the CNS and cranial ganglia (Figure 8E). To further assure we only include ENS cells, we reanalyzed the data after removing non-ENS cells as well as possible doublets (Figures 9A, 9B and 9E-9G).

After clustering the scRNA-seq data from all developmental stages, we identified 23 clusters of ENS cells ranging from progenitors and neuroblasts to immature and mature neurons (Figure 1F). With progressive ENS development, the percentage of progenitors and immature neurons decreased, whereas the percentage of mature neurons rose with largest changes occurring between 2–4 dpf, suggesting that a large degree of neuronal differentiation was transpiring during this time (Figure 9C and 9D).

Identification of ENS progenitors and neuroblasts

Putative progenitors (cluster 20, 9, 7 and 22) were assigned based on co-expression of *Phox2bb*[9,11,17], *Sox10*[18], *FoxD3*[19] and *Zeb2a*[20] (orthologous to human *ZEB2/ZFHX1B*) (Figure 1H). The progenitors also express various cell cycle genes, such as *Cdc20*[21], *Rrm2*[22] and *Cdca7a*[23] (Figure 1G, Table 1). As progenitors develop into neuroblasts (cluster 6, 14 and 1), the cells start expressing neuronal markers, like *Elavl3* (Figure 1J), but lack specific neurotransmitter genes. Transcription factors known to be involved in neuronal specification, like *Phox2a*[8], *Insm1b*[24] and *Meis1b*[25], are also expressed at this stage (Figure 1H). Early-stage neuroblasts (cluster 6, 14) are characterized by the expression of *Srrm4*, a neural-specific splicing regulator[26], in cluster 6 by *Jam2a*, a junctional adhesion molecule involved in Notch signal transmission[27], and in cluster 14 by expression of *Gata2a*[28] and receptor gene *Ackr3b*[29] known for its involvement in neuronal differentiation and maturation (Figure 9H). The late stage neuroblast (cluster 1) is marked by *Tm6sf2* and *Tmsb* (orthologous to human TMSB10), and *Tmsb10* detected in neurons[30](Figure 9H). Between the progenitor and neuroblast clusters, we identified two other clusters, 15 and 0 (Figure 1F), which emerge at 2 and 3 dpf, respectively; cluster 0 increases in cell number in subsequent days. By 6 dpf, most of the progenitors belong to these two clusters. In addition to expressing ENS progenitor genes, like *Sox10, Phox2bb, Foxd3* and *Zeb2,* C0 and C15 specifically express *Foxo1a,* whose ortholog *Foxo1* is a neural stem/progenitor marker in the mammalian CNS[31,32](Figure 1H). They also express selenoprotein *Sepp1a* (aka *Selenop*) (Figure 1H), orthologous to SEPP1/SELENOP which has been reported to be expressed in Schwann cells[33] and to increase proliferation of hippocampal neural precursor cell[34]. Moreover, *Klf15*[35] and *Ror2*[36] in cluster 0 play critical roles in the maintenance of neural stem cells. *Ccdc80*[37], *Hbegfb*[38] and *Moxd1*[39] detected in C15 also are present in neural stem cells. Given that the Schwann cell precursor (SCP) marker *Pmp22* is expressed in all progenitor clusters and SCPs are known to make an important contribution to the ENS[40-44], we speculate that cells in cluster 15 (*Foxo1a*/*Ccdc80*) and 0 (*Foxo1a*/*Ror2*) are likely reserve progenitors derived from vagal neural crest or Schwann cell precursors that contribute to later expansion of the ENS neuronal populations.

Next, we examined localization of enteric progenitors based on co-expression of *Phox2bb* and *Sox10* and neurons via coexpression of the pan-neuronal markers *Elavl3* (Figure 1J) and *Elavl4* (Figure 9H). Consistent with previous studies, neurons are first detected at 2 dpf, when progenitors are migrating in two parallel migration streams on the left and right side of the gut (Figure 1, I and J), followed by circumferential migration[45-47]. By 3 dpf, the wavefront of the migrating enteric neural crest cells has reached the end of the gut. Consistent with this, our scRNA-seq data demonstrate there are still many progenitors in the gut at 6 dpf and whole mount imaging of co-expression of *Phox2bb* and *Sox10* suggests that these progenitors are scattered throughout the gut.

Identification of enteric neuron subtypes by the combinatorial expression of neurotransmission genes

To better characterize enteric neurons, we applied the RNA velocity analysis with the UniTVelo[48] package and trajectory inference using the scFates[49] package to uncover the developmental dynamics from ENS progenitors to mature neurons (Figure 2, A and B). The analyses reveal eight mature neuronal subtypes—enteric neurons (EN) 1-7, characterized by co-expression of *Elavl3* together with high expression of known neuropeptide and neurotransmitter-related genes[50] (Figure 2A-C) and Cluster 21, composed of two groups of *Galn*-expressing neurons flanking the region anterior to the foregut and emerging early at 2dpf (Figures 2C and 9J). As the enteric neurons mature, they express *Nos1* (*nitric oxide synthase 1*), *Vip*/*Vipb* (*vasoactive intestinal peptides*), *Slc18a3a* (*solute carrier family 18 member 3a*; vesicular acetylcholine transporter) and *Galn* (Now named as *Gal*; *galanin/GMAP prepropeptide*) (Figure 2C and Figure 9J). EN1 is (clusters 10, 13) characterized by *Tph1b* (*tryptophan hydroxylase 1b*) and *Ddc* (*dopa decarboxylase*) expression, two enzymes involved in serotonin synthesis (Figure 2C, Figure 10A). EN2-4 are part of a large group (comprised of clusters 2, 3, 4, 5, 12, 17, 18). EN2 (cluster 2) expresses *Adcyap1b* (*adenylate cyclase activating polypeptide 1b*, aka *Pacap1b*), *Nos1* and *Vipb*, likely of inhibitory motor neuron character[51]. EN3 (cluster 17) and EN4 (cluster 18) are characterized by expression of *Adcyap1b/Vip/Vipb/Tph1b/Nmu* and *Adcyap1b/Vip/Vipb/Slc18a3a*, respectively. Two small subgroups of neurons are identified in EN5 (cluster 19). They share common marker genes *Slc18a3a*, *Tac3a*

(*tachykinin precursor 3a*) and *Cart2* (*cocaine- and amphetamine-regulated transcript 2*), and have unique markers *Nos1* and *Adcyap1b*, respectively. EN6, 7 (clusters 11, 8, 4) are characterized by expression of *Slc18a3a/Nmu/Tac3a/Cart2* and *Slc18a3a/Nmu/Tac3a*, respectively. Unlike in the mouse and human scRNA-seq data[52,53], we failed to detect expression of *Tac1* (products of this gene include Substance P and Neurokinin A) but found high expression of its paralog *Tac3a*. EN6 and EN7 also express calbindin proteins *Calb1* and *Calb2a* (Figure 10B). Taken together, they express characteristics of excitatory motor neurons[51,52].

Multiplex spatiotemporal analysis reveals the distribution of enteric neuronal subtypes in the developing gut

From rostral to caudal, the zebrafish gastrointestinal (GI) tract is composed of a bulky intestinal bulb (foregut), mid-intestine (midgut) and caudal segment (hindgut)[54]. The compact nature of the zebrafish gut enables visualization of transcripts throughout the developing gut, something that has been intractable in amniotes. Unlike the mammalian ENS which is composed of interconnected ganglia, neurons in the zebrafish ENS are distributed throughout the gut as individual or small clusters of cells[47,55].

To uncover the spatiotemporal distribution of various cell types in the ENS, we dissected the developing gut from 2 (52, 56, and 60 hpf), 3, 4 and 6 dpf zebrafish for whole-mount imaging with 9 neurotransmitter or neuropeptide(-related) genes. We detected expression of peptide and neurotransmitter genes *Nos1*, *Vip*, *Vipb* and *Slc18a3a* as early as 52 hpf (Figure 2D), followed by *Adcyap1b* at 56 hpf and *Nmu*, *Tac3a* and *Cart2* at 60 hpf (Figure 2G-M*).* Combinatorial expression as detected by sequential Hybridization Chain Reaction (HCR)[56] suggests that there are 7 main subtypes of enteric neurons labeled EN1-7 plus a transitional population C12 (Table 2) (Figure 2C). By 6 dpf, zebrafish begin to feed, and the gut is relatively mature, enabling validation of the spatial localization of these distinct classes of ENS neuronal subtypes (Figure 3A-L).

By merging 9 channels together, we examined the order of emergence of enteric neurons as well as their spatial localization. EN2 (*Adcyap1b/Nos1/Vipb*) was first to arise at 56 hpf (Figure 2O). EN2 is the largest neuronal subpopulation, representing more than 30% of enteric neurons (Figure 3C). They span a vast region of the gut but are sparse in

the anterior- and posterior-most regions (Figure 3F) Figure 3E (Figure 3E. At 56 hpf, almost all cells that express *Slc18a3a* also possess one or more inhibitory motor neuron marker - *Adcyap1b*, *Nos1*, *Vip, Vipb*. Indeed, many neurons in the foregut and midgut co-express all these markers *Adcyap1b*/*Nos1*/*Vip*/*Vipb/Slc18a3a* (Figure 2P). These are likely transitioning to EN4 (*Adcyap1b*/*Vip*/*Vipb/Slc18a3a*), in which *Nos1* is turned off. EN4 was first detected at 60 hpf (Figure 2R) with numbers increasing as the ENS develops, concomitant with a decrease in neurons expressing *Adcyap1b*/*Nos1*/*Vip*/*Vipb/Slc18a3a*. This further supports the trajectory analysis, suggesting EN2 and EN4 share common parents. Some cells retain *Adcyap1b/Nos1/Vipb* expression and move into EN2, while others express *Vip* and *Sla18a3a* but not *Nos1* as they differentiate into EN4.

EN7 (*Slc18a3a/Nmu/Tac3a*) appears at 60 hpf (Figure 2Q) followed by EN6 (*Slc18a3a/Nmu/Tac3a/Cart2*). A subset of *Slc18a3a*/*Nmu* neurons also are likely to be EN7 neurons. but with lower *tac3a* expression, which is difficult to detect by HCR. EN6 and EN7 account for ~10% and ~25% of the total population, respectively (Figure 3C). However, no EN6 or EN7 neurons were observed in the posterior terminus of the gut, where EN5 cells localize. Intriguingly, the density of EN6 increases from anterior to the posterior, while the distribution of EN7 is relatively even across the gut. (Figure 3K, L).

EN1 (*Tph1b*) arises at 3 dpf (Figure 2S). EN1 is composed of three different flavors of cells: *Tph1b*, *Tph1b/Vipb* and *Tph1b/Vipb*/*Vip,* consistent with the scRNA-seq results that *Vip* and *Vipb* are present in EN1 (Figure 3E) and that *Tph1b* expression arises at 3 dpf as the neurons reach maturity (Figure 2C, N). These cells are distributed throughout the gut, and account for 10% of the total detected cells, with *Tph1b/Vipb* neurons representing the majority (Figure 3C).

By 4 dpf and 6 dpf, we detected emergence of EN5 (*Slc18a3a/Tac3a/Cart2/Nos1)* and EN3 (*Adcyap1b/Vip/Vipb/Tph1b/Nmu*) (Figure 2U, V), respectively, consistent with the scRNA-seq results suggesting that these two subtypes arise later in development. EN5 is composed of early neurons (*Slc18a3a/Tac3a/Cart2*) and two types of mature neurons (Figure 3J). These express *Slc18a3a/Tac3a/Cart2/Adcyap1b* and S*lc18a3a/Tac3a/Cart2/Nos1*, with the latter being the dominant population. This subtype takes up about 5% of the enteric neurons and is confined to the caudal-most portion of the gut at the stages examined, suggesting a unique function in the hindgut (Figure 3C).

In addition to EN1-7, we also found many *Adcyap1b*/*Nos1*/*Vipb*/*Vip* expressing cells, matching cluster 12 (C12) cells, which may reflect a transitional state from immature neuron to EN3 and EN4 according to the trajectory analysis (Figure 3D). C12 cells are mostly located in anterior and posterior termini and sparse in the middle; they comprise ~10% of the total population (Figure 3C, G). EN3 mainly localizes in the intestinal bulb and EN4 in midgut and hindgut (Figure 3H, I). Both subtypes represent about 5% of enteric neurons (Figure 3C). Many *Vip*+ and *Vipb*+ cells were observed spreading throughout the gut. Given that the ENS expands as zebrafish grow, and *Vip* as well as *Vipb* are the pioneer markers in EN2-4, these cells are likely immature neurons.

Developmental trajectories provide clues to lineage specification

To gain insight into the potential cell lineage progression from ENS progenitors to mature neuronal subtypes, we applied the scFates package for trajectory and bifurcation analysis (Figure 4A-C). Clusters 15 (C15) and 0 (C0) harbor progenitor marker genes (*Sox10/Phox2bb/Foxd3*/*Zeb2)* and represent a potential progenitor pool for later expansion of the ENS. The C15 branch is characterized by expression of unique transcription factors *Foxo1a/Nr4a2b* and by 2dpf diverges from the mainstream progenitor. By 3dpf, the C0 branch emerges and is characterized by expression of *Foxo1a/Atf5b* (Figure 13A-D).

Neuroblasts are inferred to first bifurcate into two branches (EN1/2/3/4/C12 and EN5/6/7), defined by the complementary expression of *Hmx3a* and *Tox* (Figure 4D). The expression pattern of *Prdm1a* initiates in progenitors and continues in emerging immature EN5/6/7 neurons, further corroborating specification of this branch likely at the neuroblast stage (Figure 13D). The first branch soon bifurcates into two groups - EN1, characterized by the expression of *Satb2/Bnc2* and EN2/3/4/C21, expressing *Ebf1a* (Figure 4C, D). The C21 cluster becomes distinct from EN2/3/4 neurons via upregulation of *Ebf3a* at early stages, and subsequently *Pbx1a/Pbx3b/Onecut1* in mature neurons (Figure 13D). EN2 continuously expresses *Ebf1a* and turns on *Smad3a* at the terminal stage, while EN3/4 gradually downregulate *Ebf1a* and develop into EN3, characterized by expression of *Pbx1a/Pbx3b/Id1/Smad9,* and EN4 marked by *Pbx1a/Pbx3b/Foxp1a* (Figure 4C, D)

The EN5/6/7 cells branch, expressing *Gata3*, bifurcates from EN5 which expresses *Egr3/Ascl1*(Figure 4C, D). EN5 is composed of two subclusters *Slc18a3a/Tac3a/Cart2/Adcyap1b* and S*lc18a3a/Tac3a/Cart2/Nos1,* as validated by multiplex spatial analysis. Transcription factor *Nr0b1* is specifically expressed in the former and *Foxj1b/Smad9* in the latter (Figure 13D). EN6 and EN7 finally bifurcate by expressing different transcription factor combinations *Gata3/Egr3 and Gata3/Pbx1a/Mafb*, respectively (Figure 4C).

Our results agree with previous work[52] showing that the ENS progenitors give rise to different subtypes of neurons through multiple bifurcations steps.

Cell-type specific transcription factors shape the maturation of ENS neurons

To further address how ENS neurons are guided toward different fates and thus understand how the complex neural network is built, we focused on identification of potential fate-determining transcription factors in EN1, EN2/3/4 and EN5/6/7 branches using CRISPR/Cas9 technology. gRNA targeting tyrosinase, an enzyme mainly involved in melanin synthesis, was used as a control, such that sibling embryos from the same parents were injected with *Tyr*-gRNAs or transcription factor gRNAs (Figure 5A). To this end, we used 3 crRNA:tracrRNAs targeting the same gene, as these have been shown to be sufficient to generate mutation in 80-100% of sequenced alleles[57]. Crispants were raised in separate containers; dissected gut tissues from control and crispants were mounted on the same slide for parallel processing by HCR. An advantage of using zebrafish is that we can dissect and image the entire length of the gut. Thus, we separately examined effects on subregions of the gut divided into roughly equal lengths corresponding to foregut, midgut and hindgut.

Bifurcation analysis reveals that transcription factor *Ebf1a* expression initiates at the branchpoint between the EN1 and EN2/3/4/C12 lineages (Figure 5D). We noted high expression of *Ebf1a* is maintained in the EN2 (*Adcyap1b*/*Nos1/Vipb*), but not in EN3 (*Adcyap1b*/*Vipb*/*Vip*/*Slc18a3a*) or EN4 *Adcyap1b*/*Nmu*/*Vip*/(*Vipb*)/(*Tph1b*)) lineages (Figure 5C). Double fluorescent in situ hybridization further confirmed *Ebf1a* signal in most but not all the *Vipb*-positive cells at 5dpf (Figure 5B; Figure S7B), consistent with scRNA-seq results.

The homologs of zebrafish *Ebf1a* - *Ebf1* have been shown to be expressed in the mouse and human ENS[52,58,59], but the function of *Ebf1* has been largely elusive. Therefore, we tested the function of *Ebf1a* in zebrafish compared to control *Tyr*-gRNAs guts. Knockout of *Ebf1a* using 3 guides resulted in >94% mutation rate (Table 3-7; Figure 14G). The results show that *Ebf1a*-knockout leads to a significant reduction of *Adcyap1b*+ neurons (Figure 5E, F) by ~80% in the foregut and ~40% in the midgut and hindgut, respectively. Its loss also results in a remarkable decrease of *Nos1* expression and significant loss of *Vipb* expression (Figure 5E, F), particularly in the foregut and midgut. However, we noted less effect on *Vip* expression (Figure 5E, F), which is the primary marker of EN3 and EN4 neurons. Taking multiplex HCR (Figure 3A) and scRNA-seq (Figure 5C) results into account, *Ebf1a* appears to play an important role in the differentiation of the EN2 lineage. We also observed a slight decrease of *Tph1b*+ and *Slc18a3a*+ cells in the foregut but an increase in the hindgut of experimental compared to control guts. The total number of neurons follows a similar pattern. Given that the EN2 lineage is the first to emerge, this may reflect a change in migratory behavior of precursors or timing of differentiation of neuroblasts. In contrast, there was no change in *Cart2*+ expression, PH3 positive cells or number of neurons in the whole gut between experimental and control guts. Taken together, the results suggest that *Ebf1a* functions in differentiation but not survival of the EN2 neuronal lineage (likely inhibitory motor neurons), and with little effect on EN3 or EN4.

Next, we examined candidate regulators that emerge at the initiation of the excitatory motor neuron branch. We discovered that *Gata3* is expressed in EN6 and EN7, but not EN5, thus closely associated with the bifurcation that leads to the excitatory lineage decision (Figure 6). As *Gata3* transcript expression has not been previously noted in the ENS, we performed three rounds of sequential HCR staining to compare the expression of *Gata3, Nmu, Cart2, Nos1* and *Adcyap1b* in the same sample (Figure 14A). *Gata3/Nmu* cells (presumably EN7) are distributed throughout a broad region of the gut (Figure 6A-A", yellow arrowheads), whereas *Gata3/Nmu/Cart2* cells (presumably EN6) are mainly confined to the hindgut (Figure 6A-A", white arrowheads). Detected throughout the gut are cells that express *Gata3* but lack other marker genes (Figure 6A-A", cyan arrowheads); these are likely to be immature neurons that have yet to activate neurotransmitter genes.

Finally, we also observed *Cart2/Nos1* and *Cart2/Adcyap1b* cells, as well as cells with only *Cart2* (presumably EN5, Figure 6A''-A"', purple arrowheads) in the hindgut, consistent with our scRNA-seq results.

Knockout of *Gata3* using 3 guides resulted in 95% mutation rate (Figure 14G; Table 3-7). After loss of *Gata3*, we noted a profound reduction of *Slc18a3a*$^{+}$ neurons by ~ 40% in the foregut, and significant loss of ~70% and ~60% *Slc18a3a*$^{+}$ neurons in the midgut and hindgut, respectively (Figure 6D-E). Similarly, we observed a 70-80% decrease of *Nmu*+ cells in all three gut subregions. In contrast, we detected a concomitant increase in the number *Cart2*-positive neurons (Figure 6D-E). Moreover, the localization of *Cart2* expands throughout the whole gut, rather than being restricted to the terminal portion as in controls. Although the number of *Tac3a*+ cells was only slightly changed, the expression level of *Tac3a* appeared to be upregulated in each cell. This suggests that *Gata3* activates *Slc18a3a* and *Nmu* expression while repressing *Cart2* expression. Interestingly, we noted an increase of *Nos1*+ cells, most evident in the foregut. Close examination of the Gata3-KO sample revealed many *Cart2/Nos1* cells (possibly EN5) in the foregut and midgut, whereas these cells are normally confined to the hindgut (Figure 6F). Taking the expression patterns of *Gata3* and *Cart2* into account (Figure 6A-B), we hypothesize that *Gata3* specifies and maintains EN6/7 lineages but suppresses the EN5 lineage. Expression of *Vip* and *Tph1b* was unaffected by *Gata3* perturbation (Figure 14E). These results are consistent with *Gata3* primarily playing an essential role in excitatory motor neuron development.

Enhanced expression of *Satb2* was noted in the serotonergic neuron lineage and associated with expression of marker *Tph1b* (Figure 7A-C). Consistent with our findings, the homolog of zebrafish *Satb2* have been shown to be expressed in the mouse ENS, partially co-expressed with serotonin[59]. HCR results show that *Satb2* signal colocalizes with *Tph1b* in the foregut region. Surprisingly, *Satb2* was expressed not only in ENS neurons, but also in other gut tissues ranging from the posterior part of the foregut to the end of the gut (Figure 7A; Figure 14C, D).

We detected Satb2 expression at the bifurcation between EN1 and EN2 lineages. Analogous to the experiments above, we next interrogated its function using CRISPR/Cas9-mediated perturbation. Knockout of *Satb2* using 3 guides resulted in more than 90% mutation rate (Figure 14G; Table 3-7), causing selective reduction of *Tph1b*-

positive neurons in the foregut and midgut, but only has a slight effect on neurons in the hindgut (Figure 7D, E). In contrast, we noted little effect on the expression of *Nos1* and *Vip* in EN2 and EN3/4 lineages, or *Slc18a3a* and *Cart2* in EN5/6/7 lineages, suggesting that *Satb2* functions preferentially on serotonergic neurons during ENS development (Figure 7D, E).

Altogether, our loss-of-function results reveal novel roles for *Ebf1a, Gata3* and *Satb2* in neurons that appear to reflect inhibitory, excitatory and serotonergic lineages, respectively. *Gata3* expression has not been previously noted in the ENS, nor has the function of any of these transcription factors been previously determined during ENS development.

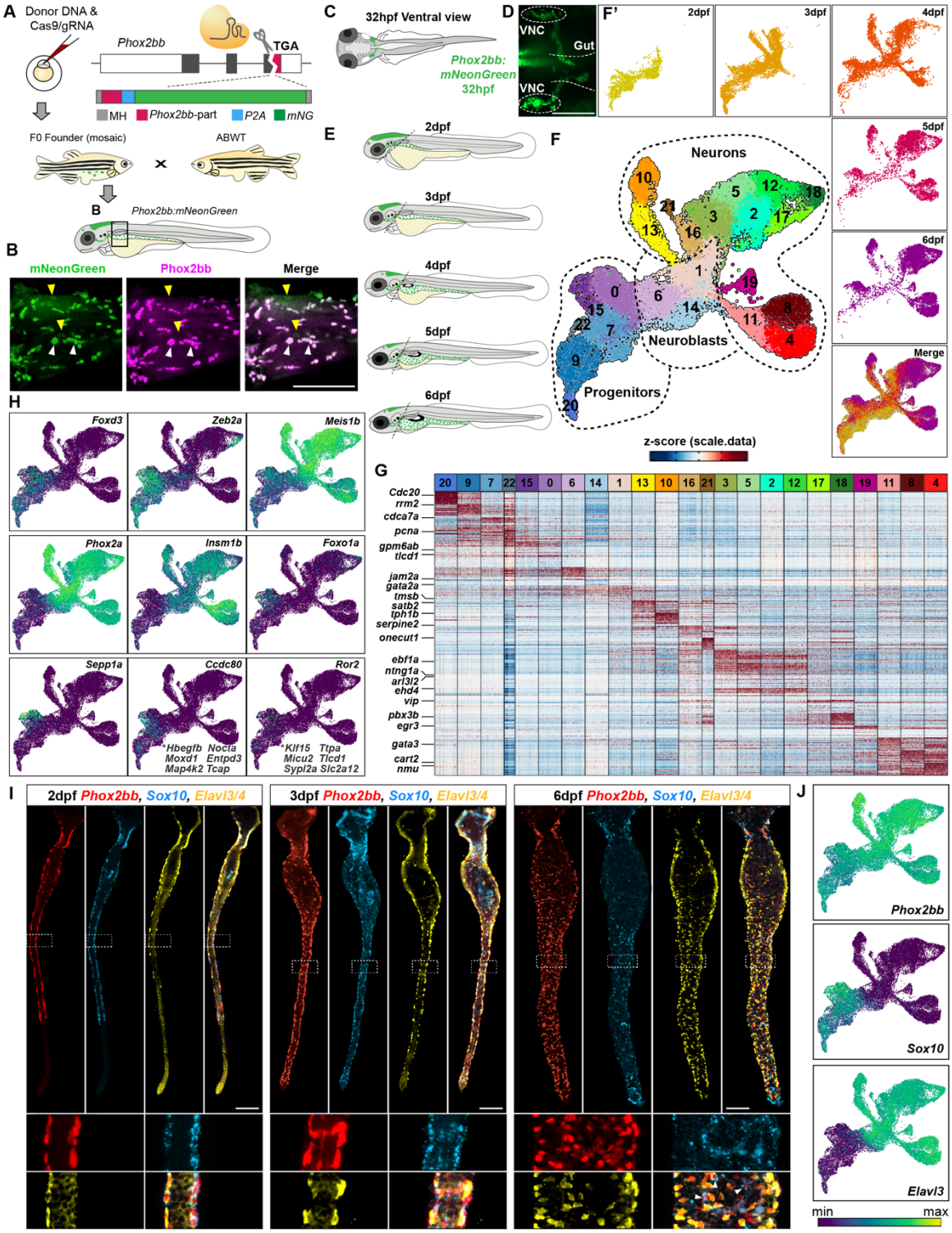

Figure 1: Single-cell transcriptome analysis reveals cell-type heterogeneity in zebrafish enteric nervous system during embryogenesis. (A) Schematic diagram showing strategy for generation of Tg(*Phox2bb*:*mNeonGreen*) fish through

microhomology-mediated end joining mechanism. **(B)** mNeonGreen and Phox2bb immunostaining colocalize in the foregut at 3dpf. White arrowheads indicate enteric neurons. Yellow arrowheads indicate autofluorescent cells in the green channel. **(C)** Schematics of vagal neural crest localization at 32 hpf. **(D)** Ventral view of vagal neural crest expressing mNeonGreen at 32 hpf. **(E)** Schematics showing site of dissection in embryos and larvae at 2-6 dpf. **(F, F')** UMAP plot of enteric neural cells colored by clusters and corresponding days in F'. **(G)** Heat map showing differentially expressed genes in each cluster. **(H)** UMAP plots of marker genes expressed in progenitors and neurons. *Genes display a similar expression pattern with the marker genes shown in corresponding plots. **(I)** Spatial expression of *Phox2bb*, *Sox10* and *Elavl3/4* at 2, 3 and 6 dpf revealing the distribution of enteric progenitors and neurons in the developing zebrafish gut imaged in whole mount. Dashed rectangles indicate areas enlarged below image. Arrowheads indicate progenitors co-expressing *Phox2bb* and *Sox10*. Samples were stained by HCR to reveal *Sox10* expression, then fixed and immunostained with anti-Phox2b and anti-HuC/D (Elavl3/4) antibodies. **(J)** UMAP plots of *Phox2bb*, *Sox10* and *Elavl3.* Scale bar: 100 um.

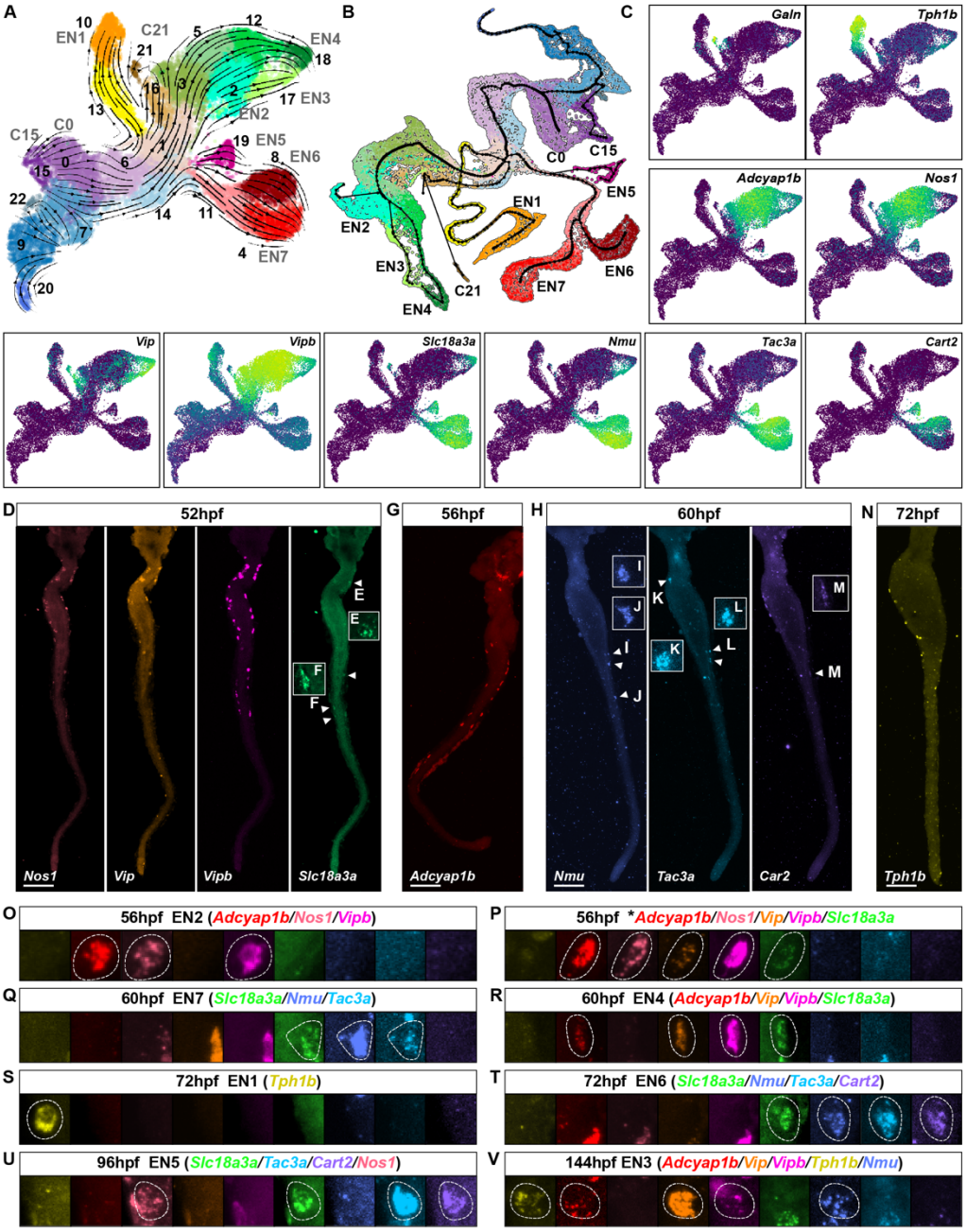

Figure 2: Single cell RNA-seq analysis reveals major subtypes of mature enteric neurons. **(A)** RNA velocity and **(B)** scFates single cell analysis shows the developmental trajectory of ENS neurons from progenitor root to mature neurons. **(C)** UMAP of highly expressed neurotransmitters, neuropeptide and related genes. **(D-N)** HCR images showing the expression of marker genes at different time points. Scale bar: 100 um. (**O-V**) Higher magnification of neuronal subtypes at different time points.

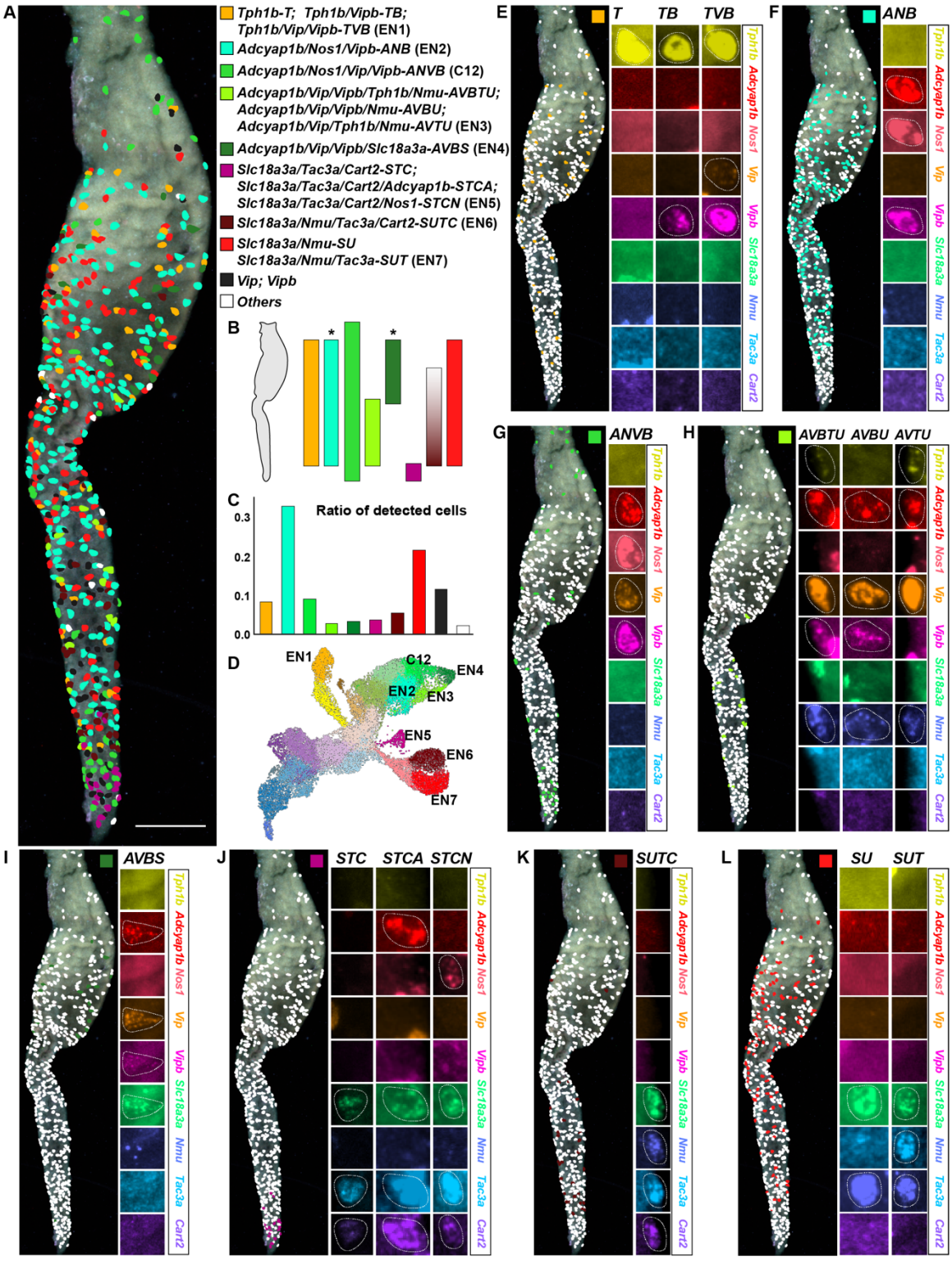

Figure 3: Spatial localization of specific ENS neuronal subtypes throughout the gut. (**A**) Color painting of ENS subtypes in the gut of a 6 dpf zebrafish. 9 neurotransmitter-related genes were identified in the same sample using sequential multiplex HCR.

Combinatorial expression of these 9 genes revealed several distinct neuronal subtypes. **(B)** Schematic showing the spatial distribution of specific ENS subtypes in the gut. **(C)** Ratio of number of cells per subtype relative to the entire population. **(D)** UMAP with colors corresponding to different types of ENS neurons subtypes revealed by HCR. **(E-L)** Spatial information of different types of ENS cells in the gut and average intensity projection images of 9 neurotransmitter-related genes in representative cells. *T*: *Tph1b*, *TB*: *Tph1b/Vipb*, *TVB*: *Tph1b/Vip/Vipb*, *ANB*: *Adcyap1b/Nos1/Vipb*, *ANVB*: *Adcyap1b/Nos1/Vip/Vipb*, *AVBTU*: *Adcyap1b/Vip/Vipb/Tph1b/Nmu*, *AVBU*: *Adcyap1b/Vip/Vipb/Nmu*, *AVTU*: *Adcyap1b/Vip/ Tph1b/Nmu*, *AVBS*: *Adcyap1b/Vip/Vipb/Slc18a3a*, *STC*: *Slc18a3a/Tac3a/Cart2*, *STCA*: *Slc18a3a/Tac3a/Cart2/Adcyap1b*, *STCN*: *Slc18a3a/Tac3a/Cart2/Nos1*, *SUTC*: *Slc18a3a/Nmu/Tac3a/Cart2*, *SU*: *Slc18a3a/Nmu*, *SUT*: *Slc18a3a/Nmu/Tac3a*. Scale bar: 100 um.

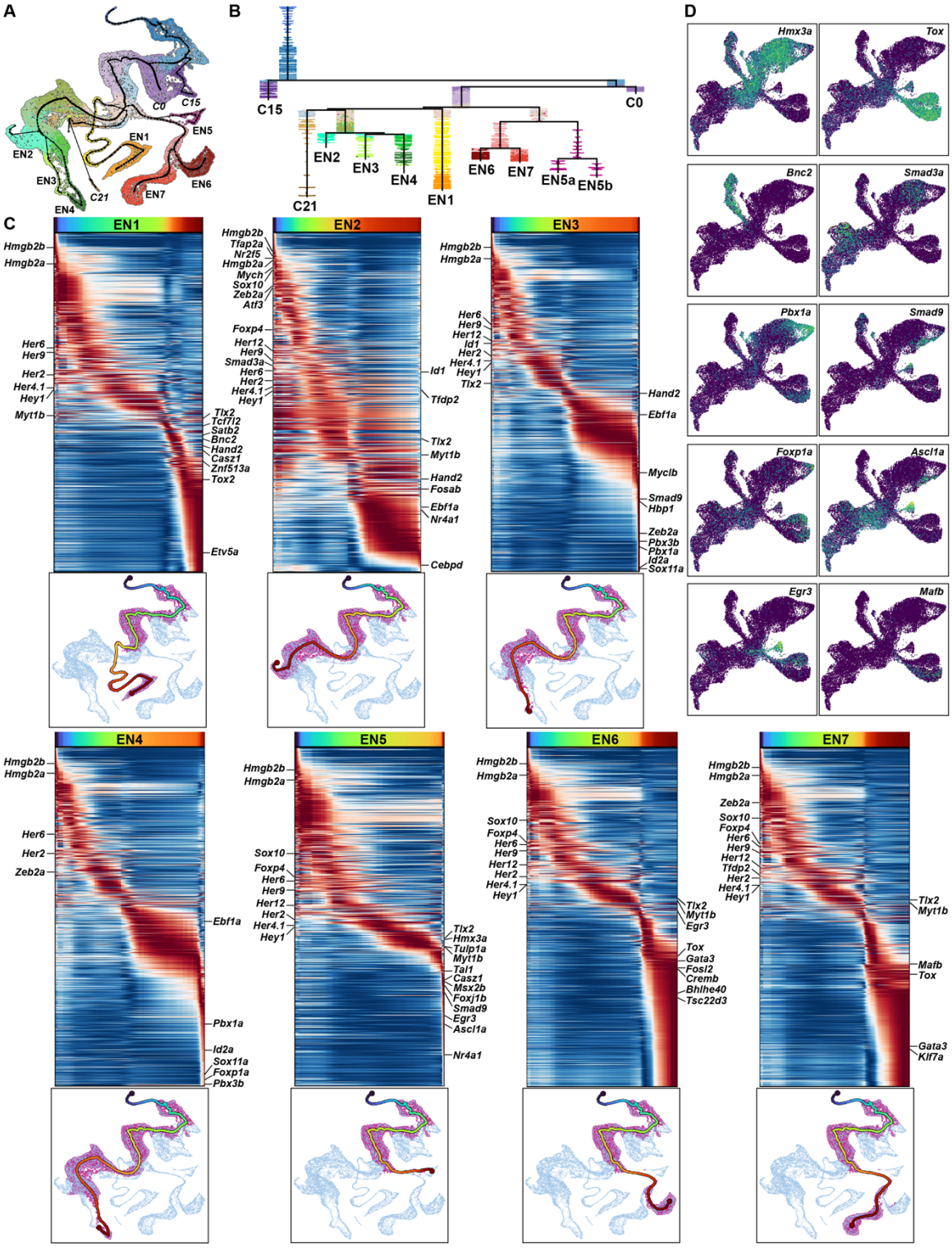

Figure 4: Developmental trajectory analysis reveals emergence of subtypes of ENS neurons. **(A)** scFates analysis shows lineage progression of ENS neurons from progenitor root to mature neuronal subtypes. **(B)** Dendrogram showing bifurcation of

lineage decisions during ENS development. **(C)** Heatmaps and UMAPs of EN1–EN7, highlighting representative transcription factors in each of the lineages. **(D)** UMAPs showing marker genes representative of different clusters.

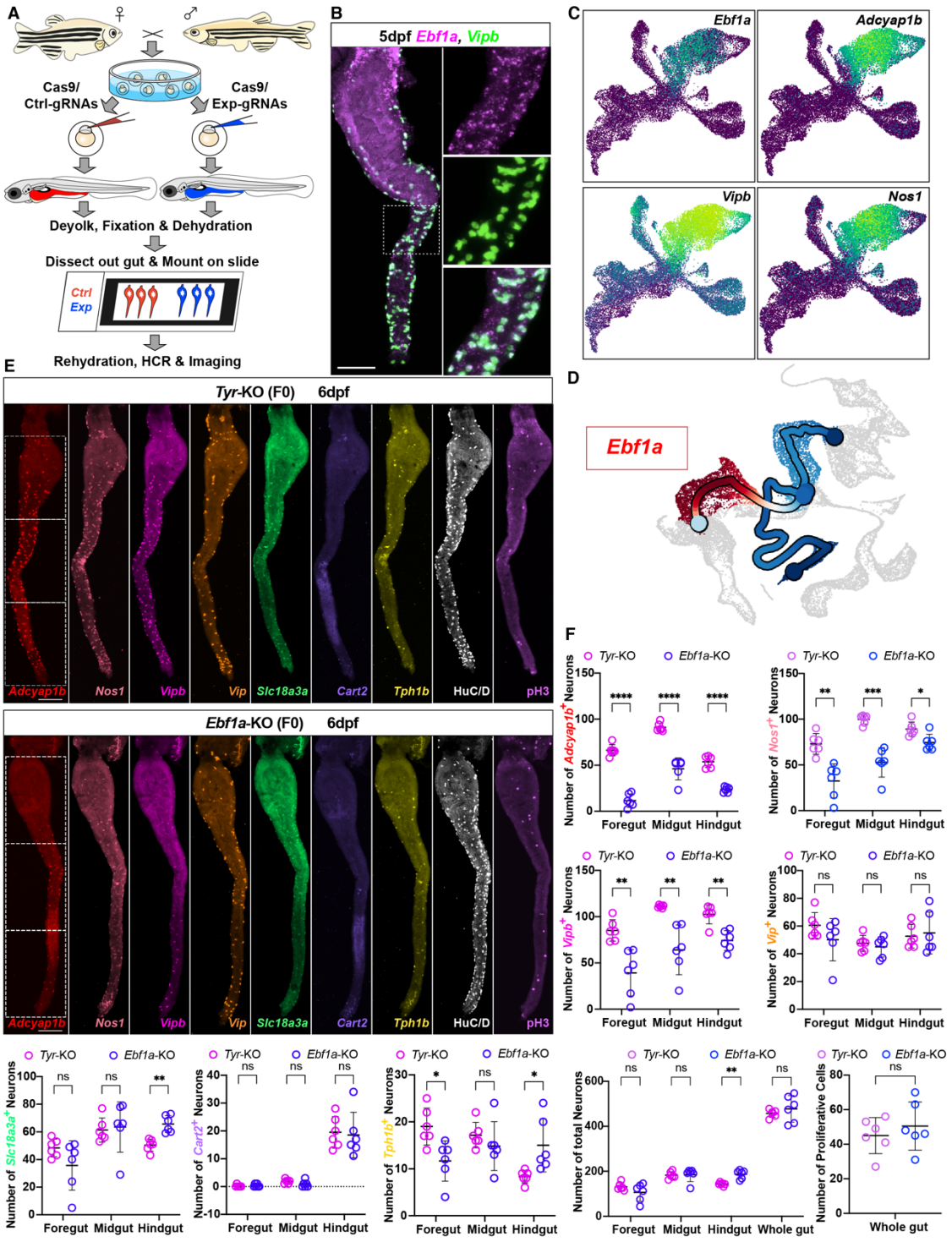

Figure 5: Expression and function of *Ebf1a* in the developing ENS. (A) Schematic diagram illustrating the perturbation approach. Briefly, Cas9 and 3 guide RNAs or control guide RNAs were injected into 1 cell stage embryos. The guts were dissected from sibling control and experimental embryos and processed by HCR. **(B)** Expression

pattern of *Ebf1a* and *Vipb* validated by HCR imaging. **(C)** UMAP of *Ebf1a* and other co-expressed marker genes. **(D)** Bifurcation analysis indicates that *Ebf1a* may be a key driver of cell fate decisions at the EN1 and EN2 transition. Quantitation of the numbers of neurons in foregut, midgut and hindgut reveals that loss of *Ebf1a* results in loss of *Nos1* and *Vipb* at all levels of the gut, but an increase in total neuron number in the hindgut. **(E, F)** HCR of neuropeptides and neurotransmitter genes and immunostaining of neuronal marker HuCD and proliferation marker PH3. Loss of *Ebf1a* causes loss of *nos1* and *vipb* without affecting other ENS markers. Scale bar: 100 um. The statistical analysis is performed with the software GraphPad Prism 10. ns: $P \geq 0.05$, *: $P < 0.05$, **: $P < 0.01$, ***: $P < 0.001$, ****: $P < 0.0001$.

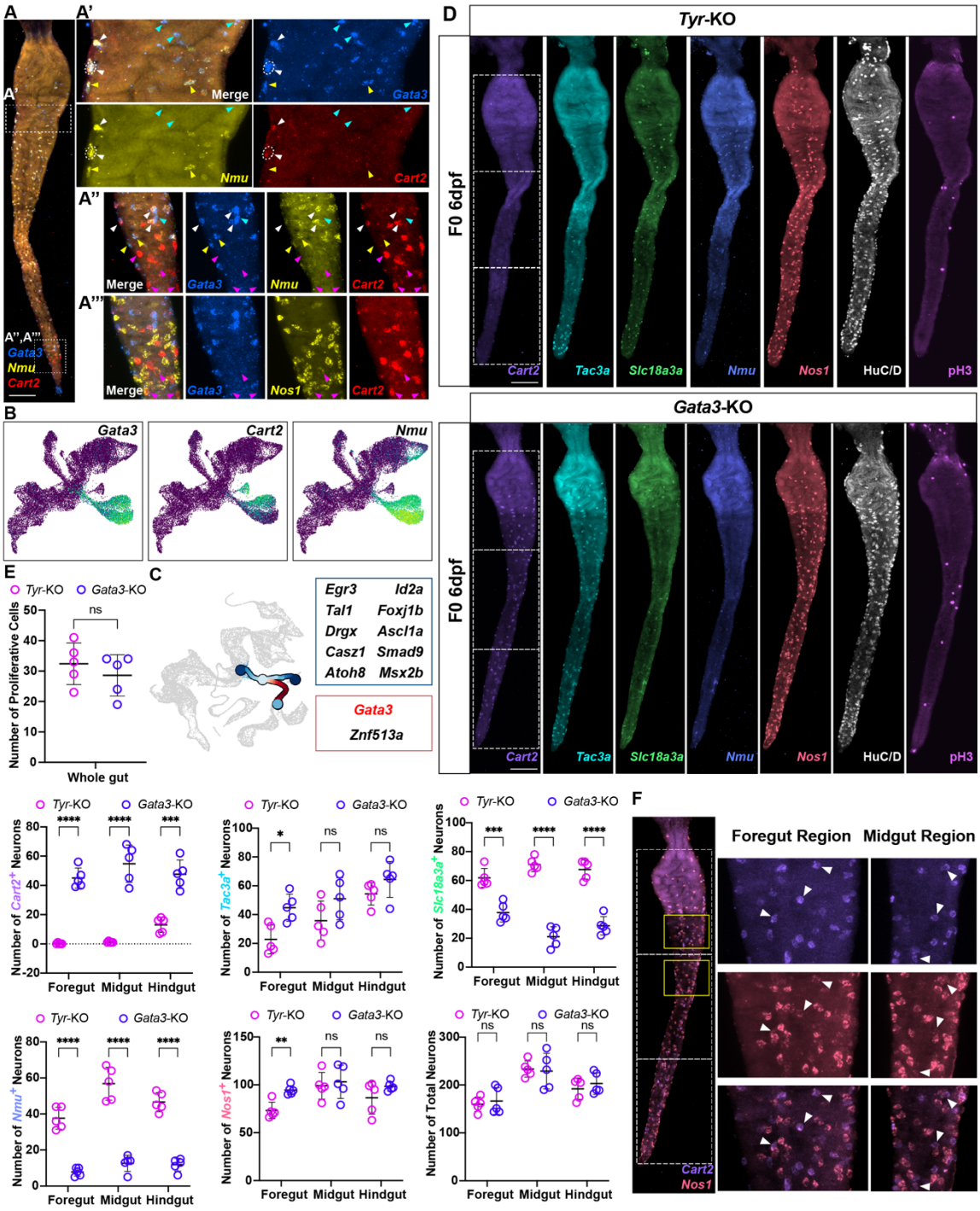

Figure 6: Expression and function of *Gata3* in the developing ENS. (A) Expression pattern of *gata3* and EN5, EN6 and EN7 markers *Nmu, Cart1* and *Nos1*. (A', A", A"' are higher magnification views) **(B)** UMAP of the *gata3* and other co-expressed marker genes. **(C)** *Gata3* is expressed in the bifurcation between EN5 and EN6/7. **(D)** HCR of neuropeptides and neurotransmitter genes and immunostaining of neuronal marker HuCD

and proliferation marker PH3. Loss of *Gata3* causes loss of *Nmu* and *Slc118a3a but* increases *cart2* expression without affecting other ENS markers. **(E)** Quantitation of the numbers of neurons in foregut, midgut and hindgut reveals that loss of *Gata3* results in loss of *Nmu* and *Slc118a3a* at all levels of the gut, while increasing *Cart2* throughout the gut. **(F)** Many *Cart2*+ cells detected in *Gata3*-KO embryos are *Cart2+/Nos1*+ cells, indicating they are likely to be EN5 cells. Scale bar: 100 um. The statistical analysis is performed with the software GraphPad Prism 10. ns: $P \geq 0.05$, *: $P < 0.05$, **: $P < 0.01$, ***: $P < 0.001$, ****: $P < 0.0001$.

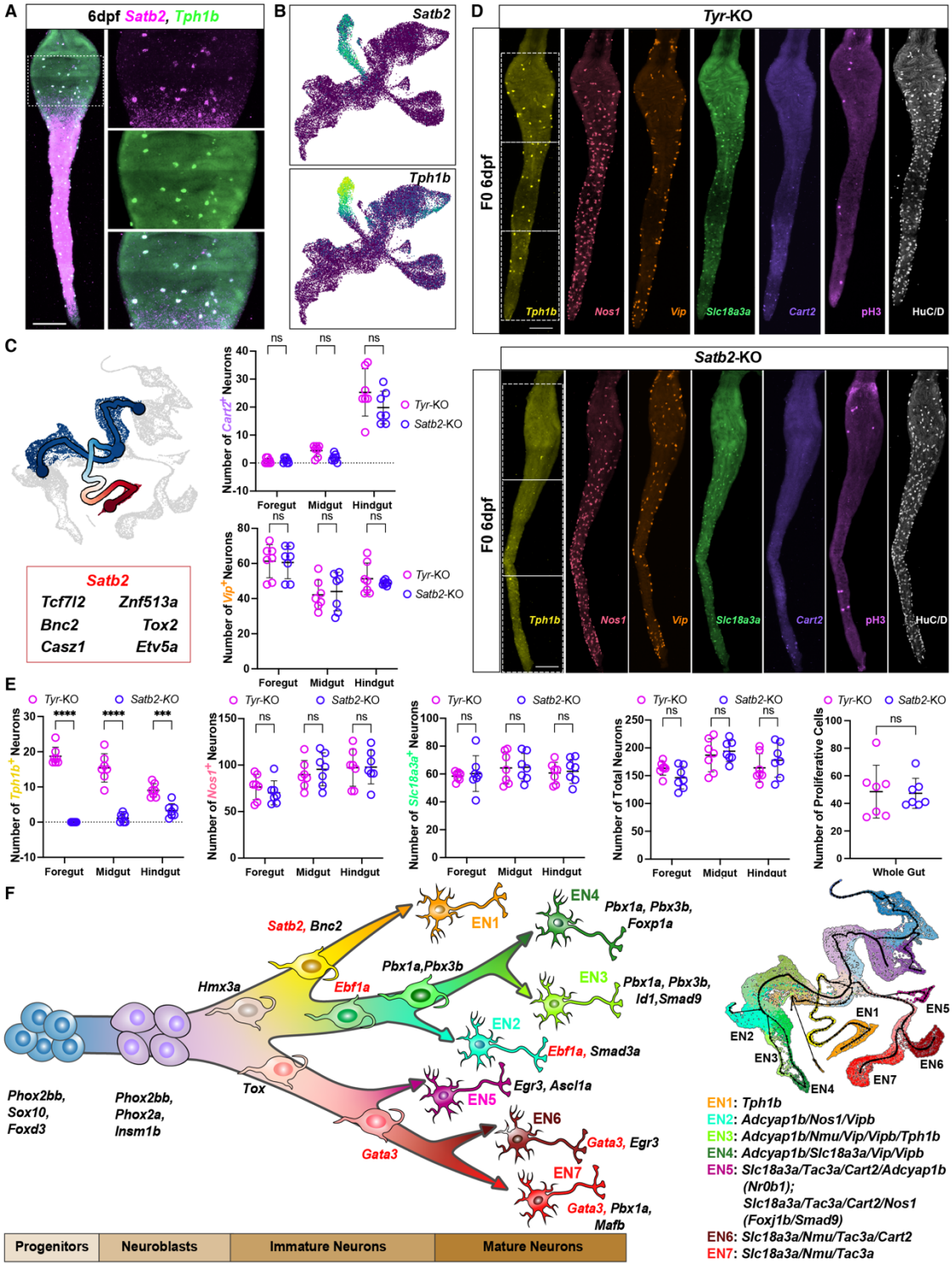

Figure 7: Expression and function of *Satb2* in the developing ENS. (A) Expression pattern of *Satb2* and *Tph1b*. **(B)** UMAP of the *Satb2* and *Tph1b* marker genes. **(C)** Bifurcation analysis indicates that *Satb2* is a potential driver of cell fate decisions during

the transition of the neuroblasts to EN1 and the common ancestors of EN2/3/4. **(D, E)** Quantification analysis of HCR imaging results of neuropeptides and neurotransmitter genes and immunostaining of neuronal marker HuCD and proliferation marker PH3. Loss of *Satb2* decreases the number of *Tph1b*-positive neurons, especially in the foregut and midgut. **(F)** Schematic diagram summarizing the developmental trajectory of zebrafish ENS neurons and revealing the transcription factors expressed in each neuronal subtype. Scale bar: 100 um. The statistical analysis is performed with the software GraphPad Prism 10. ns: $P \geq 0.05$, *: $P < 0.05$, **: $P < 0.01$, ***: $P < 0.001$, ****: $P < 0.0001$.

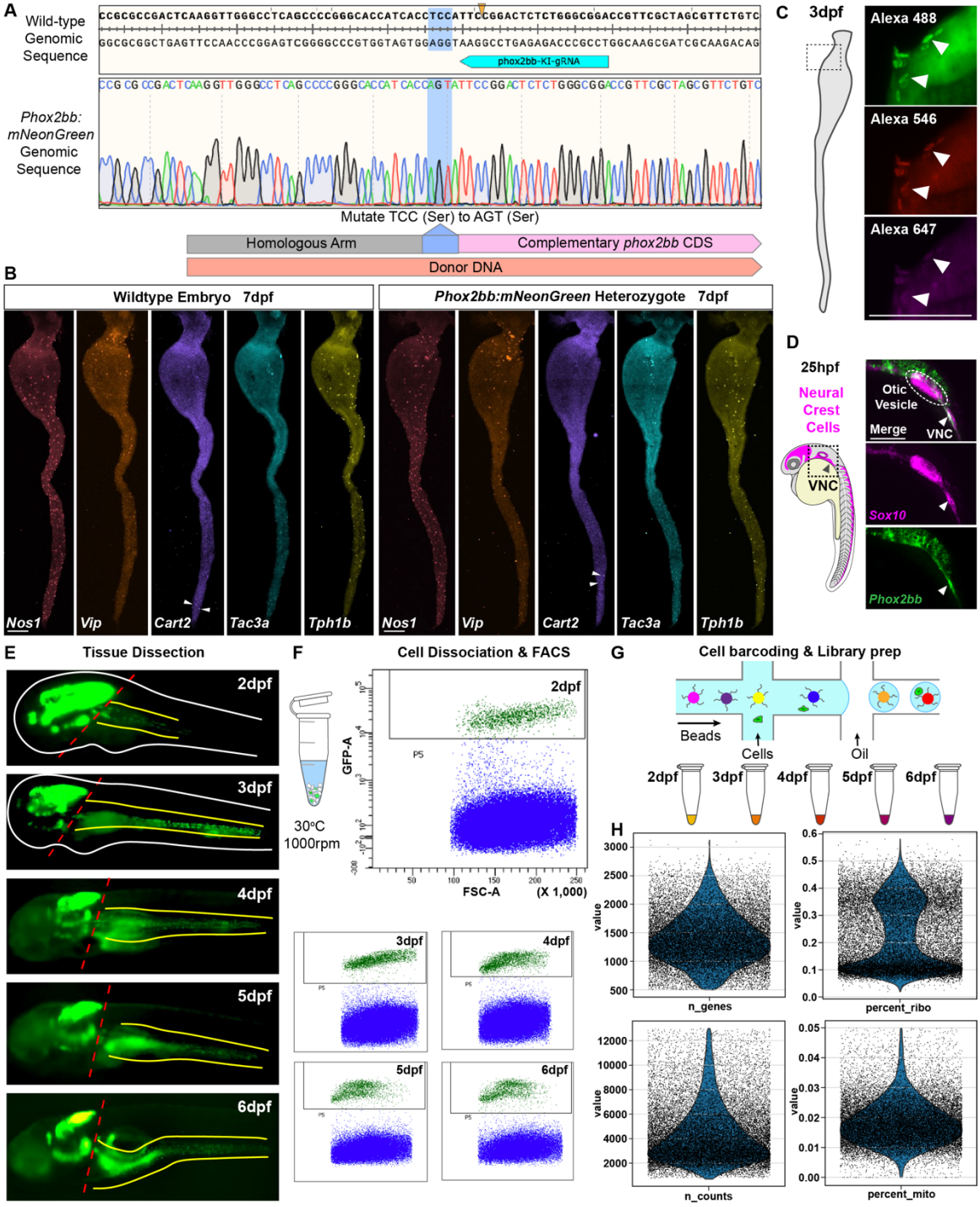

Figure 8: Validation of Tg(*Phox2bb:mNeonGreen*) line and experimental procedure for scRNA-seq of the developing ENS. (A) Genomic sequencing of a Tg(*Phox2bb:mNeonGreen*) fish showing the insertion of donor DNA into the genome with a synonymous mutation in the Serine coding region near the CRISPR/Cas9 cleavage

point. **(B)** Representative neuronal marker staining in wild type and *Phox2bb:mNeonGreen* heterozygotes at 7dpf. **(C)** Cells from adjacent tissues have strong autofluorescence. Wild-type intestinal tissue with no staining, as labeled in the schematic of zebrafish gut at 3 dpf shown on the left, was imaged using a confocal LSM 800 under 20X objective. These autofluorescent cells could be detected in three channels illuminated by the green (488 nm), red (561 nm) and far-red (640 nm) lasers, but the signals in the 640 nm channel was much weaker than those in the 488 nm channel. **(D)** Lateral view of a 25 hpf zebrafish embryo showing the localization of vagal neural crest determined by the co-expression of *Phox2bb* and *Sox10* in the post-otic region. **(E-G)** Experimental procedure of scRNA-seq analysis to explore ENS development. **(H)** Violin plots showing the quality control results of the scRNA-seq data and presenting the distribution of cells according to the number of genes (n_genes) and counts (n_counts), and the percentage of mitochondrial and ribosomal reads. Scale bar: 100 um.

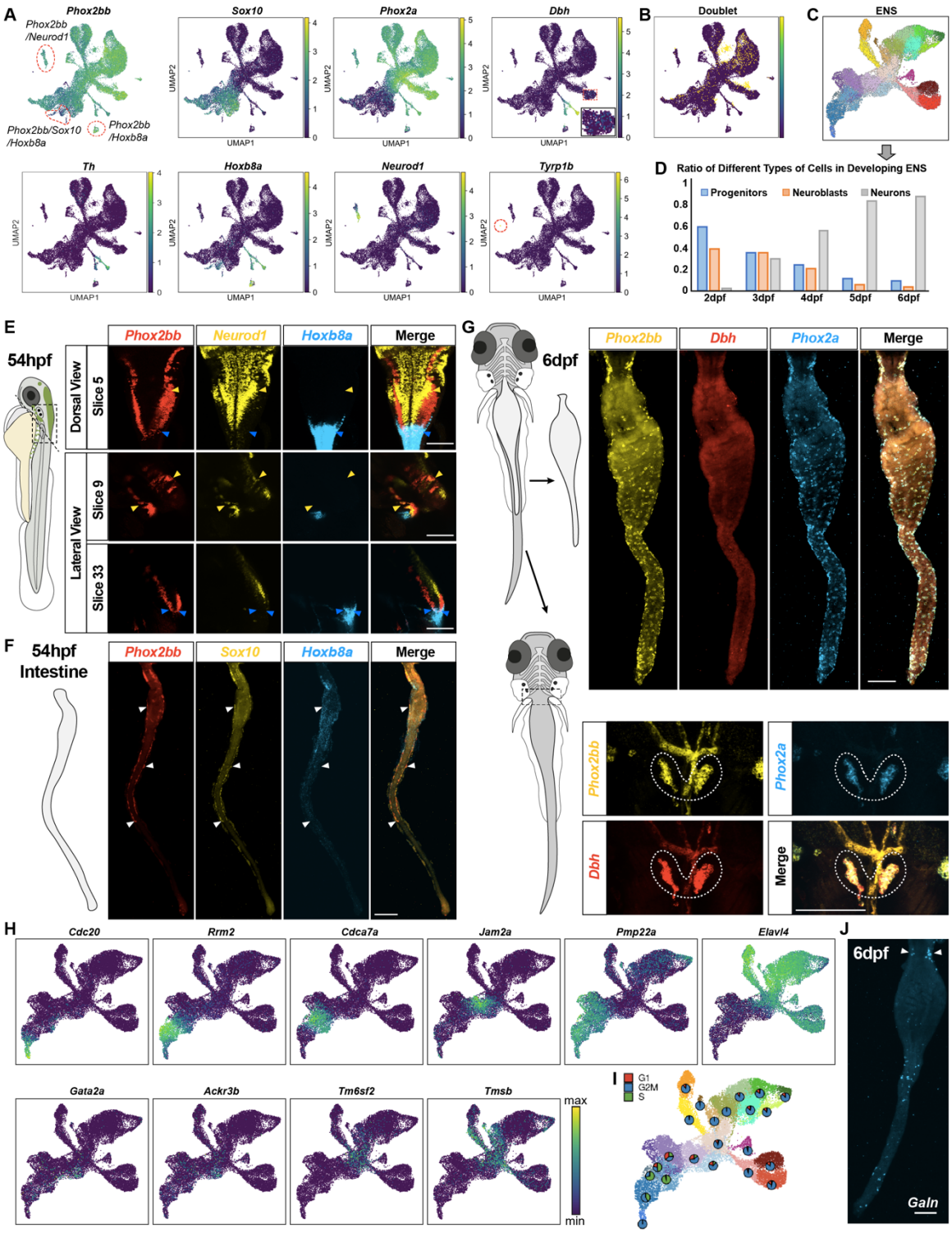

Figure 9: Validation of ENS versus non-ENS cells. (A) UMAP plots representing expression of marker genes. **(B)** UMAP plot showing doublets. **(C, D)** Ratio of different classes of ENS cells **(C)** at each developmental stage. **(E)** Marker genes used to

distinguish ENS (*Phox2bb*) cells from CNS, cranial ganglia (*Phox2bb, Hoxb8a*, *Neurod1)* and superior cervical ganglia (*Phox2bb, Dbh*). *Phox2bb/Hoxb8a* and *Phox2bb/Neurod1* double-positive cells in (A) are likely to be from CNS or cranial ganglia. **(F)** Expression of marker genes *Phox2bb*, *Sox10* and *Hoxb8a* in the gut. Arrowheads point to representative ENS progenitors (*Phox2bb/Sox10*). *Hoxb8a* likely expresses in the surrounding tissue, but not in ENS cells. The *Phox2bb/Sox10/Hoxb8a* cells in **(A)** are probably non-ENS cells derived from the neural crest, such as sympathetic neurons that express *Hoxb8* as previously reported[60]. Because these cells are in the post-otic region and express *Phox2bb*, they were captured after cell sorting. **(G)** Observation of marker genes *Phox2bb*, *Phox2a* and *Dbh* in the gut and the trunk. *Dbh* is present in the trunk sympathetic ganglia, but no high expression was noted in the gut. Scale bar: 100 um. (**H**) UMAP plot of marker genes. (**I**) Cell cycle phase of cells in each cluster. (**J**) *Galn* expression in the esophageal neurons.

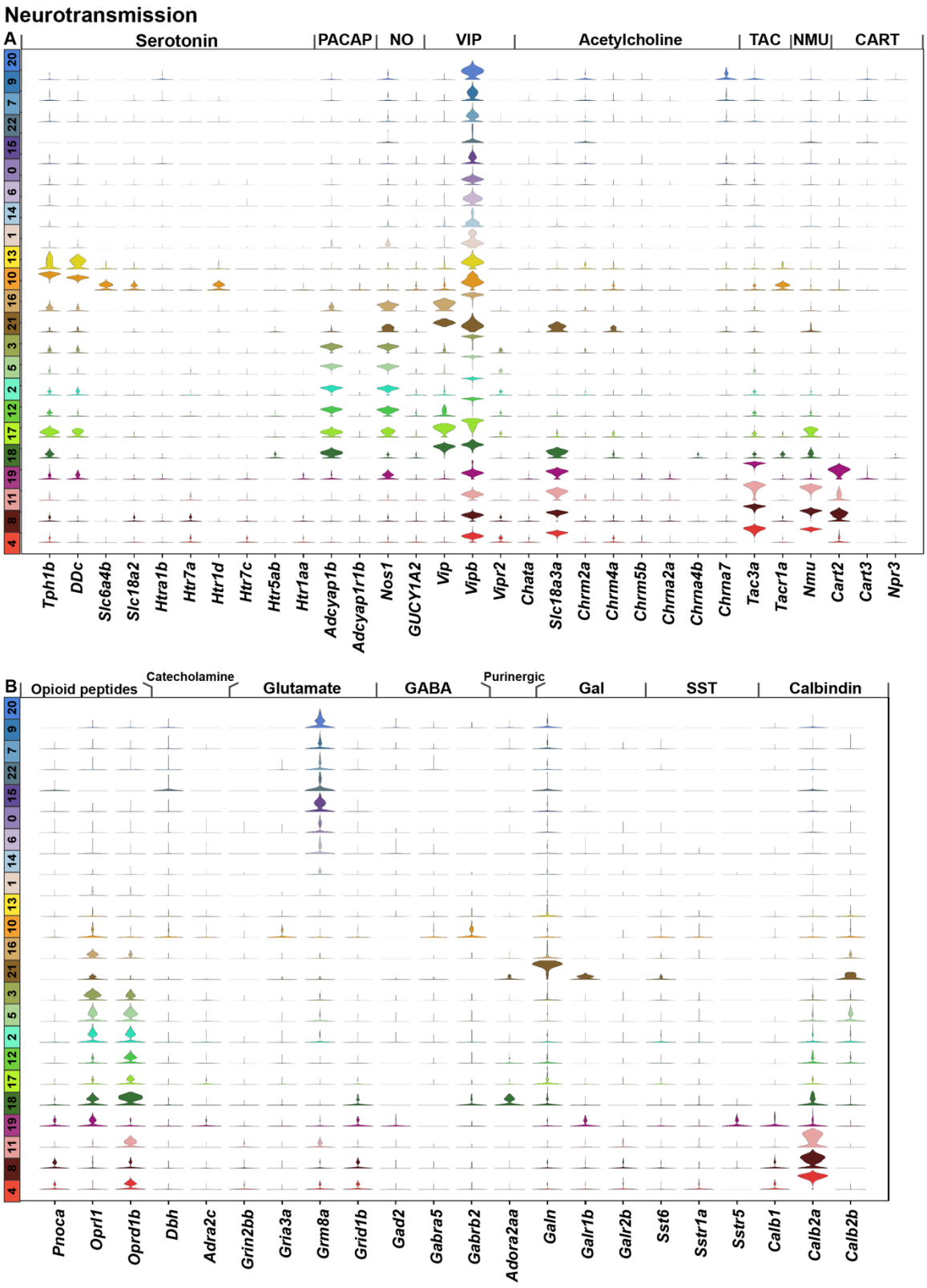
Neurotransmission
A
Serotonin
PACAP
NO
VIP
Acetylcholine
TAC
NMU
CART
Tph1b
DDc
Slc6a4b
Slc18a2
Htra1b
Htr7a
Htr1d
Htr7c
Htr5ab
Htr1aa
Adcyap1b
Adcyap1r1b
Nos1
GUCY1A2
Vip
Vipb
Vipr2
Chata
Slc18a3a
Chrm2a
Chrm4a
Chrm5b
Chrna2a
Chrna4b
Chrna7
Tac3a
Tacr1a
Nmu
Cart2
Cart3
Npr3
B
Opioid peptides
Catecholamine
Glutamate
GABA
Purinergic
Gal
SST
Calbindin
Pnoca
Oprl1
Oprd1b
Dbh
Adra2c
Grin2bb
Gria3a
Grm8a
Grid1b
Gad2
Gabra5
Gabrb2
Adora2aa
Galn
Galr1b
Galr2b
Sst6
Sstr1a
Sstr5
Calb1
Calb2a
Calb2b

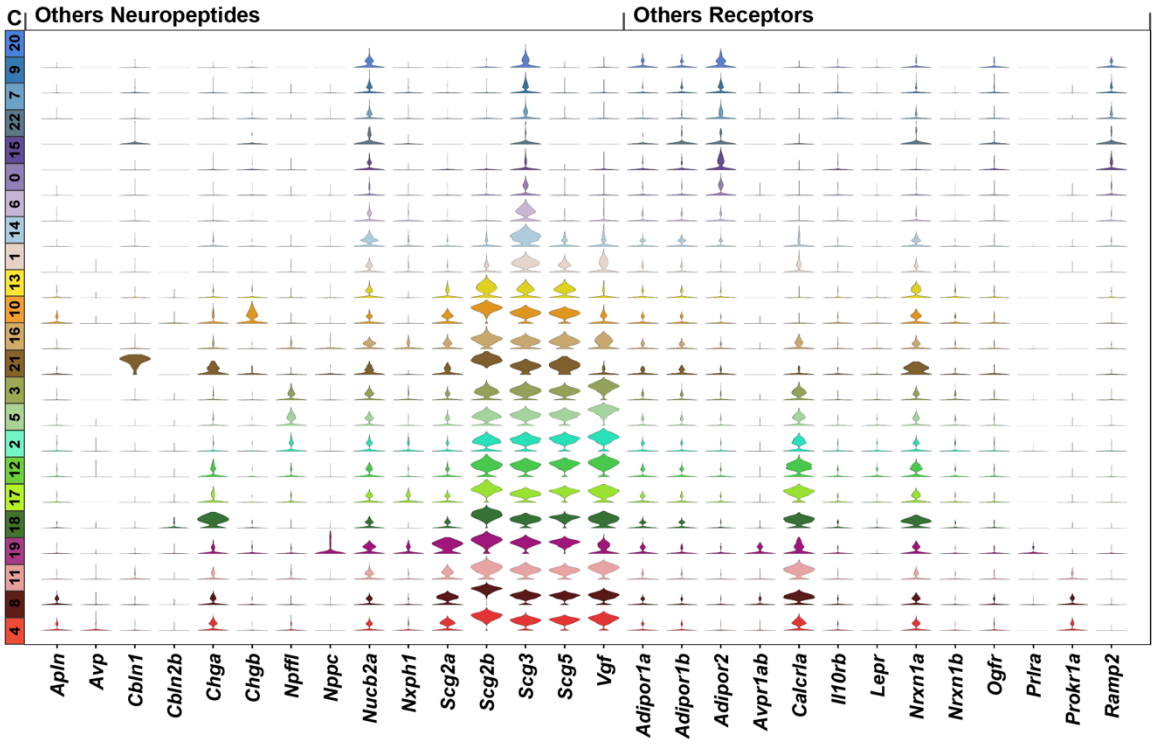
C
Others Neuropeptides
Others Receptors
20 9 7 22 15 0 6 14 1 13 10 16 21 3 5 2 12 17 18 19 11 8 4
Apln
Avp
Cbln1
Cbln2b
Chga
Chgb
Npffl
Nppc
Nucb2a
Nxph1
Scg2a
Scg2b
Scg3
Scg5
Vgf
Adipor1a
Adipor1b
Adipor2
Avpr1ab
Calcrla
Il10rb
Lepr
Nrxn1a
Nrxn1b
Ogfr
Prlra
Prokr1a
Ramp2

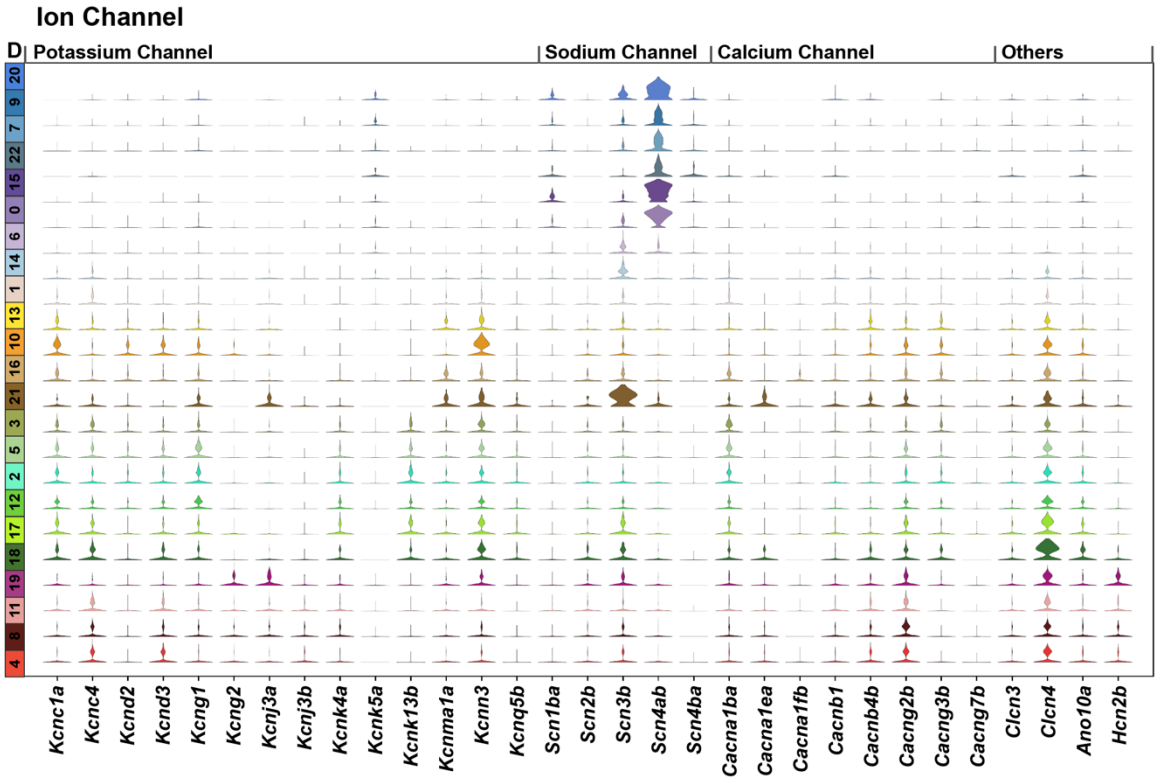
Ion Channel
D
Potassium Channel
Sodium Channel
Calcium Channel
Others
20 9 7 22 15 0 6 14 1 13 10 16 21 3 5 2 12 17 18 19 11 8 4
Kcnc1a
Kcnc4
Kcnd2
Kcnd3
Kcng1
Kcng2
Kcnj3a
Kcnj3b
Kcnk4a
Kcnk5a
Kcnk13b
Kcnma1a
Kcnn3
Kcnq5b
Scn1ba
Scn2b
Scn3b
Scn4ab
Scn4ba
Cacna1ba
Cacna1ea
Cacna1fb
Cacnb1
Cacnb4b
Cacng2b
Cacng3b
Cacng7b
Clcn3
Clcn4
Ano10a
Hcn2b

Signaling Molecules

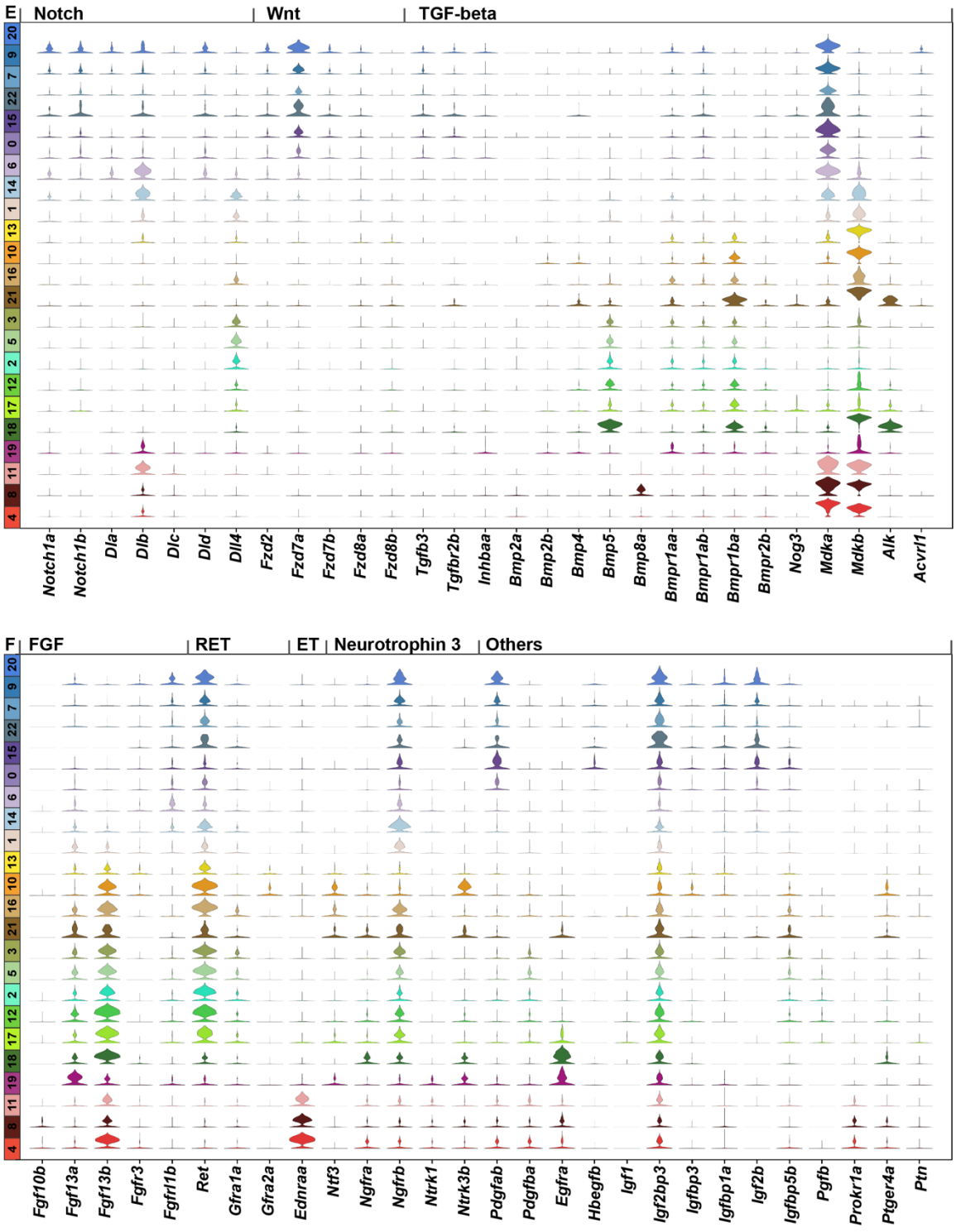

Membrane Trafficking

G

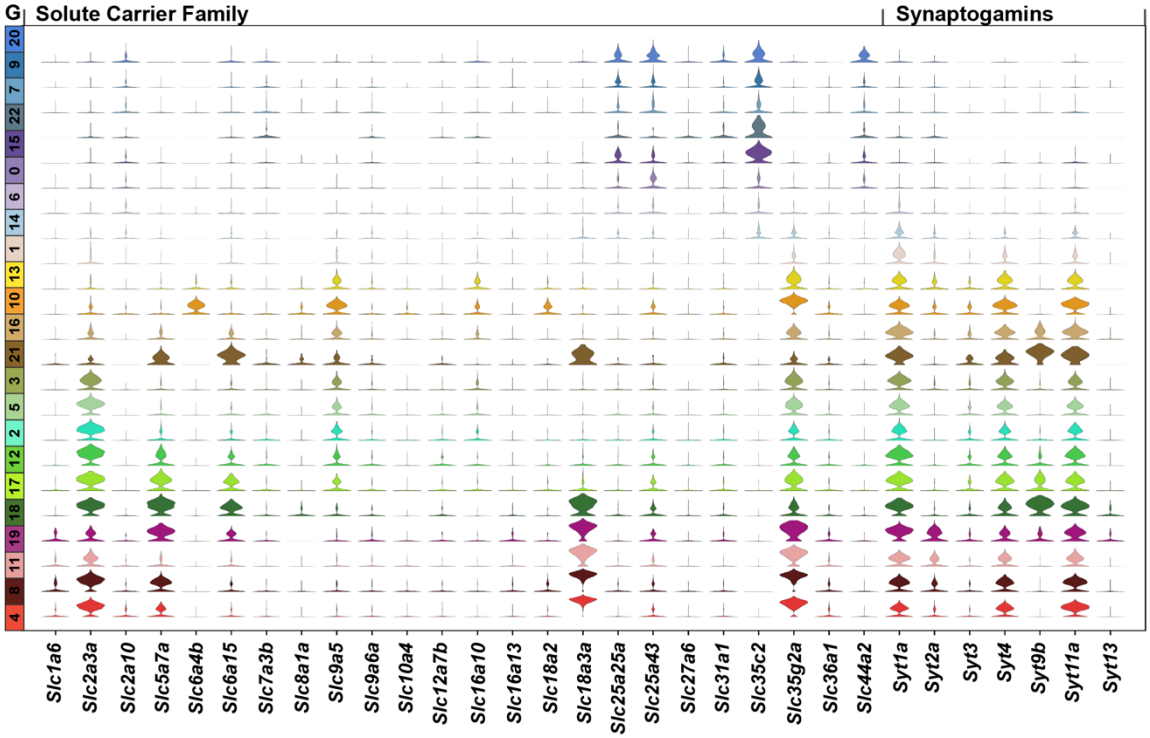

Transcription Factors

H

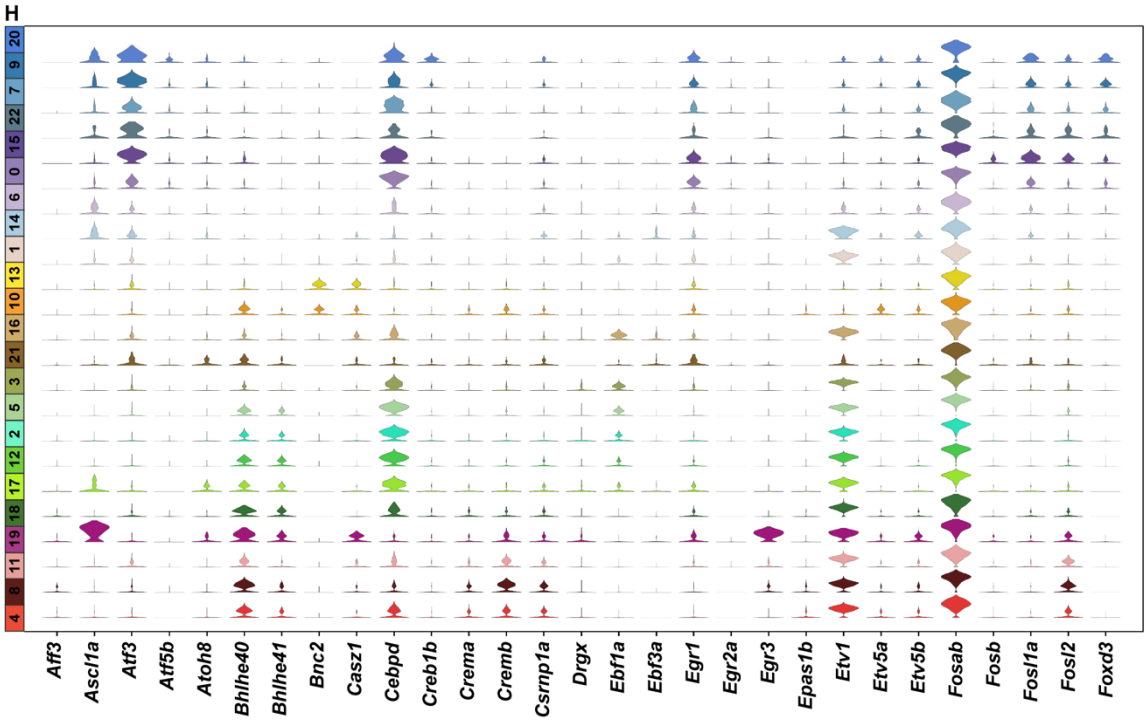

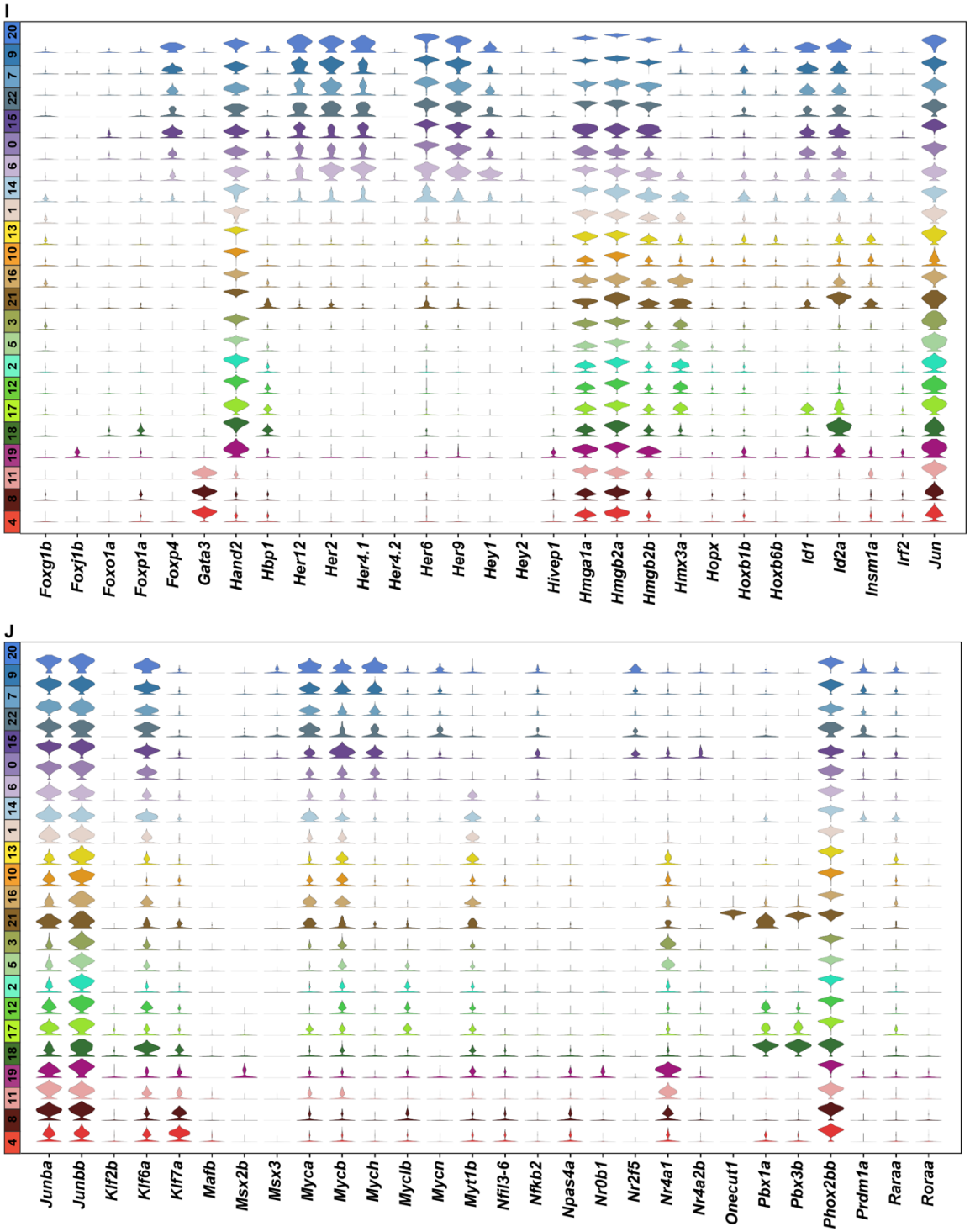
I
J
Foxg1b
Foxj1b
Foxo1a
Foxp1a
Foxp4
Gata3
Hand2
Hbp1
Her12
Her2
Her4.1
Her4.2
Her6
Her9
Hey1
Hey2
Hivep1
Hmga1a
Hmgb2a
Hmgb2b
Hmx3a
Hopx
Hoxb1b
Hoxb6b
Id1
Id2a
Insm1a
Irf2
Jun
Junba
Junbb
Klf2b
Klf6a
Klf7a
Mafb
Msx2b
Msx3
Myca
Mycb
Mych
Myclb
Mycn
Myt1b
Nfil3-6
Nfkb2
Npas4a
Nr0b1
Nr2f5
Nr4a1
Nr4a2b
Onecut1
Pbx1a
Pbx3b
Phox2bb
Prdm1a
Raraa
Roraa

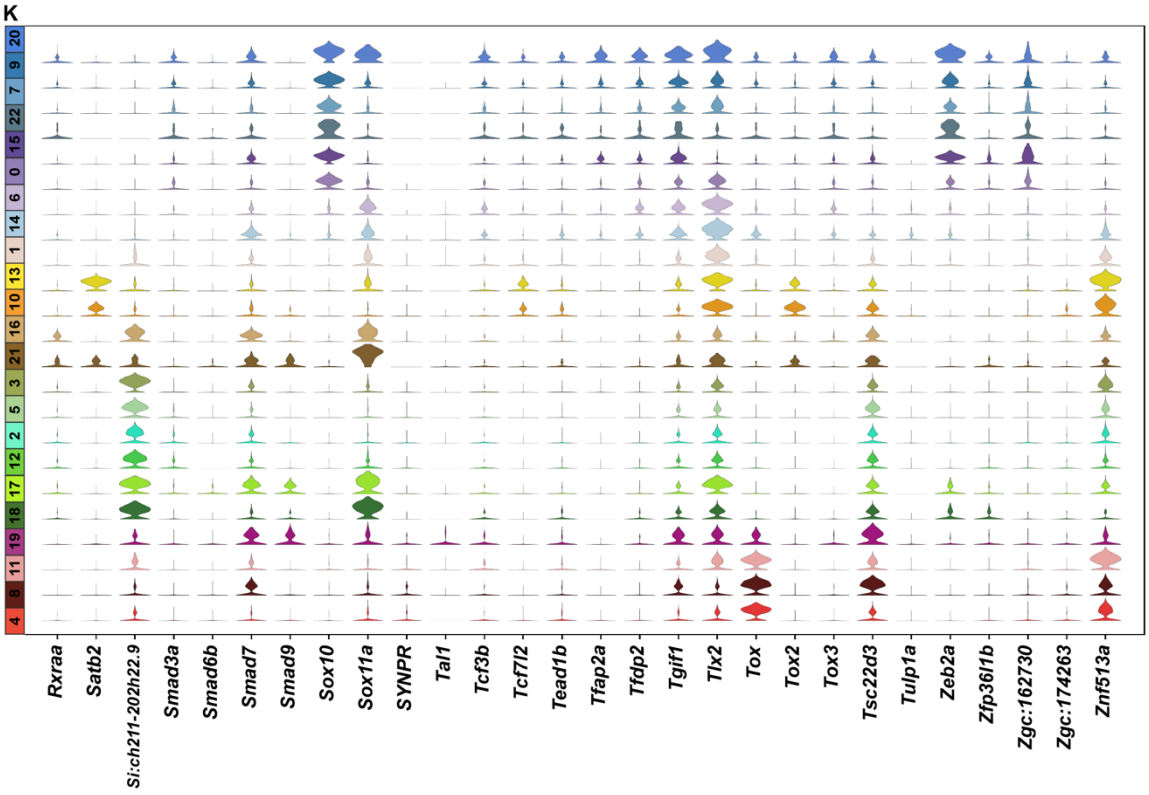

Marker Genes

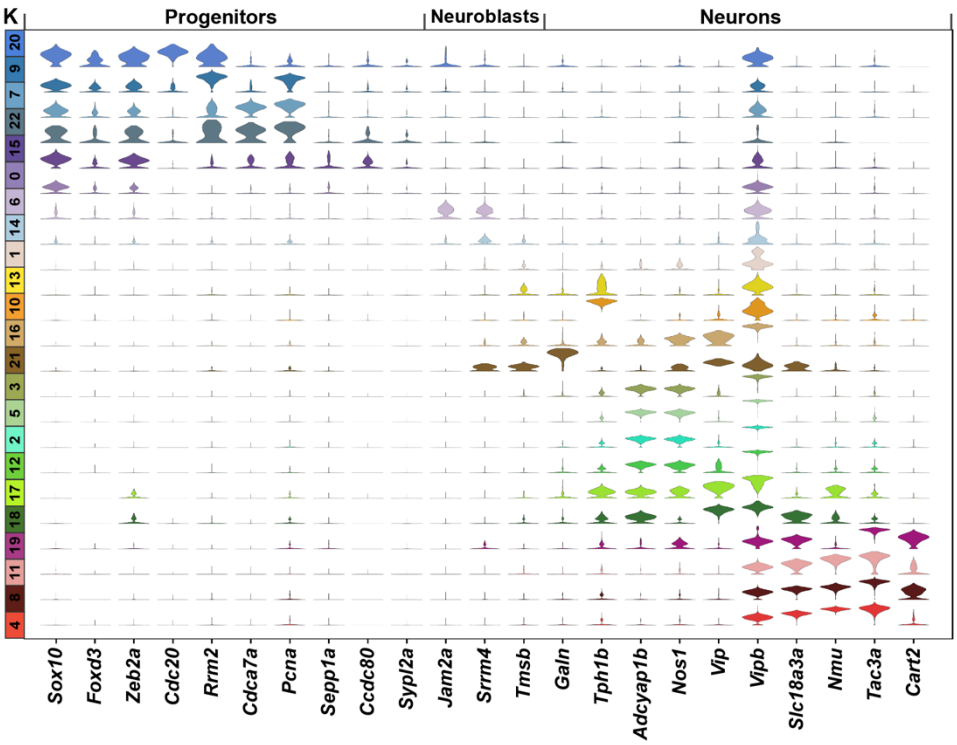

Figure 10: Violin plot displaying the expression of genes involved in neurotransmission and membrane trafficking; genes encoding ion channels, signaling molecules, and transcription factors; and genes marking ENS progenitors, neuroblasts, and neurons.

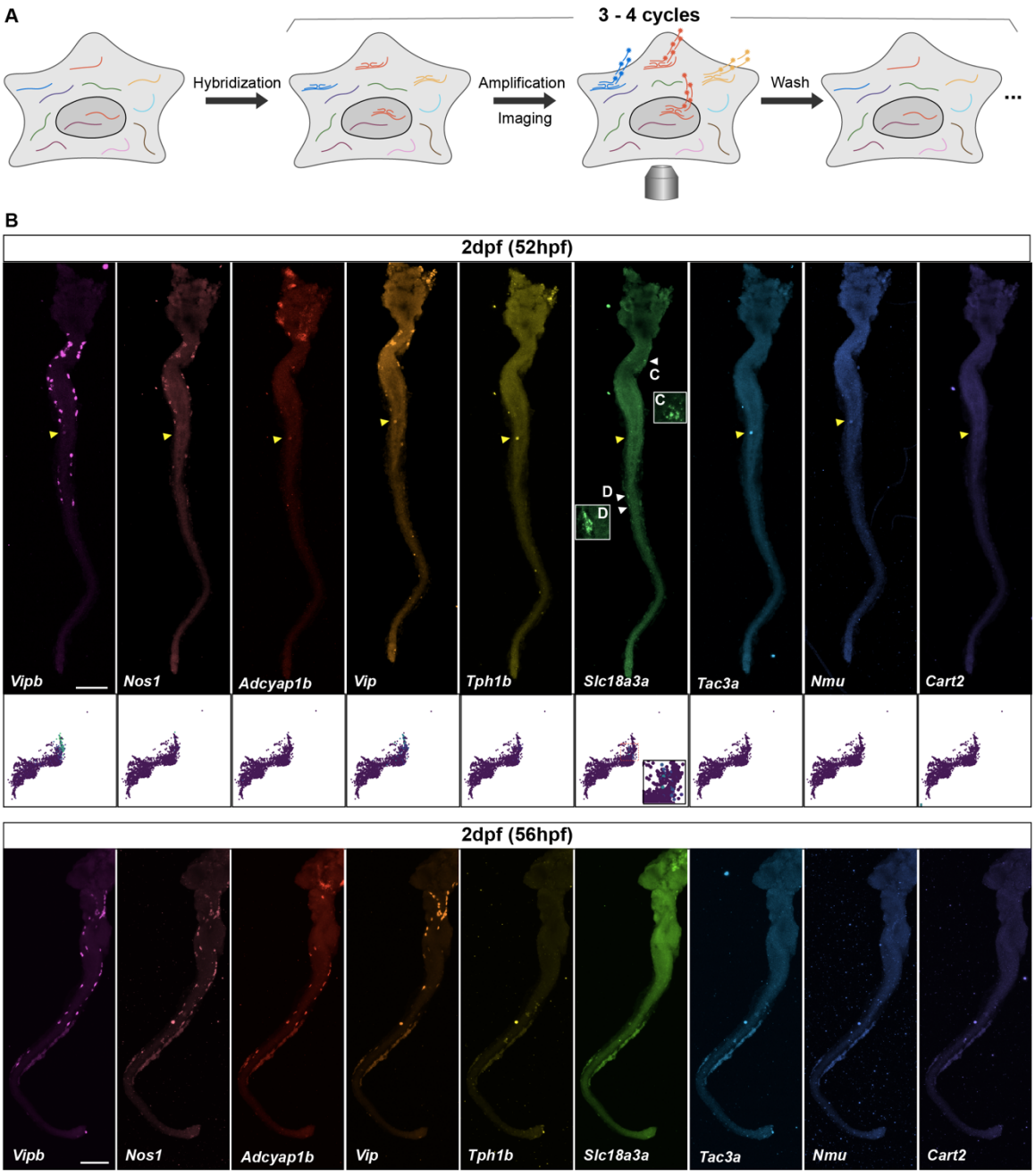
A
3 - 4 cycles
Hybridization
Amplification
Imaging
Wash
...
B
2dpf (52hpf)
Vipb
Nos1
Adcyap1b
Vip
Tph1b
Slc18a3a
Tac3a
Nmu
Cart2
C
D
2dpf (56hpf)

E

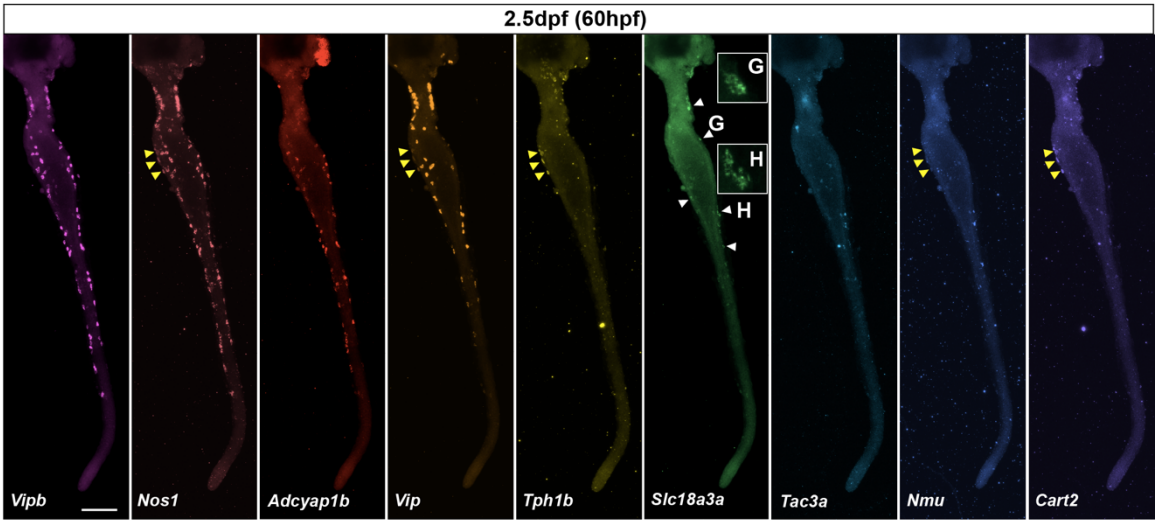
2.5dpf (60hpf)
G
G
H
H
Vipb
Nos1
Adcyap1b
Vip
Tph1b
Slc18a3a
Tac3a
Nmu
Cart2

F

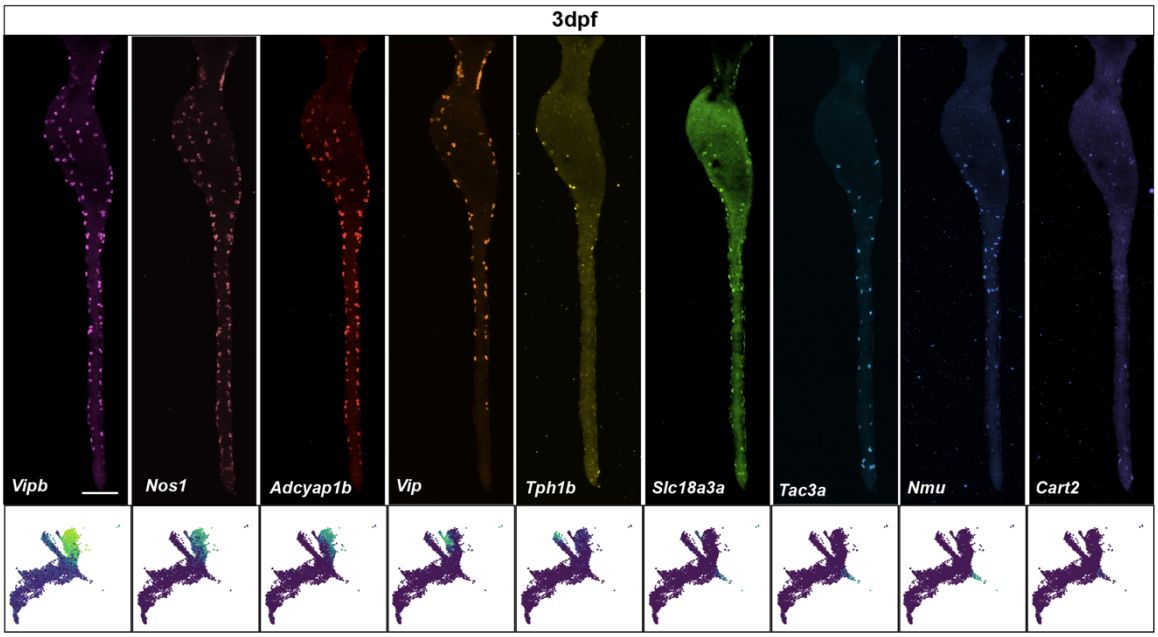
3dpf
Vipb
Nos1
Adcyap1b
Vip
Tph1b
Slc18a3a
Tac3a
Nmu
Cart2

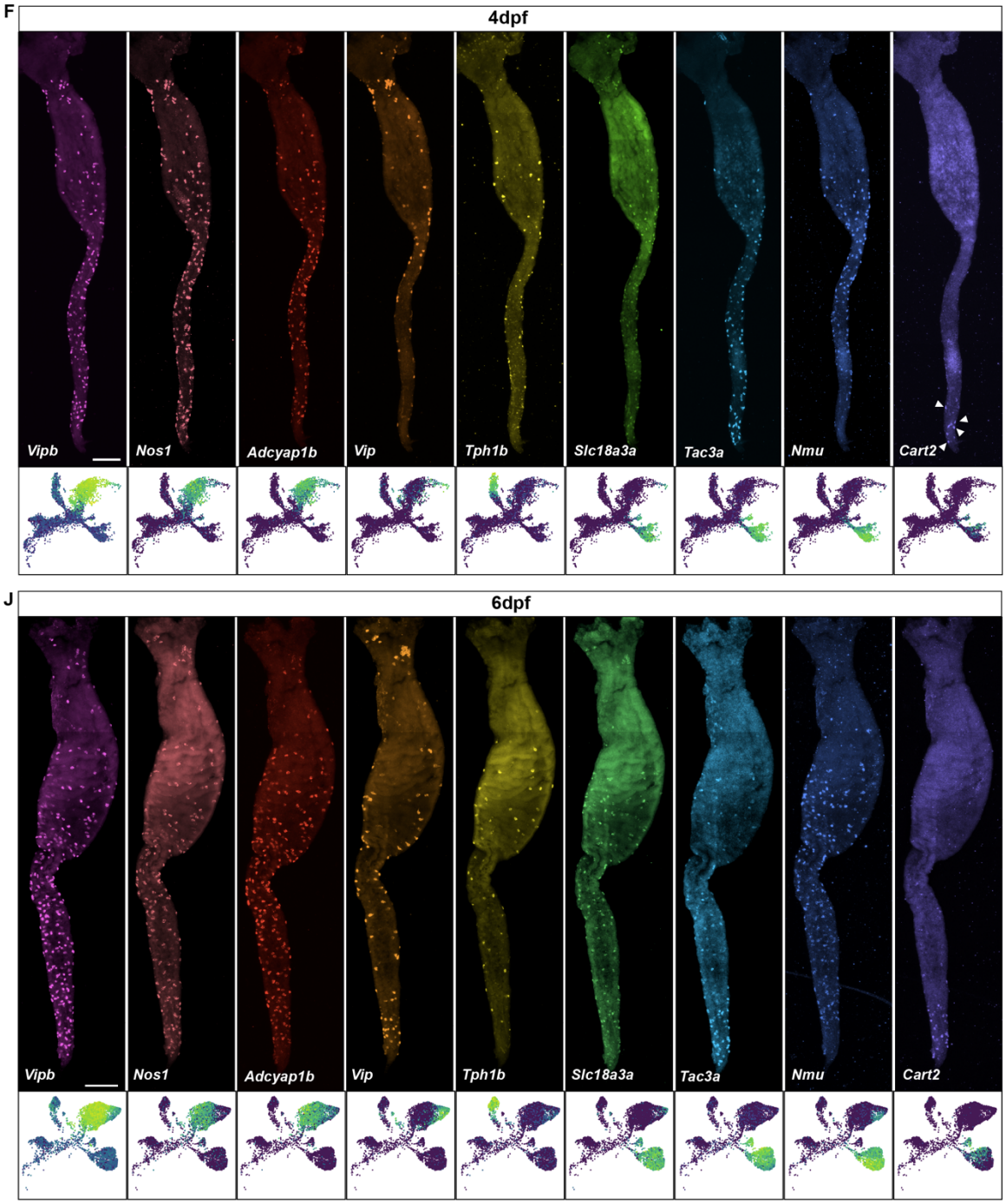

Figure 11: Spatiotemporal expression of multiple marker genes in one sample revealed by sequential HCR. (A) Schematic showing the procedure of sequential HCR. After performing one round of HCR, the sample is washed with formamide to remove the probes and hairpins. Then the sample receives the next round of HCR staining. **(B-J)**

Images and UMAP plots showing the expression of marker genes at different time points. Scale bars: 100 um.

* To ensure accurate comparison, the scale of gene expression for a given gene in the UMAP plots was standardized across all the time points.

*White arrowheads point out specific cells and yellow arrowheads indicate autofluorescent dots in the samples.

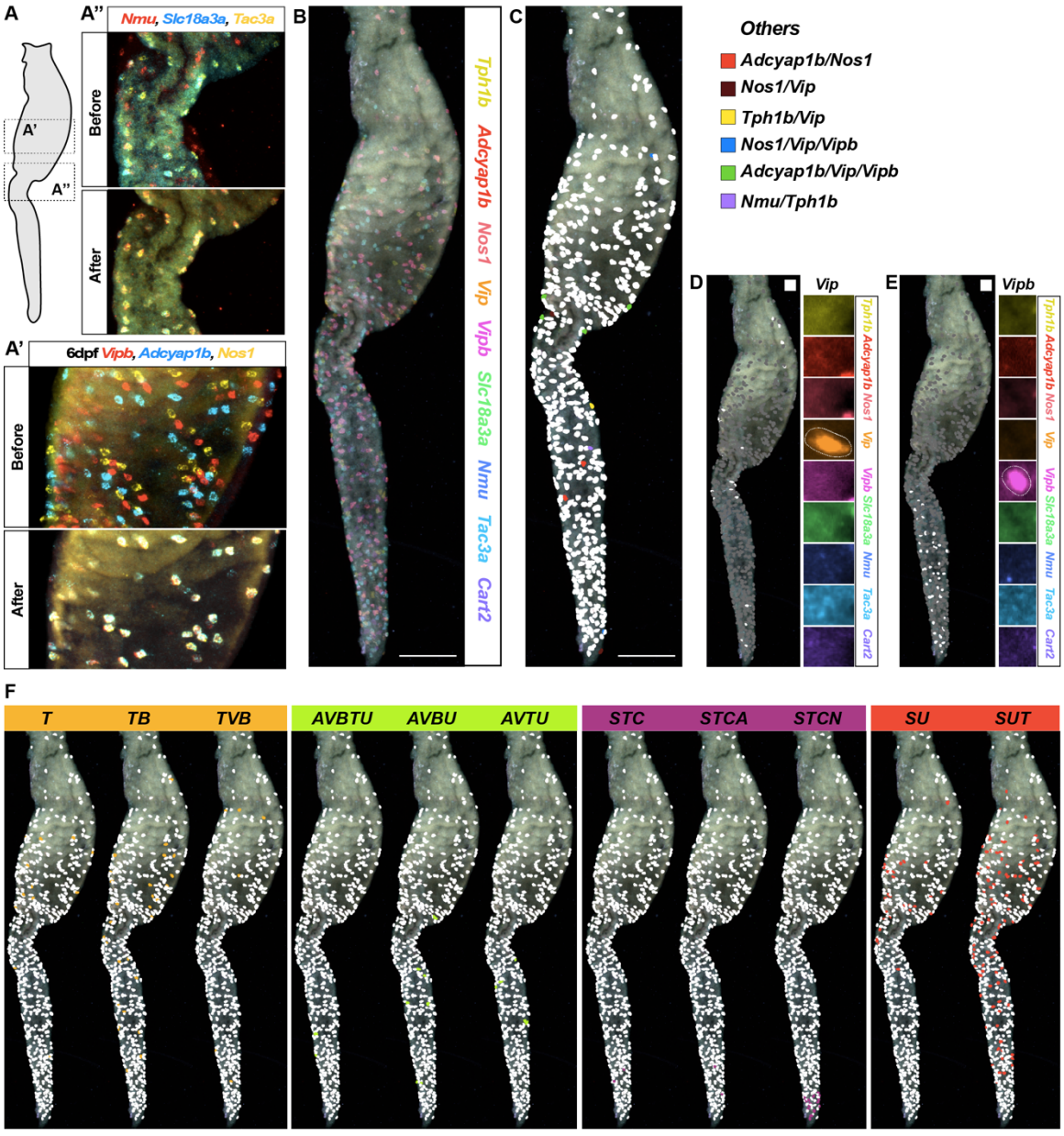

Figure 12: Merged images of 9 neurotransmitter-related genes. (A) Using ImageJ plugins—Template Matching and Image Stabilizer to merge images from different HCR-staining and imaging cycles. During the imaging phase, we collected 4 tiles in x-y plane and ~20 slices along z direction to cover the signals in the whole gut. For each gene, we first used average intensity projection to compress the raw data into a single image. Images from different imaging cycles inevitably have displacement in the x-y plane. Therefore, we used Template Matching and Image Stabilizer plugins to correct the deviations. After this correction, the same cells in different focal planes could merge. **(B)**

Processed image showing the expression of 9 genes simultaneously. Scale bars: 100 μm. **(C)** Spatial distribution of rare types of cells collectively named "Others." Cells occupying less than 1% (number < 5) of all the analyzed ENS cells are combined and named "Others." **(D, E)** Distribution of *Vip* and *Vipb* subtypes of neurons within each cluster in the gut. (**F**) Distribution of subtypes of neurons throughout the gut. *T*: *Tph1b*, *TB*: *Tph1b/Vipb*, *TVB*: *Tph1b/Vip/Vipb*, *AVBTU*: *Adcyap1b/Vip/Vipb/Tph1b/Nmu*, *AVBU*: *Adcyap1b/Vip/ Vipb/Nmu*, *AVTU*: *Adcyap1b/Vip/Tph1b/Nmu*, *STC*: *Slc18a3a/Tac3a/Cart2*, *STCA*: *Slc18a3a/Tac3a/Cart2/Adcyap1b*, *STCN*: *Slc18a3a/Tac3a/Cart2/Nos1*, *SU*: *Slc18a3a/ Nmu*, *SUT*: *Slc18a3a/Nmu/Tac3a*. Scale bars: 100 um.

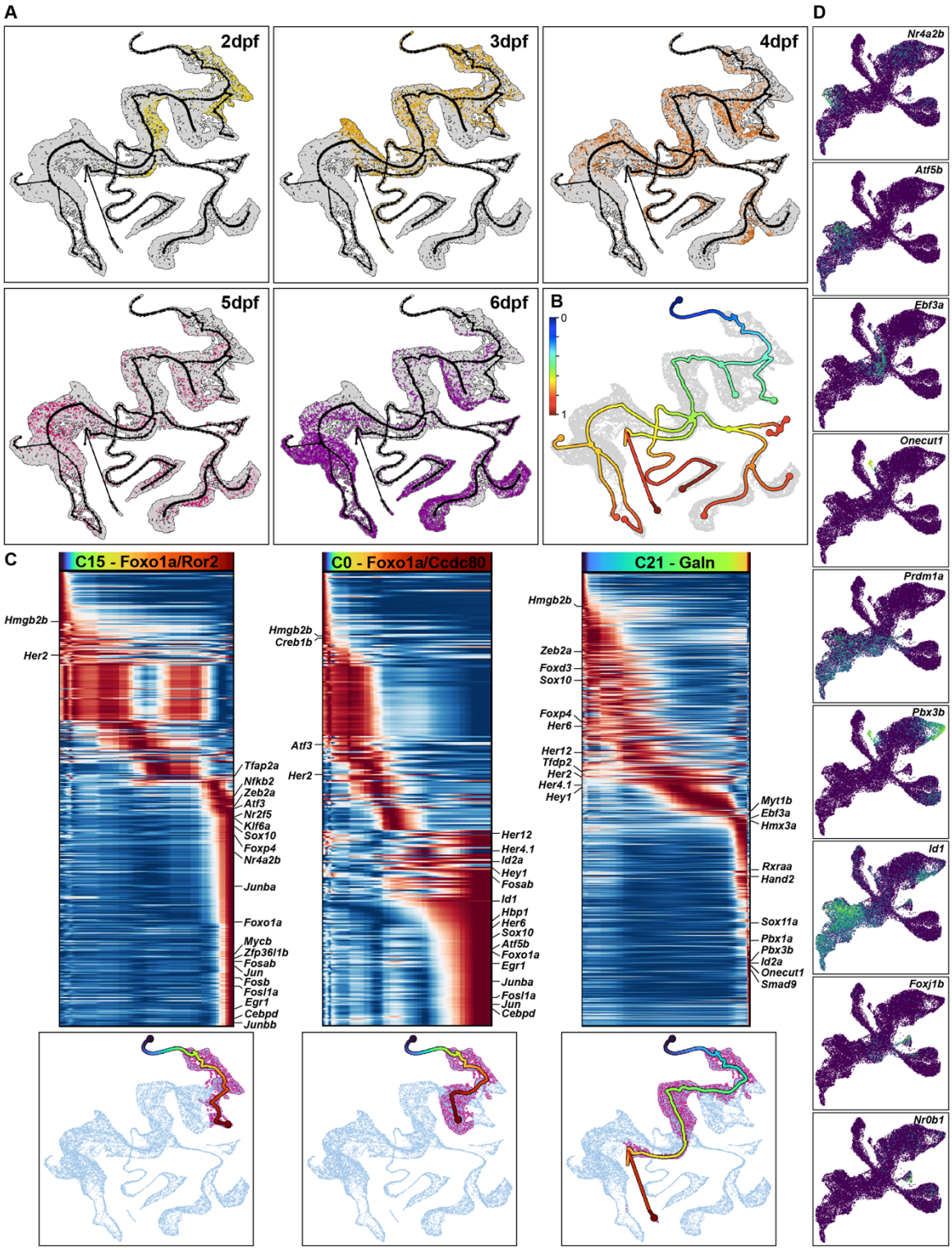
A
2dpf
3dpf
4dpf
5dpf
6dpf
B
0
1
C
C15 - Foxo1a/Ror2
Hmgb2b
Her2
Tfap2a
Nfkb2
Zeb2a
Atf3
Nr2f5
Klf6a
Sox10
Foxp4
Nr4a2b
Junba
Foxo1a
Mycb
Zfp36l1b
Fosab
Jun
Fosb
Fosl1a
Egr1
Cebpd
Junbb
C0 - Foxo1a/Ccdc80
Hmgb2b
Creb1b
Atf3
Her2
Her12
Her4.1
Id2a
Hey1
Fosab
Id1
Hbp1
Her6
Sox10
Atf5b
Foxo1a
Egr1
Junba
Fosl1a
Jun
Cebpd
C21 - Galn
Hmgb2b
Zeb2a
Foxd3
Sox10
Foxp4
Her6
Her12
Tfdp2
Her2
Her4.1
Hey1
Myt1b
Ebf3a
Hmx3a
Rxraa
Hand2
Sox11a
Pbx1a
Pbx3b
Id2a
Onecut1
Smad9
D
Nr4a2b
Atf5b
Ebf3a
Onecut1
Prdm1a
Pbx3b
Id1
Foxj1b
Nr0b1

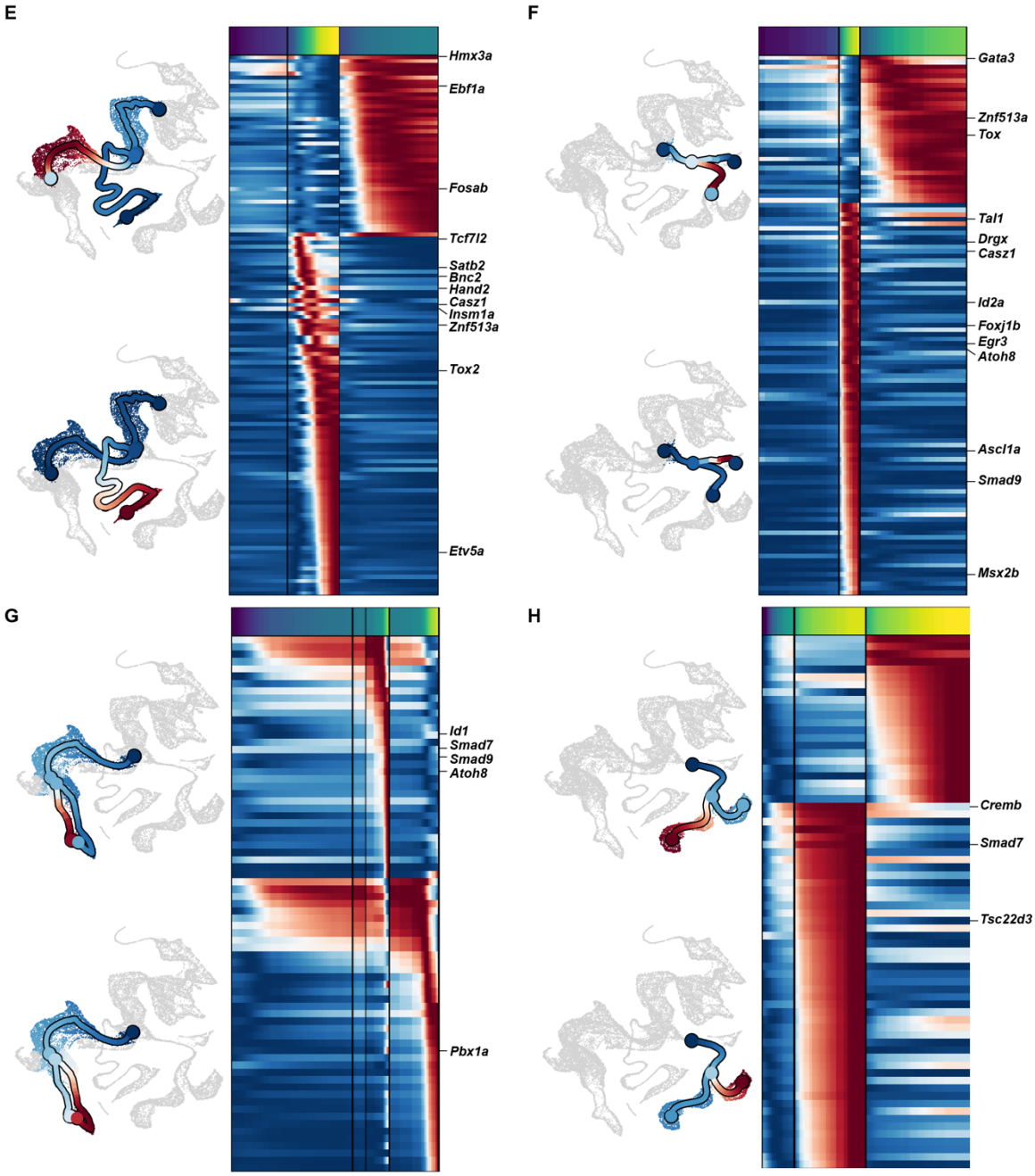

Figure 13: Lineage trajectories and bifurcation analysis. (A) UMAP plots with trajectories and different time points. (**B**) Pseudo-type analysis of ENS development. **(C)** Heatmaps and UMAPs of C15, C0, C21 highlighting transcription factors in each of the lineages. **(D)** UMAPs showing marker genes representative of different clusters. **(E**) Heatmaps and UMAPs showing trajectory from precursor to EN1 vs neuroblasts undergoing differentiation into EN2/EN3/EN4. **(F)** Heatmaps and UMAPs showing EN5

vs neuroblasts undergoing differentiation into EN6/EN7. **(G)** Heatmaps and UMAPs showing EN3 vs EN4. **(H)** Heatmaps and UMAPs showing EN6 vs EN7.

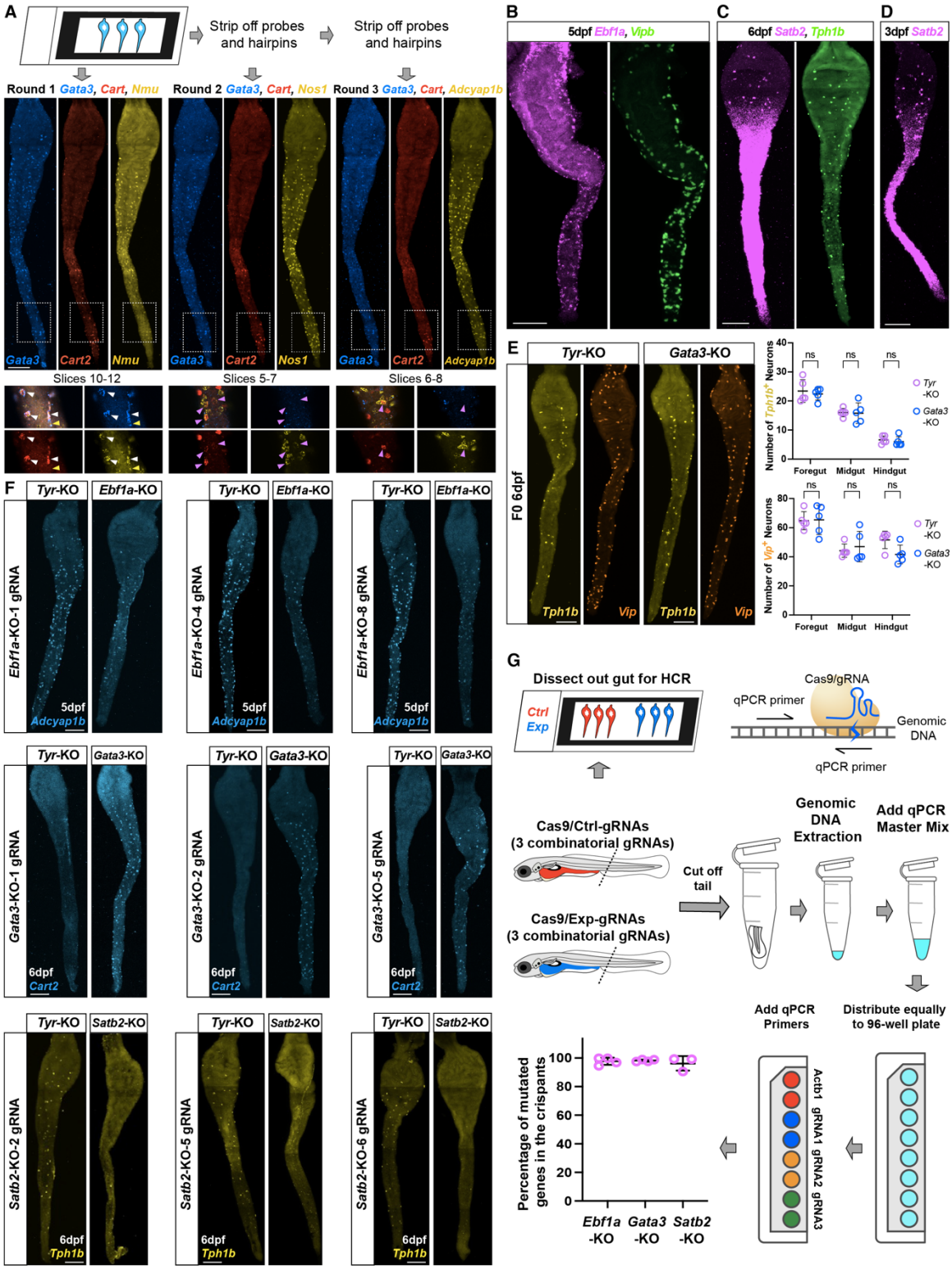

Figure 14: Expression and functions of transcription factors *Ebf1a*, *Satb2* and *Gata3* in the ENS. (**A**) Experimental procedure for multiplex HCR staining and whole

mount views of zebrafish guts showing the expression of transcription factors (*Gata3*) and corresponding marker genes (*Cart2, Nmu, Nos1, Adcyap1b*) that co-distribute with them in scRNA-seq clusters. (**B-C**) Whole mount view of zebrafish guts showing the expression of transcription factors (*Satb2* and *Ebf1a*) and corresponding marker genes (*Tph1b, Vipb*) that co-distribute with them in scRNA-seq clusters. (**D**) Expression of *Satb2* at 3dpf. (**E**) *Gata3*-knockout causes no change in *Tph1b* and *Vip* expression. The statistical analysis is performed with the software GraphPad Prism 10. ns: $P \geq 0.05$, *: $P < 0.05$, **: $P < 0.01$, ***: $P < 0.001$, ****: $P < 0.0001$. **(F)** Even single guides gave profound phenotypes as assayed by HCR for indicated marker genes. **(G)** Schematic of experimental design for qPCR analysis of mutational rate after CrispR-Cas9 using 3 guide RNAs to knockout *Ebf1a, Gata3* and *Satb2.* The results show a mutation percentage of >90% for each of these transcription factors. Scale bar: 100um.

Table 1. Marker genes identified in each cluster.

cluster	gene	p_val	p_val_adj	avg_log2FC
20	ube2c	5.87E-125	1.12E-121	10.976
20	si:ch211-69g19.2	1.14E-123	2.16E-120	12.803
20	tuba8l	2.12E-122	4.03E-119	9.092
20	mad2l1	1.09E-121	2.06E-118	8.927
20	cdc20	1.32E-121	2.50E-118	9.410
20	ccnb1	2.21E-121	4.19E-118	9.750
20	tpx2	3.89E-121	7.39E-118	8.233
20	cdk1	9.14E-121	1.73E-117	9.225
20	kpna2	9.39E-121	1.78E-117	12.962
20	aurkb	1.72E-119	3.27E-116	6.808
20	hmgb2a	1.03E-118	1.96E-115	4.847
20	hmgn2	1.60E-115	3.03E-112	4.252
20	top2a	7.88E-112	1.50E-108	7.501
20	ccnb3	4.27E-107	8.11E-104	9.143
20	hmgb2b	1.62E-106	3.07E-103	4.501
20	kif11	1.87E-104	3.55E-101	9.356
20	kifc1	3.61E-104	6.85E-101	1.266
20	tacc3	2.81E-99	5.33E-96	9.126
20	mki67	6.24E-98	1.18E-94	7.117
20	CABZ01058261.1	7.36E-97	1.40E-93	4.947
9	rrm2	0	0	8.811
9	mibp	0	0	7.282
9	stmn1a	0	0	6.039
9	rrm1	0	0	5.809
9	kiaa0101	0	0	5.732
9	ccna2	0	0	5.630
9	cks1b	0	0	5.385
9	CABZ01074745.1	0	0	4.958
9	tuba8l4	0	0	4.391
9	hmgb2a	0	0	3.946
9	chaf1a	0	0	3.886
9	banf1	0	0	3.808
9	aurkb	0	0	3.775
9	nutf2l	0	0	3.468
9	lbr	0	0	2.996
9	hmgb2b	0	0	2.367
9	dlx2a	0	0	2.113

9	hmgn2	0	0	1.815
9	neil1	0	0	1.449
9	gata2a	0	0	1.011
7	cdca7a	0	0	7.140
7	mcm4	0	0	6.111
7	mcm2	0	0	5.874
7	mcm5	0	0	5.661
7	pcna	0	0	1.843
7	nasp	7.27E-264	1.38E-260	3.758
7	fen1	5.41E-252	1.03E-248	2.416
7	si:ch211-156b7.4	4.52E-226	8.58E-223	3.346
7	nop58	1.97E-218	3.74E-215	2.804
7	gins2	1.89E-211	3.58E-208	5.096
7	myl4	1.60E-208	3.04E-205	1.330
7	hbegfa	6.81E-184	1.29E-180	1.587
7	lig1	1.80E-182	3.41E-179	2.332
7	rpa3	8.80E-176	1.67E-172	2.770
7	cpn1	1.19E-170	2.26E-167	2.724
7	dkc1	3.44E-166	6.53E-163	2.863
7	dnajc9	4.72E-151	8.96E-148	3.091
7	nutf2l	1.92E-149	3.65E-146	3.456
7	stmn1a	8.20E-148	1.56E-144	1.855
7	hells	2.01E-145	3.81E-142	4.310
22	hmgb2b	1.05E-54	2.00E-51	6.681
22	hmga1a	2.04E-53	3.86E-50	4.804
22	qkia	1.78E-49	3.37E-46	5.629
22	pcna	2.19E-49	4.15E-46	3.091
22	cdca7a	5.17E-49	9.81E-46	4.124
22	mcm5	4.69E-47	8.91E-44	4.450
22	hmgb2a	1.26E-46	2.38E-43	2.983
22	mcm2	7.75E-45	1.47E-41	4.868
22	rrm2	1.62E-44	3.07E-41	1.111
22	mcm4	2.91E-44	5.52E-41	5.223
22	rpl3	8.44E-44	1.60E-40	3.358
22	fabp7a	1.31E-43	2.48E-40	4.108
22	lig1	1.78E-43	3.38E-40	6.206
22	chaf1a	4.50E-43	8.54E-40	5.641
22	tuba8l3	8.03E-43	1.52E-39	5.389
22	rpl7a	1.39E-42	2.64E-39	3.348
22	nasp	2.04E-42	3.87E-39	4.476

22	CABZ01074745.1	2.66E-42	5.04E-39	5.309
22	pmp22a	5.23E-42	9.92E-39	6.907
22	rps7	5.54E-42	1.05E-38	3.239
15	fabp7a	2.26E-216	4.29E-213	4.707
15	sparc	1.17E-209	2.22E-206	4.454
15	qkia	5.06E-178	9.61E-175	2.823
15	krt18b	1.63E-166	3.09E-163	5.881
15	sdc4	1.60E-162	3.04E-159	5.098
15	pmp22a	3.88E-159	7.36E-156	3.117
15	sox10	5.86E-158	1.11E-154	3.959
15	marcksl1b	6.62E-154	1.26E-150	1.420
15	sulf2b	6.07E-150	1.15E-146	2.708
15	socs3b	1.27E-143	2.41E-140	2.840
15	lrig3	2.10E-141	3.99E-138	1.375
15	pon3.2	3.04E-138	5.78E-135	3.595
15	gpm6ab	5.17E-134	9.82E-131	4.673
15	gbx1	6.45E-133	1.22E-129	1.645
15	hsbp1l1	1.39E-132	2.65E-129	2.741
15	epas1a	1.17E-131	2.22E-128	3.017
15	junba	1.34E-128	2.54E-125	3.104
15	triobpa	1.83E-128	3.48E-125	1.843
15	s100v2	1.67E-124	3.17E-121	2.202
15	hbegfa	3.52E-123	6.68E-120	3.378
0	her6	0	0	5.739
0	tlcd1	0	0	5.330
0	eef1da	0	0	5.326
0	socs3b	0	0	4.848
0	ror2	0	0	4.775
0	CABZ01055522.1	0	0	4.775
0	micu2	0	0	4.752
0	nrgna	0	0	4.478
0	gbp3	0	0	4.436
0	lysmd4	0	0	4.414
0	prickle1b	0	0	4.392
0	slc2a12	0	0	4.370
0	ttpa	0	0	4.345
0	sypl2a	0	0	4.344
0	apol1	0	0	4.327
0	hgd	0	0	4.313
0	triobpa	0	0	4.273

0	si:ch211-191a24.4	0	0	4.265
0	klf15	0	0	4.204
0	si:dkey-238i5.2	0	0	4.186
6	AL929185.1	0	0	6.831
6	si:ch211-193l2.4	0	0	5.420
6	si:ch211-222l21.1	0	0	4.663
6	si:ch211-193l2.7	0	0	3.464
6	rpl11	0	0	1.225
6	rps7	2.53E-299	4.80E-296	1.269
6	rpl3	1.03E-289	1.96E-286	1.104
6	RPL41	6.64E-282	1.26E-278	1.267
6	her4.1	1.87E-280	3.54E-277	5.421
6	rpl7a	1.74E-274	3.30E-271	1.070
6	hmga1a	3.49E-272	6.63E-269	2.107
6	her2	1.39E-256	2.64E-253	4.337
6	CR812832.1	1.60E-255	3.03E-252	2.941
6	hey1	2.20E-236	4.18E-233	5.122
6	rplp0	7.51E-233	1.43E-229	1.115
6	srrm4	2.96E-145	5.62E-142	5.474
6	ppfibp1b	2.35E-137	4.46E-134	1.100
6	auts2b	5.10E-135	9.69E-132	1.691
6	dlb	4.75E-131	9.01E-128	2.036
6	jam2a	3.52E-128	6.69E-125	7.658
14	hbae3	0	0	3.396
14	hbbe1.3	0	0	3.396
14	pah	0	0	2.257
14	nt5c2l1	0	0	2.150
14	dlx2a	2.63E-246	4.98E-243	2.663
14	si:dkey-25o16.2	1.53E-238	2.91E-235	2.643
14	tm6sf2	1.50E-197	2.85E-194	2.334
14	gata2a	4.53E-164	8.59E-161	3.775
14	ackr3b	1.20E-140	2.27E-137	2.991
14	ebf3a	2.88E-131	5.47E-128	3.963
14	rsrp1	3.09E-55	5.87E-52	1.283
14	cyp26a1	3.53E-20	6.70E-17	1.754
14	hoxb1b	6.97E-12	1.32E-08	1.055
1	cited4b	1.50E-242	2.85E-239	4.206
1	rsrp1	1.09E-204	2.08E-201	1.362
1	hsp90aa1.2	5.43E-189	1.03E-185	1.856
1	rpl11	2.49E-153	4.73E-150	1.068

1	hand2	1.90E-152	3.61E-149	1.106
1	myt1b	7.85E-152	1.49E-148	2.777
1	actb1	7.65E-135	1.45E-131	3.205
1	AL929077.2	3.77E-127	7.15E-124	3.025
1	cd82a	1.14E-109	2.16E-106	3.528
1	adgre10	3.45E-78	6.54E-75	1.161
1	si:ch211-260e23.9	1.19E-67	2.26E-64	4.318
1	CR812832.1	1.62E-62	3.07E-59	1.747
1	sult6b1	2.78E-61	5.28E-58	1.225
1	zfand5b	6.27E-36	1.19E-32	3.530
1	zgc:77784	6.48E-30	1.23E-26	1.404
1	tle3a	6.81E-22	1.29E-18	1.019
1	brd1b	8.69E-22	1.65E-18	1.846
1	tmsb	1.19E-19	2.26E-16	2.493
1	nfkbiab	1.22E-16	2.32E-13	1.144
1	tm6sf2	7.84E-14	1.49E-10	4.212
13	mdkb	0	0	3.636
13	hand2	0	0	3.261
13	marcksl1b	0	0	2.226
13	satb2	4.99E-290	9.47E-287	5.594
13	tubb5	2.70E-249	5.13E-246	3.367
13	tuba1c	7.53E-232	1.43E-228	1.916
13	stmn2b	2.18E-183	4.14E-180	2.869
13	spata22	1.11E-176	2.11E-173	5.342
13	znf513a	6.36E-153	1.21E-149	2.034
13	gpm6ab	2.00E-141	3.79E-138	1.951
13	gap43	1.30E-131	2.47E-128	1.475
13	bnc2	1.30E-121	2.46E-118	4.979
13	rasgrp3	2.52E-106	4.78E-103	3.497
13	tmsb	4.02E-75	7.63E-72	3.436
13	tcf7l2	3.76E-73	7.14E-70	4.398
13	pcdh19	4.78E-69	9.07E-66	2.519
13	dok6	1.03E-64	1.96E-61	3.698
13	efna2b	3.29E-61	6.25E-58	3.051
13	zgc:153426	1.16E-60	2.21E-57	3.166
13	tox2	4.32E-59	8.20E-56	1.689
10	tph1b	0	0	9.574
10	ddc	0	0	8.882
10	CABZ01069081.1	0	0	8.407
10	hpca	0	0	8.404

10	arpp21	0	0	7.677
10	crhbp	0	0	7.152
10	marcksl1b	0	0	4.608
10	hand2	0	0	2.435
10	tmem178	3.03E-299	5.74E-296	5.506
10	ahcyl1	1.58E-260	3.00E-257	6.604
10	ckbb	4.19E-237	7.95E-234	2.567
10	kifc1	4.49E-233	8.51E-230	7.769
10	mns1	8.89E-233	1.69E-229	10.411
10	slc35g2a	6.44E-200	1.22E-196	2.667
10	mdkb	1.11E-173	2.11E-170	1.488
10	asic4a	1.11E-165	2.11E-162	7.359
10	synpr	1.01E-155	1.93E-152	7.962
10	gpm6aa	3.86E-155	7.32E-152	5.191
10	boka	1.40E-147	2.65E-144	1.579
10	pcmtd2	5.97E-146	1.13E-142	1.492
16	serpine2	4.45E-180	8.44E-177	5.430
16	gap43	8.05E-169	1.53E-165	1.232
16	cadm4	5.34E-154	1.01E-150	2.593
16	tuba1c	1.49E-146	2.83E-143	1.272
16	stmn2b	5.23E-143	9.92E-140	1.234
16	hmx3a	2.97E-126	5.63E-123	2.464
16	tubb5	2.42E-117	4.59E-114	3.516
16	gpm6ab	1.85E-111	3.51E-108	2.276
16	sox11a	6.44E-103	1.22E-99	2.401
16	epha7	2.13E-75	4.04E-72	2.577
16	syt9b	3.84E-70	7.29E-67	2.234
16	mllt11	1.08E-66	2.05E-63	1.072
16	rpa3	8.66E-65	1.64E-61	1.115
16	ebf1a	6.58E-64	1.25E-60	2.003
16	FAM163A	1.33E-57	2.52E-54	1.603
16	nanos1	8.00E-57	1.52E-53	1.143
16	tenm3	4.09E-55	7.75E-52	1.470
16	cntn4	4.57E-55	8.67E-52	2.289
16	ntf3	5.43E-55	1.03E-51	2.154
16	sypb	7.17E-54	1.36E-50	2.636
21	onecut1	7.76E-69	1.47E-65	13.252
21	pbx3b	8.84E-65	1.68E-61	6.354
21	galn	8.86E-65	1.68E-61	13.198
21	cbln1	2.33E-62	4.42E-59	10.961

21	si:ch211-215d8.2	1.29E-53	2.45E-50	12.278
21	id2a	3.46E-50	6.58E-47	3.404
21	syt9b	5.70E-49	1.08E-45	5.661
21	sox11a	7.65E-46	1.45E-42	5.776
21	mdkb	6.30E-45	1.20E-41	1.685
21	serpine2	8.04E-44	1.53E-40	3.896
21	hand2	3.73E-39	7.09E-36	1.098
21	ptmaa	1.05E-31	2.00E-28	3.386
21	edil3a	1.52E-30	2.89E-27	7.059
21	slc6a15	9.37E-29	1.78E-25	5.453
21	tubb2	6.18E-27	1.17E-23	7.902
21	tmsb	2.60E-26	4.94E-23	4.145
21	mllt11	2.97E-26	5.64E-23	1.416
21	ptprga	3.54E-26	6.72E-23	1.066
21	cplx1	3.37E-25	6.39E-22	2.753
21	anxa13l	6.81E-24	1.29E-20	2.439
3	stmn2b	0	0	3.523
3	si:ch211-202h22.9	0	0	3.336
3	sult6b1	0	0	3.263
3	oprl1	0	0	2.750
3	tuba1c	0	0	2.368
3	si:dkeyp-120h9.1	0	0	2.083
3	tubb2b	0	0	1.965
3	gap43	0	0	1.854
3	dgkaa	0	0	1.362
3	si:ch73-193i22.1	0	0	1.283
3	ehd4	0	0	1.268
3	plcxd3	0	0	1.256
3	adcyap1b	0	0	1.101
3	cygb2	9.16E-298	1.74E-294	1.526
3	arl4d	5.98E-253	1.13E-249	1.438
3	si:dkey-280e21.3	2.76E-243	5.25E-240	2.738
3	nr4a1	4.15E-221	7.88E-218	3.461
3	ebf1a	3.54E-205	6.72E-202	2.266
3	zgc:153426	8.42E-200	1.60E-196	2.701
3	si:ch211-269c21.2	1.14E-199	2.17E-196	3.441
5	nos1	0	0	3.699
5	adcyap1b	0	0	3.638
5	plcxd3	0	0	3.605
5	rgs4	0	0	3.007

5	ehd4	0	0	2.874
5	cygb2	0	0	2.592
5	si:ch73-193i22.1	0	0	2.394
5	dgkaa	0	0	1.993
5	vgf	0	0	1.412
5	sult6b1	0	0	1.366
5	atp1b1a	0	0	1.120
5	atp2b3b	2.76E-284	5.24E-281	3.014
5	myadmb	8.06E-190	1.53E-186	2.245
5	atp2b3a	1.38E-186	2.63E-183	3.143
5	arl4d	7.63E-184	1.45E-180	1.757
5	si:ch211-195b15.8	4.07E-126	7.73E-123	1.358
5	fosab	3.38E-118	6.41E-115	1.374
5	ada	9.30E-117	1.77E-113	1.285
5	map2k1	2.06E-116	3.90E-113	3.298
5	ntng1a	1.93E-88	3.67E-85	3.410
2	si:dkeyp-111e5.4	0	0	3.449
2	bpifcl	0	0	2.896
2	arl3l2	0	0	2.769
2	rims2a	0	0	2.533
2	trpc5b	0	0	2.493
2	si:ch73-193i22.1	0	0	2.443
2	zgc:152977	0	0	2.200
2	hs3st1l2	0	0	2.175
2	hsd11b2	0	0	2.136
2	tnfaip2a	0	0	2.060
2	ppp1r13ba	0	0	2.040
2	fam169aa	0	0	2.039
2	dgkaa	0	0	1.973
2	si:dkey-85k7.7	0	0	1.939
2	AL929435.1	0	0	1.885
2	ezh1	0	0	1.866
2	cysltr1	0	0	1.814
2	nptnb	0	0	1.752
2	tapbp.1	0	0	1.707
2	si:dkey-18a10.3	0	0	1.657
12	si:ch73-193i22.1	7.31E-285	1.39E-281	1.636
12	atp1b1a	1.12E-195	2.13E-192	1.642
12	ehd4	6.95E-190	1.32E-186	1.567
12	ada	2.20E-159	4.18E-156	3.130

12	rgs4	1.17E-153	2.21E-150	3.859
12	dgkaa	2.20E-153	4.18E-150	1.409
12	fam107b	4.01E-147	7.61E-144	4.070
12	si:dkeyp-120h9.1	1.34E-96	2.54E-93	1.015
12	CABZ01092746.1	1.41E-86	2.68E-83	1.224
12	hbae3	2.61E-86	4.96E-83	1.425
12	zgc:152977	1.84E-83	3.49E-80	1.663
12	hbbe1.3	4.44E-82	8.42E-79	1.425
12	atp2b3b	6.84E-80	1.30E-76	1.580
12	cbx7b	7.35E-80	1.40E-76	1.749
12	si:ch211-213a13.2	1.35E-78	2.56E-75	2.240
12	rrbp1b	6.99E-78	1.33E-74	1.827
12	syce2	7.08E-76	1.34E-72	1.265
12	si:ch211-63p21.1	8.64E-71	1.64E-67	1.096
12	si:ch211-198m17.1	1.77E-70	3.37E-67	2.088
12	si:dkey-18a10.3	1.93E-62	3.67E-59	1.317
17	vip	1.51E-200	2.87E-197	5.630
17	kctd12.2	1.11E-180	2.11E-177	3.737
17	calcrla	7.72E-106	1.46E-102	3.232
17	fxyd1	2.98E-83	5.65E-80	1.142
17	zgc:152977	1.15E-82	2.17E-79	1.601
17	si:ch211-213a13.2	2.20E-80	4.17E-77	1.382
17	cbx7b	4.21E-78	7.99E-75	2.331
17	col7a1	9.82E-77	1.86E-73	2.718
17	atoh8	1.62E-75	3.07E-72	3.491
17	gria3a	9.62E-74	1.83E-70	2.022
17	rrbp1b	1.36E-73	2.58E-70	1.760
17	sox11a	1.81E-70	3.44E-67	3.476
17	pcmtd2	4.38E-67	8.31E-64	1.634
17	ttll10	1.88E-66	3.57E-63	1.979
17	ppp1r13ba	2.76E-64	5.23E-61	1.321
17	camk2n1a	3.16E-63	6.00E-60	2.654
17	tmem123	8.99E-61	1.71E-57	2.956
17	pip4k2ab	1.88E-58	3.57E-55	1.969
17	fam169aa	4.74E-58	9.00E-55	1.414
17	si:dkey-14k9.2	1.11E-56	2.11E-53	1.846
18	lyve1a	1.41E-212	2.68E-209	9.079
18	ppp1r1b	4.36E-207	8.28E-204	8.757
18	vip	1.52E-199	2.88E-196	5.114
18	spock3	6.21E-175	1.18E-171	1.683

18	mdkb	5.72E-172	1.08E-168	4.189
18	pbx1a	1.24E-161	2.35E-158	6.668
18	pbx3b	5.26E-159	9.98E-156	5.479
18	tnfaip8l2b	1.68E-146	3.18E-143	7.270
18	cpn1	1.42E-133	2.70E-130	2.659
18	emp3b	1.66E-129	3.15E-126	7.522
18	zgc:162698	3.00E-129	5.69E-126	5.907
18	sult4a1	1.55E-109	2.94E-106	2.428
18	anxa13l	3.55E-106	6.74E-103	3.708
18	si:dkey-7j14.5	4.48E-102	8.51E-99	4.829
18	id2a	8.29E-92	1.57E-88	3.528
18	sox11a	1.37E-90	2.61E-87	3.684
18	arrb2b	1.72E-90	3.26E-87	6.010
18	map1aa	3.33E-82	6.33E-79	4.974
18	si:dkey-196j8.2	2.37E-81	4.49E-78	6.344
18	FP236545.1	3.62E-79	6.88E-76	1.258
19	cart2	5.70E-132	1.08E-128	5.873
19	egr3	6.22E-99	1.18E-95	7.794
19	fxyd1	9.90E-94	1.88E-90	3.239
19	mapk8ip3	9.30E-89	1.77E-85	9.169
19	spock3	1.09E-88	2.07E-85	5.668
19	chl1b	6.62E-88	1.26E-84	1.473
19	mmp17b	6.84E-79	1.30E-75	1.921
19	rai14	4.39E-77	8.33E-74	2.549
19	pik3r3b	6.45E-77	1.22E-73	3.598
19	scinla	1.14E-75	2.16E-72	1.867
19	arap3	3.50E-75	6.65E-72	1.188
19	ascl1a	2.50E-74	4.75E-71	7.625
19	BX936305.1	3.65E-74	6.92E-71	1.215
19	prickle1b	1.69E-70	3.21E-67	1.453
19	rrbp1b	8.46E-70	1.60E-66	2.451
19	si:dkey-100n10.2	2.37E-69	4.50E-66	7.326
19	myo1b	5.31E-69	1.01E-65	2.752
19	cbfa2t3	5.28E-68	1.00E-64	2.585
19	sowahab	8.74E-68	1.66E-64	3.143
19	rnd1b	1.13E-67	2.14E-64	1.085
11	nmu	0	0	1.263
11	fhl1b	3.07E-298	5.83E-295	3.249
11	prdx1	1.12E-287	2.12E-284	3.428
11	chl1b	4.35E-252	8.25E-249	3.433

11	fxyd1	6.67E-228	1.27E-224	2.124
11	tuba1c	3.79E-211	7.20E-208	1.304
11	tox	3.24E-175	6.15E-172	2.523
11	atp1a1a.2	2.84E-173	5.39E-170	3.319
11	calcrla	3.12E-160	5.91E-157	4.087
11	gata3	2.30E-156	4.36E-153	1.456
11	dlb	6.73E-140	1.28E-136	3.476
11	arl4aa	4.14E-135	7.86E-132	1.710
11	ptmaa	9.61E-135	1.82E-131	1.436
11	calb2a	9.70E-111	1.84E-107	2.708
11	ndrg3b	5.38E-99	1.02E-95	1.202
11	ednraa	4.93E-90	9.36E-87	1.084
11	vgf	3.24E-81	6.15E-78	1.335
11	nr4a1	1.29E-75	2.45E-72	2.707
11	ptprga	3.43E-73	6.52E-70	1.868
11	CABZ01095157.1	7.00E-68	1.33E-64	4.491
8	s1pr1	0	0	6.502
8	zgc:101731	0	0	5.949
8	scg2b	0	0	5.923
8	tac3a	0	0	4.900
8	pik3ip1	0	0	4.076
8	slc35g2a	0	0	4.065
8	tob1a	0	0	3.786
8	slc18a3a	0	0	2.277
8	fhl1b	0	0	1.532
8	higd1a	1.22E-302	2.31E-299	4.153
8	snap25b	2.52E-295	4.77E-292	4.192
8	ckbb	2.24E-293	4.25E-290	2.048
8	gata3	7.11E-274	1.35E-270	2.979
8	pam	2.34E-262	4.44E-259	3.710
8	slc2a3a	2.59E-213	4.91E-210	4.679
8	rasd1	9.73E-205	1.85E-201	2.779
8	hsd3b7	1.04E-191	1.98E-188	2.062
8	tox	2.25E-186	4.27E-183	3.594
8	cart2	4.07E-180	7.72E-177	4.099
8	dnmt3ab	5.63E-178	1.07E-174	5.363
4	FP015823.1	0	0	6.914
4	FP015823.2	0	0	6.630
4	mdka	0	0	6.056
4	calb2a	0	0	5.430

4	nmu	0	0	5.428
4	ednraa	0	0	5.128
4	arl4aa	0	0	4.500
4	slc18a3a	0	0	4.107
4	gata3	0	0	3.760
4	atp1a1a.2	0	0	3.667
4	fhl1b	0	0	3.633
4	ndrg3b	0	0	3.459
4	tmsb1	0	0	3.252
4	snap25b	0	0	3.206
4	spock3	0	0	2.725
4	atp1b1a	0	0	2.677
4	tac3a	0	0	2.357
4	ckbb	0	0	2.042
4	slc35g2a	0	0	1.127
4	tox	5.93E-307	1.13E-303	2.854

Table 2. Spatial Expression of multiple marker genes in the zebrafish ENS at 6 dpf revealed by sequential HCR.

Label	vipb	nos1	adcyap1b	vip	tph1b	slc18a3a	tac3a	nmu	cart2
1	√	√	√	√					
2	√	√		√					
3	√	√	√	√					
4		√		√		√			
5		√		√		√			
6		√		√		√			
7		√		√		√			
8		√		√		√			
9	√	√	√	√					
10	√	√	√	√					
11	√	√	√	√					
12	√	√	√	√					
13	√	√	√	√					
14				√		√			
15		√		√		√			
16		√		√		√			
17		√		√		√			
18		√		√		√			
19		√		√		√			
20	√	√	√	√					
21		√		√		√			
22		√		√		√			
23	√	√	√	√					
24	√	√		√					
25				√		√			
26	√	√	√	√					
27	√	√	√	√					
28	√	√	√	√					
29	√	√	√	√					
30	√	√	√	√					
31	√	√	√	√					
32	√	√	√	√					
33	√	√	√	√					
34						√	√	√	
35	√	√	√	√					
36	√	√	√	√					

37	√	√	√	√					
38	√				√				
39	√	√	√	√					
40	√	√	√						
41	√	√	√	√					
42						√	√	√	
43	√			√	√				
44	√	√	√	√					
45	√	√	√						
46	√	√	√						
47	√	√	√						
48	√	√	√						
49	√	√	√						
50	√	√	√						
51	√			√	√				
52	√	√	√						
53	√	√	√						
54	√			√	√				
55	√		√	√		√			
56	√	√		√					
57				√					
58	√	√	√						
59	√	√	√						
60	√	√	√						
61	√	√	√						
62	√	√	√						
63	√	√	√	√					
64	√	√	√						
65						√	√	√	
66					√				
67	√	√	√						
68						√	√	√	
69	√		√	√		√			
70						√	√	√	
71	√	√	√						
72					√				
73	√		√	√		√			
74						√	√	√	√
75						√	√	√	
76						√	√	√	

77	√	√	√						
78					√				
79						√	√	√	
80						√	√	√	
81	√				√				
82	√	√	√			√	√	√	
83	√		√	√		√			
84	√	√	√						
85	√	√	√						
86	√	√	√						
87						√	√	√	
88	√	√	√						
89	√	√	√						
90					√				
91						√	√	√	
92						√	√	√	
93	√	√	√						
94						√	√	√	
95	√	√	√						
96	√	√	√						
97	√	√	√						
98	√				√				
99	√	√	√						
100	√	√	√						
101	√				√				
102	√	√	√						
103	√		√	√		√			
104						√		√	
105	√				√				
106						√	√	√	√
107	√	√	√						
108						√		√	
109						√		√	
110						√	√	√	
111						√	√	√	
112						√		√	
113						√	√	√	
114	√		√	√		√			
115						√	√	√	
116						√	√	√	

117	√		√		√		√			
118	√	√	√							
119	√		√		√		√			
120						√				
121							√	√	√	
122							√	√	√	
123	√	√	√							
124	√	√	√							
125	√		√		√		√			
126							√	√	√	√
127	√	√	√							
128							√		√	
129	√		√		√		√			
130							√	√	√	
131					√					
132	√		√		√		√			
133	√	√	√							
134							√	√	√	
135							√	√	√	
136							√	√	√	
137	√				√	√				
138							√	√	√	
139							√	√	√	
140	√	√	√							
141	√					√				
142	√					√				
143							√	√	√	
144							√	√	√	
145					√					
146					√					
147	√	√	√							
148							√		√	
149	√	√	√							
150							√	√	√	
151	√	√	√							
152	√		√		√		√			
153	√	√	√							
154	√					√				
155	√	√	√							
156	√	√	√							

157						√	√	√
158	√	√	√					
159	√	√	√					
160	√	√	√					
161	√	√	√					
162	√				√			
163	√	√	√					
164	√	√	√					
165	√	√	√					
166	√				√			
167	√	√	√					
168	√		√	√		√		
169						√	√	√
170						√		√
171					√			
172	√	√	√					
173						√	√	√
174					√			
175						√	√	√
176	√	√	√	√				
177	√	√	√					
178						√		√
179						√		√
180					√			
181	√	√	√	√				
182	√	√	√					
183	√	√	√					
184						√	√	√
185	√	√	√	√				
186	√				√			
187						√	√	√
188						√		√
189	√	√	√	√				
190	√		√	√		√		
191						√		√
192	√	√	√					
193	√	√	√					
194	√		√	√		√		
195	√	√	√					
196	√	√	√					

197	√	√	√						
198	√				√				
199						√		√	√
200					√				
201	√	√	√						
202	√	√	√						
203	√	√	√	√					
204						√		√	√
205	√				√				
206	√	√	√						
207	√		√	√					
208					√				
209	√		√	√		√			
210				√					
211	√	√	√						
212						√			√
213						√		√	√
214	√	√	√						
215	√	√	√						
216						√		√	√
217						√		√	√
218	√	√	√						
219	√	√	√						
220	√	√	√						
221						√			√
222				√					
223	√	√	√						
224						√			√
225	√	√	√						
226						√			√
227	√				√				
228						√		√	√
229			√	√		√			
230	√	√	√						
231	√	√	√						
232						√		√	√
233	√	√	√						
234	√	√	√						
235	√	√	√						
236	√	√	√						

237	√	√	√						
238	√	√	√						
239	√		√	√		√			
240						√			√
241	√	√	√						
242	√		√	√					√
243	√				√				
244	√	√	√						
245	√	√	√						
246	√	√	√						
247						√		√	√
248		√		√					
249	√	√	√						
250						√			√
251	√	√	√						
252						√		√	√
253						√		√	√
254	√	√	√						
255	√	√	√						
256						√		√	√
257	√		√	√					
258						√		√	√
259						√			√
260	√	√	√						
261	√				√				
262	√	√	√						
263	√	√	√						
264						√		√	√
265	√	√	√						
266	√	√	√	√					
267						√		√	√
268						√		√	√
269	√		√	√					
270						√		√	√
271	√	√	√						
272	√	√	√						
273						√			√
274						√		√	√
275	√	√	√						
276						√		√	√

277	√	√	√						
278	√				√				
279	√	√	√						
280						√			√
281	√	√	√						
282	√	√	√						
283						√		√	√
284				√					
285	√	√	√						
286	√	√	√						
287				√					
288	√				√				
289						√			√
290						√		√	√
291	√	√	√						
292	√	√	√						
293	√	√	√						
294				√					
295	√	√	√						
296	√	√	√						
297				√					
298	√	√	√						
299	√	√	√						
300						√		√	√
301	√	√	√						
302	√	√	√						
303	√	√	√						
304	√	√	√						
305	√	√	√						
306						√		√	√
307						√		√	√
308						√		√	√
309	√								
310				√					
311						√		√	√
312	√	√	√						
313				√					
314	√	√	√	√					
315	√	√	√	√					
316	√	√	√						

317						√		√	√	√
318						√		√	√	
319	√	√	√							
320	√				√					
321	√									
322	√				√					
323						√		√	√	√
324	√	√	√							
325			√	√	√				√	
326						√		√	√	
327					√					
328	√	√	√							
329						√		√	√	
330	√	√	√							
331	√	√	√							
332	√	√	√							
333	√	√	√							
334	√	√	√							
335	√									
336						√		√	√	
337	√	√	√	√						
338	√									
339	√	√	√							
340	√	√	√							
341						√			√	
342	√		√	√					√	
343						√		√	√	
344						√		√	√	
345						√		√	√	
346	√	√	√							
347						√		√	√	
348	√	√	√							
349				√	√					
350	√	√	√							
351	√	√	√							
352	√	√	√							
353	√									
354			√	√	√				√	
355	√	√	√							
356	√									

357	√	√	√							
358	√	√	√							
359	√		√	√					√	
360						√		√	√	√
361						√		√	√	√
362			√	√	√				√	
363	√	√	√							
364						√		√	√	
365	√	√	√							
366						√		√	√	
367						√		√	√	
368	√				√					
369	√	√	√							
370	√	√	√							
371	√	√	√							
372	√	√	√							
373	√	√	√							
374						√		√	√	
375	√	√	√							
376	√	√	√							
377	√									
378	√									
379						√		√	√	√
380	√									
381	√	√	√							
382				√	√				√	
383	√	√	√							
384	√		√	√					√	
385	√									
386	√				√					
387						√		√	√	√
388	√	√	√							
389						√		√	√	
390						√		√	√	
391	√									
392		√	√							
393	√	√	√							
394	√		√	√					√	
395						√		√	√	
396	√	√	√							

397						√		√	√	√
398	√	√	√							
399	√									
400	√				√					
401	√									
402	√	√	√							
403	√									
404	√									
405						√		√	√	
406	√	√	√							
407	√									
408						√		√	√	√
409	√	√	√							
410	√	√	√	√						
411	√	√	√							
412	√	√	√							
413						√		√	√	√
414	√	√	√	√						
415	√									
416	√	√	√							
417	√				√					
418	√				√					
419						√		√	√	
420		√	√							
421						√		√	√	
422			√	√	√				√	
423			√	√	√				√	
424	√									
425						√		√	√	√
426	√	√	√							
427	√	√	√							
428	√									
429	√									
430	√	√	√	√						
431	√									
432	√	√	√							
433	√	√	√							
434	√				√					
435	√	√	√							
436	√		√	√	√				√	

437						√		√	√	√
438						√		√	√	√
439						√		√	√	√
440	√	√	√							
441	√									
442	√									
443	√									
444	√									
445	√	√	√							
446	√									
447						√		√	√	
448						√		√	√	√
449	√	√	√							
450	√									
451	√	√	√							
452	√	√	√							
453	√	√	√							
454	√			√	√					
455						√		√	√	√
456	√		√	√	√				√	
457	√	√	√							
458	√	√	√							
459						√		√	√	
460						√		√	√	
461	√									
462	√	√	√							
463	√									
464	√	√	√							
465	√	√	√							
466	√									
467	√									
468	√	√	√							
469						√		√	√	√
470						√		√	√	
471	√									
472	√	√	√	√						
473	√				√					
474					√					
475						√		√	√	
476						√		√	√	

477						√	√	√	
478						√	√	√	√
479	√	√	√	√					
480	√	√	√						
481	√								
482	√	√	√						
483			√			√	√		√
484				√					
485	√	√	√						
486	√	√	√	√					
487	√	√	√						
488	√				√				
489	√	√	√						
490	√								
491						√	√	√	
492						√	√	√	√
493						√	√	√	√
494						√	√		√
495						√	√	√	
496	√	√	√	√					
497						√	√	√	√
498						√	√	√	√
499	√	√	√	√					
500						√	√	√	√
501	√	√	√						
502						√	√	√	
503	√	√	√						
504	√	√	√						
505	√	√	√						
506			√	√				√	
507						√	√	√	
508						√	√		√
509	√	√	√						
510	√		√	√				√	
511	√								
512	√			√	√				
513				√					
514	√	√	√	√					
515	√	√	√	√					
516	√	√	√						

517	√								
518					√	√	√	√	
519					√	√	√	√	
520					√	√	√	√	
521	√	√	√	√					
522					√	√	√	√	
523					√	√	√	√	
524		√			√	√		√	
525	√	√	√	√					
526	√	√	√	√					
527	√	√	√	√					
528	√	√	√	√					
529	√	√	√	√	√				
530	√	√	√	√					
531	√	√	√	√					
532	√	√	√	√					
533	√								
534	√	√	√	√					
535	√	√	√	√					
536		√			√	√		√	
537	√								
538		√			√	√		√	
539		√			√	√		√	
540			√		√	√		√	
541		√			√	√		√	
542	√	√	√	√					
543	√	√	√	√					
544	√	√	√	√					
545		√			√	√		√	
546				√					
547		√			√	√		√	
548	√								
549	√	√	√	√					
550		√			√	√		√	
551		√			√	√		√	
552	√								
553		√			√	√		√	
554	√								
555	√	√		√					
556		√			√	√		√	

557	√	√	√						
558		√				√	√		√
559	√								
560	√	√	√	√					
561		√				√	√		√
562	√	√	√	√					
563		√				√	√		√
564	√								
565		√				√	√		√
566		√				√	√		√
567		√		√					
568				√					
569				√					
570				√					
571				√					
572						√		√	
573	√	√	√	√					
574						√		√	
575	√		√	√					
576						√	√	√	
577						√	√	√	
578					√			√	
579				√					
580						√	√	√	
581						√		√	
582						√		√	
583						√	√	√	
584	√	√	√						
585						√		√	
586	√	√	√						

Table 3. crRNA sequence

	crRNA sequence
Tyr-KO-1	GGACTGGAGGACTTCTGGGG
Tyr-KO-2	GATGCATTATTACGTGTCCC
Tyr-KO-3	GAACCTCTGCCTCTCGGTAG
Ebf1a-KO-1	CGTATAGCGCTAATACGAAG
Ebf1a-KO-4	GAAAGCGTCGCATGTCTCGT
Ebf1a-KO-8	GGTAAGCGCTCAGGGTCGCC
Gata3-KO-1	CGTACTACGGGAACCCGGTT
Gata3-KO-2	GGGAAAGGCCCAAGGTTCCA
Gata3-KO-5	GCATGAGGTCCCAGCTCGTC
Satb2-KO-2	GAGACTGCTCTCCTCGCCCT
Satb2-KO-5	GGGCGTTGCGTACTGTTGCG
Satb2-KO-6	GGTTGGAGCCGGGCTCTCCA

Table 4. Primer sequences used in qPCR experiment

Primer sequences in qPCR experiment	
actb1-for	GCACAGCTTCTCCTTGATGTCA
actb1-rev	GATCTGGCTGGTCGTGACCT
ebf1a-1-for	CCATCATCATTCTGTCTGTCTTTCTTC
ebf1a-1-rev	TCGTATAGCGCTAATACGAAGTGGA
ebf1a-4-for	GTCAATGTCACAGAAAACGGACATC
ebf1a-4-rev	CGTCGCATGTCTCGTGGGT
ebf1a-8-for	GGGTGTTGAATTTCCCTGCG
ebf1a-8-rev	CTCAGGGTCGCCCGGGT
gata3-1-for	CCCGAACCGGGTTCCCG
gata3-1-rev	CCCAGGACTGGGACACTCCTAC
gata3-2-for	GGAAGGTGAAGAGATGTGGGCTG
gata3-2-rev	CCCCTGGAACCTTGGGCC
gata3-5-for	GACAGCTAGGGAGCTTACATTGTGT
gata3-5-rev	TGCCAGACGAGCTGGGACCT
satb2-2-for	AGCCGAGGGCGAGGAGAG
satb2-2-rev	TGGAGCAGATGGATGGAGGGA
satb2-5-for	GTTGCGTACTGTTGCGTGGTTC
satb2-5-rev	TTGACCTGGCCTGCTGCA
satb2-6-for	AGCCGGGCTCTCCAGGGC
satb2-6-rev	TCTTATCAACCAGCAGCTGGCC

Table 5. Cq value in qPCR experiment

The amplified region in Actb1 gene is used as the reference for quantitative PCR analysis.

We noticed different cleavage efficiency of each gRNA, and the most efficient gRNAs detected in each Ebf1a-KO, Gata3-KO and Satb2-KO embryo were highlighted with yellow color, whose relative cycle number comparing to the control (Tyr-KO) is the largest.

***Ebf1a*-KO**

Ebf1a-1, *Ebf1a*-4 and *Ebf1a*-8 are regions mutated by the 3 *Ebf1a*-KO gRNAs.

	Actb1	*Ebf1a*-1	*Ebf1a*-4	*Ebf1a*-8
Tyr-Embryo1	22.59	23.97	24.01	23.59
Tyr-Embryo2	24.07	25.96	25.79	25.1
Tyr-Embryo3	23.41	25.1	24.91	24.41
Tyr-Embryo4	22.95	24.61	24.45	23.89

	Actb1	*Ebf1a*-1	*Ebf1a*-4	*Ebf1a*-8
Ebf1a-Embryo1	24.44	35.41	31.28	25.34
Ebf1a-Embryo2	24.67	31.3	28.07	26.06
Ebf1a-Embryo3	22.61	33.54	24.98	23.78
Ebf1a-Embryo4	23.96	29.83	29.1	25.2

***Gata3*-KO**

Gata3-1, *Gata3*-2 and *Gata3*-5 are regions mutated by the 3 *Gata3*-KO gRNAs.

	Actb1	*Gata3*-1	*Gata3*-2	*Gata3*-5
Tyr-Embryo1	22.79	25.12	23.51	24.77
Tyr-Embryo2	22.89	25.26	23.58	24.83
Tyr-Embryo3	21.8	ND	22.78	ND
Tyr-Embryo4	21.49	ND	22.47	ND

	Actb1	*Gata3*-1	*Gata3*-2	*Gata3*-5
Gata3-Embryo1	23.99	32.91	29.36	27.12
Gata3-Embryo2	23.28	31	28.99	29.91
Gata3-Embryo3	21.73	ND	27.91	ND
Gata3-Embryo4	21.62	ND	28.88	ND

ND: not detected. For Tyr-Embryo3/4 & Gata3-Embryo3/4, we only detected the efficiency of the Gata3-KO-2 gRNA.

***Satb2*-KO**

Satb2-2, *Satb2*-5 and *Satb2*-6 are regions mutated by the 3 *Satb2*-KO gRNAs.

	Actb1	*Satb2*-2	*Satb2*-5	*Satb2*-6
Tyr-Embryo1	23.17	24.19	24.51	23.43
Tyr-Embryo2	24.59	25.73	25.71	23.77
Tyr-Embryo3	23.35	24.47	24.7	23.26

	Actb1	*Satb2*-2	*Satb2*-5	*Satb2*-6
Satb2-Embryo1	22.52	24.71	27.19	23.7
Satb2-Embryo2	23.06	31.23	29.38	23.74
Satb2-Embryo3	22.89	30.76	25.23	23.59

Table 6. Primer sequences used in the detection of Indels generated by CRISPR/Cas9 system.

Primer sequences in this sequencing experiment	
ebf1a-1-for	GCAATTCACGTGTGCTATTTCAGGGCTT
ebf1a-1-rev	CCATTTTCACTCAAATTTGCAAAACCGATATGT
ebf1a-4-for	CCTGAAATTCTTCCTCAAATGTAACCAG
ebf1a-4-rev	CTGTAACACATATTATTTGCTATACGGAATGC
ebf1a-8-for	TGCCTTGTGGTTGCAAACTGCTAAAGC
ebf1a-8-rev	CCCGTTGAATAAGTGCATCATCTGGGTATTT
gata3-1-for	GCGGATCCAATTTTGTATTCGAGCTTTTGAC
gata3-1-rev	CCAGGGTACTAAAAAGATGTGAAACCAGTG
gata3-2-for	GGCCTTTGACGTGCAGTTTCACAGTT
gata3-2-rev	GATTGAGGCCATGCTCCGACTATGAGC
gata3-5-for	CGGGAAAATGTCATCAGTTTTAATGGGCAC
gata3-5-rev	GGGTCAATTGAATAGGTCTTGCGAAATGC
satb2-2-for	GCAGGTGTGAGTAAATGTGAGGGC
satb2-2-rev	GGTCTTCTCTGTTAGCTAATGATTTCC
satb2-5-for	GGCCAGGCTAAACTTTTTATCTGCACTTCT
satb2-5-rev	GAAATGGCCCGTGAATGCAAGGAATTTC
satb2-6-for	TCAGTCTCAGCCTCCACCTCAAGGG
satb2-6-rev	TGACCCCAGATTAATAAAGGGGCTAAGCC

Table 7. Indel sequences detected in each embryo

The genomic DNAs used for this experiment are different from those for the qPCR experiment, so we used successive numbers to name the samples.

We listed the representative Indel sequence in each embryo.

PAM sequence of each gRNA is displayed in blue color. Mutated or inserted sequences are in red color and deleted sequences are shown with "-" symbol.

***Ebf1a*-KO**	
Ebf1a-KO-1 Region	
Wildtype:	CGTATAGCGCTAATACGAAGTGGAAG
Ebf1a-Embryo5	CGTATAGCGCTAAAGATAAG - - GAAG
Ebf1a-Embryo6	CGTATAGCGCTAATAC - - - - - - - - AG
Ebf1a-KO-4 Region	
Wildtype:	GAAAGCGTCGCATGTCTCGTGGGTTCC
Ebf1a-Embryo7	GAAAGCGTCGCATGTCT - - - GGGTTCC
Ebf1a-Embryo8	GAAAGCGTCGCATGTC - -GTGGGTTCC
Ebf1a-KO-8 Region	
Wildtype:	GGTAAGCGCTCAGGGTCGCCCGGGTGT
Ebf1a-Embryo9	GGTAAGCGCTCAGGGTC - - - CGGGTGT
Ebf1a-Embryo10	GGTAAGCGC - - - - - CCCCCCCGGGTGT
***Gata3*-KO**	
Gata3-KO-1 Region	
Wildtype:	CGTACTACGGGAACCCGGTTCGGGCCGT
Gata3-Embryo5	CGTACTA - - - - - - - - - - - - CGGGCCGT
Gata3-Embryo6	CGTACTACGGGAACCCGG - - - - - ACCGT
Gata3-KO-2 Region	
Wildtype:	GGGAAAGGCCCAAGGTTCCAGGGGGAGG
Gata3-Embryo7	GGGAAAGGCCCAAGGTT - - - - - - - - - - -
Gata3-Embryo8	GGGAAAGG -
Gata3-KO-5 Region	
Wildtype:	GCATGAGGTCCCAGCTCGTCTGGCAGC
Gata3-Embryo9	GCATGACTGGCAAACTTGCGCATGACTGGCAGC
Gata3-Embryo10	GCATGAGGTCCCAG - - -GTCTGGCAGC

***Satb2*-KO**

Satb2-KO-2 Region	
Wildtype:	GAGACTGCTCTCCTCGCCCTCGGCTAC
Satb2-Embryo4	GAGACTGCTCTCCTCG - - - - - - GCTAC
Satb2-Embryo5	GAGACTGCTCTCCTC - - - - - - - - - - - -
Satb2-KO-5 Region	
Wildtype:	GGGCGTTGCGTACTGTTGCGTGGTTCC
Satb2-Embryo6	GGGCGTTGCGTACTG - - - - - TGGTTCC
Satb2-Embryo7	GAGCGTTGCG - - - - - - - - - - -TGGTTCC
Satb2-KO-6 Region	
Wildtype:	GGTTGGAGCCGGGCTCTCCAGGGCCCC
Satb2-Embryo8	GGTTGGAG - - - - - - - - - - - -AGGGCCCC
Satb2-Embryo9	GGTTGGAGCC - - - - - - - - - - -GGGCCCC

Methods

Fish husbandry

Adult fish and larvae are kept in an aquatic circulating system, where the water temperature is maintained at 26–28.5°C, and the light is adjusted to a 13/11-hour light/dark cycle. Before breeding, one pair of adult fishes is transferred to an individual tank and separated from each other by a divider. Embryos are collected in the morning within 20 minutes after pulling off the divider and raised at 28.5°C in an incubator on the same light/dark cycle as that in the aquatic system. All manipulations in the animal experiments comply with the regulations of California Institute of Technology Institutional Animal Care and Use Committee, and performed in full compliance with the U.S. laws, guidelines and policies of laboratory animal care and use.

Generation of CRISPR-Cas9 mediated knock-in line Tg(*Phox2bb*:*mNeonGreen*)

To isolate ENS cells, we generated a reporter line by inserting mNeonGreen fluorescent protein after the *Phox2bb* coding sequence, such that mNeonGreen faithfully recapitulates endogenous *Phox2bb* expression. To achieve this, we designed a *Phox2bb*-KI-guide (g) RNA (5' - TCCGCCCAGAGAGTCCGGAA) using Benchling (https://benchling.com) to target the *Phox2bb* coding sequence before the stop codon. To synthesize the gRNA, we first amplified the template of gRNA from a plasmid carrying gRNA scaffold with the forward primer: 5'-ATCACTAATACGACTCACTATAGGCCGCCCAGAGAGTCCGGAAGTTTAAGAG CTATGCTG and the reverse primer: 5'-AAAAAAGCACCGACTCGGTGCCA. In the 5'-to-3' direction, the forward primer includes (1) five nucleotides (ATCAC) to enhance the binding of T7 RNA polymerase to the promoter; (2) T7 promoter sequence (TAATACGACTCACTATA) for reverse transcription; (3) 21-nucleotide spacer (GGCCGCCCAGAGAGTCCGGAA) of *Phox2bb*-KI-gRNA by replacing the first T to GG for better yield; (4) sequence matching with the gRNA scaffold (GTTTAAGAGCTATGCTG) for amplification from the plasmid. We also synthesized donor DNA that harbored the remaining *Phox2bb* coding sequence after the cleavage site, plus a 2A self-cleaving peptide and *mNeonGreen* gene, flanked by 30-35bp microhomology arms (left microhomology arm: 5' -

CAAGGTTGGGCCTCAGCCCCGGGCACCATCACC; right microhomology arm: 5' -CGGA CTCTCTGGGCGGACCGTTCGCTAGCGTTCTG) which have identical sequences to the regions beside the cleavage site. To avoid the cleavage of donor DNA by the CRISPR/Cas9 system, we altered the PAM sequence in the donor DNA by changing the codon sequence of serine from TCC to AGT (fig. S1A). We also added three tandem SV40 nuclear localization signal (NLS) sequences after mNeonGreen to transport the fluorescent protein into the nucleus after translation. Cas9 protein, *Phox2bb*-KI-gRNA and donor DNA were co-injected into zebrafish embryos at the one-cell stage.

Donor DNA sequence:

CAAGGTTGGGCCTCAGCCCCGGGCACCATCACCAGTATTCCGGACTCTCTGG
GCGGACCGTTCGCTAGCGTTCTGTCCTCATTACAAAGACAGAACGGAGCCAA
AGCCACTTTAGTAAAGACCAGCATGTTCGCCACGAACTTCTCTCTGTTAAAGC
AAGCAGGAGACGTGGAAGAAAACCCCGGTCCTATGGTGAGCAAGGGCGAGG
AGGATAACATGGCCTCTCTCCCAGCGACACATGAGTTACACATCTTTGGCTCC
ATCAACGGTGTGGACTTTGACATGGTGGGTCAGGGCACCGGCAATCCAAATG
ATGGTTATGAGGAGTTAAACCTGAAGTCCACCAAGGGTGACCTCCAGTTCTC
CCCCTGGATTCTGGTCCCTCATATCGGGTATGGCTTCCATCAGTACCTGCCCT
ACCCTGACGGGATGTCGCCTTTCCAGGCCGCCATGGTAGATGGCTCCGGATA
CCAAGTCCATCGCACAATGCAGTTTGAAGATGGTGCCTCCCTTACTGTTAACT
ACCGCTACACCTACGAGGGAAGCCACATCAAAGGAGAGGCCCAGGTGAAGG
GGACTGGTTTCCCTGCTGACGGTCCTGTGATGACCAACTCGCTGACCGCTGCG
GACTGGTGCAGGTCGAAGAAGACTTACCCCAACGACAAAACCATCATCAGTA
CCTTTAAGTGGAGTTACACCACTGGAAATGGCAAGCGCTACCGGAGCACTGC
GCGGACCACCTACACCTTTGCCAAGCCAATGGCGGCTAACTATCTGAAGAAC
CAGCCGATGTACGTGTTCCGTAAGACGGAGCTCAAGCACTCCAAGACCGAGC
TCAACTTCAAGGAGTGGCAAAAGGCCTTTACCGATGTGATGGGCATGGACGA
GCTGTACAAGGGAGGTGGAGGTTCACCAAAAAAGAAGAGAAAGGTAGATCC
TAAGAAGAAGCGAAAGGTTGACCCAAAGAAGAAGCGTAAGGTCGAAGCATC
AAGCTGATAACGGACTCTCTGGGCGGACCGTTCGCTAGCGTTCTG

(Left/Right microhomology arms; Serine Codon alteration; *Phox2bb* coding sequence; *P2A*; *mNeonGreen;* 3xNLS)

Embryo collection and tissue dissection

We sorted and raised the F0 founder fish carrying mNeonGreen fluorescence. We outcrossed about 40 Tg(*Phox2bb: mNeonGreen*) fish of F1 generation (equal numbers of males and females) with wild-type ABWT fish to produce developmentally synchronized embryos. Embryos are raised in E3 medium (https://cshprotocols.cshlp.org/content/2011/10/pdb.rec66449) and are then transferred to 0.003% 1-phenyl-2-thiourea (PTU)/E3 medium to slow down pigmentation progress and thus diminish cellular autofluorescence effect on cell sorting. We then carefully sorted healthy F2 Tg(*Phox2bb: mNeonGreen*) embryos at the desired stages. About half were *mNeonGreen*+ following Mendelian inheritance. We dissected about 250 F2 embryos at 2dpf, about 200 embryos at 3dpf and 4dpf, and about 100 embryos at 5dpf and 6dpf. While we were unable to sex the embryos, we assume the F2 embryos have a similar number of males and females.

Cell dissociation

Embryos and larvae at 2, 3, 4, 5 and 6 dpf were anesthetized by tricaine Methanesulfonate (MS222) and the head regions were dissected away. The remainder of the embryo/larvae were kept in Ringer's Solution on ice and dissociated with Accumax cell dissociation solution at 30ºC for 20, 23, 28, 32 and 36 mins at 1000rpm in the Eppendorf thermomixer R system. The dissociation duration was optimized according to several criteria—number of cells remaining in the digestive tract after dissociation observed by fluorescent microscope, number of cells sorted out and viable after trypan blue staining. After digestion, Accumax was quenched by ice-cold resuspension buffer (Recipe listed below), and samples were then passed through a 70um cell strainer into 50ml conical tube, centrifuged at 300g for 10 mins and resuspended in 500ul fresh resuspension buffer for cell sorting.

Resuspension Buffer:

1X Hanks' Balanced Salt Solution, no calcium, no magnesium (HBSS)

10mM HEPES, adjusted to PH 8.0

2.5 mg/ml BSA

Cell barcoding, Library prep and sequencing

After sorting, mNeonGreen-positive cells were stained with trypan blue and observed under the microscope to check cell viability and cell number. 8000-1,5000 cells at different time points were loaded to the 10X Genomics instrument for single cell barcoding. Libraries were prepared with chromium single cell 3' reagent kit v2 following the manufacturer's instructions and sequenced for 3 lanes in Illumina HiSeq 4000 sequencing system.

Single-cell RNA-seq analysis - cell clustering and DEG analysis

We preprocessed the raw data from 5 different time points separately using Kallisto and bustools programs[61,62] to quantify gene abundance in single cells and generate the gene-cell matrices. We constructed a reference transcriptome for pseudoalignment based on zebrafish genome assembly GRCz10. We then read and concatenated 5 datasets generated by Kallisto and bustools programs using Scanpy package[63]. We performed quality control to first remove cells with <500 genes, and then cells with > 13,000 counts or ratio of mitochondrial genes to total genes ≥ 0.05. Genes expressed in fewer than 50 cells were also eliminated. We saved the preprocessed data, and with the remaining 24,039 cells, we detected doublets with the DoubletDetection algorithm[64] and the parameters were set as clf = doubletdetection.BoostClassifier(n_iters=30, standard_scaling = True, pseudocount = 0.1, n_jobs=-1) and doublets = clf.fix(ENS.X).predict(p_thresh=1e-16, voter_thresh=0.5). After doublet detection, we normalized the data to 10,000 total-counts per cell, and log-transformed the data. Then we identified 1715 highly variable genes by setting the threshold with minimum and maximum means equal to 0.015 and 3, respectively, and with minimum dispersion equal to 0.45. After regressing out the source of variation from expression of mitochondrial genes, we performed PCA and visualized the data in two dimensions by running the UMAP algorithm with the parameter settings as n_neighbors = 16 and n_pcs = 40. Cell clusters were further revealed using Leiden algorithm with resolution = 0.75; 21 clusters in total were discovered.

Next, we found marker genes in each cluster and inferred possible non-ENS cells. We filtered out doublets and non-ENS cell clusters. We selected the ENS cells repeated the above analysis performed PCA and visualized the data in two dimensions by running the

UMAP algorithm with the parameter settings as n_neighbors = 14 and n_pcs = 24. Cell clusters are further revealed using the Leiden algorithm with resolution = 0.9, and 23 clusters in total are discovered. The data were saved for advanced analysis.

We used the Single Cell Pipeline (SCP) algorithm[65] and transferred the data from Python to R to find differentially expressed genes in each cluster. The marker genes were screened out based on the criteria avg_log2FC >1 and p_val_adj<0.06.

Single cell data are available in GEO.

Single-cell RNA-seq analysis - RNA velocity analysis using UniTVelo package

We employed the temporally unified RNA velocity (UniTVelo) package[48] for RNA velocity and transcription rates analysis to infer the developmental progress from ENS progenitors to mature neurons. We loaded the data processed with Scanpy package and applied the dynamical mode from scVelo package[66] for preprocessing and found 1202 genes with distinct spliced and unspliced abundance information among 1898 highly variable genes. We set up the parameters as follows: velo_config.R2_ADJUST = True, velo.IROOT = 20 (One of the progenitor clusters expressing marker gene *Cdc20*), velo.FIT_OPTION = '1' (Unified-time mode), velo_config.N_TOP_GENES = 1202.

Single-cell RNA-seq analysis - developmental trajectory and bifurcation analysis with scFates package

We used scFates package[49] to find genes upregulated and downregulated along the developmental trajectory of each neuronal lineage and search for key transcription factors that play important roles in cell fate decision. We first loaded the data processed with the Scanpy package, and used Palantir[67] package for multiscale diffusion space calculation with the parameters palantir.utils.run_diffusion_maps(pca_projections, n_components = 40), palantir.utils.determine_multiscale_space(dm_res, n_eigns = 40). Then we calculated the neighborhood graph of cells with n_neighbors = 60 and the matrix use_rep = "X_palantir," and produced the UMAP plot. To infer the developmental tree, we used SimplePPT algorithm with the parameters Nodes = 1000, ppt_sigma = 0.1, ppt_lambda = 1 and ppt_nsteps = 400. We trimmed off stray leaves and tiny branches with only one node and obtained the final trajectory. With this trajectory, we defined the root node, and

performed pseudotime analysis and generated a dendrogram to reconstruct the developmental tree of the ENS. Next, we performed functions to find genes with significant variance along the tree and screened out 1258 genes. We further fit the genes along the developmental trajectory from the progenitor to each terminal cell type and labeled transcription factors in the top 200 gene list ranked by expression abundance in the heatmap plot. To identify genes driving the differentiation of neuronal subtypes, we chose a subtree containing common parent cells and two branches and then examined genes with high differential expression between the post-bifurcation branches. We set the parameter to detect minimum expression differences "effect = 0.6" and used the default settings for others in the scFate.tl.branch_specific function.

Hybridization Chain Reaction (HCR)

Zebrafish embryos at selected stages are transferred to Ringer's solution and anesthetized in 0.01% MS-222. We then used forceps to gently remove the yolks and fixed embryos overnight at 4^{o}C with 4% paraformaldehyde (PFA) dissolved in phosphate-buffered saline (PBS). The next day, we washed with PBS 3 times for 5 minutes each (3 X 5 mins) to terminate the fixation, dehydrated in methanol for 5 mins, and changed to fresh methanol for long-time storage in -20^{o}C.

The probes and reagents for HCR experiment were purchased from the Molecular Technologies resource at California Institute of Technology. Before performing HCR, we first prepared slides. We cut a rectangular-shape hole in a fragment of insulation tape and attached the tape to a superfrost slide. For tight attachment, we usually covered the superfrost slide with a plain slide and pressed the whole set for ~1 hour. Next, we transferred embryos from the freezer to 50% methanol in a RNase-free petri dish for dissection. After dissecting out the entire intact gut, it was placed in fresh methanol for 5 mins, and then transferred to the superfrost slide. After the methanol evaporated, the gut samples stuck tightly to the slide.

We rehydrated the samples by incubating in 75%, 50% and 25% methanol/PBST (0.1% Triton and 0.05% Tween20 in PBS) for 5 mins each in turn and washed off methanol with PBS for 5 X 5 mins. Then we added the HCR probe hybridization buffer and incubated at 37^{o}C for 30 mins. For long incubations, slides were placed in a moist chamber. In the

meantime, we prepared probe solution by adding 8 to 24 pmol of each probe mixture to hybridization buffer depending on the expression levels of genes of interest. Then, we removed the hybridization buffer from the slide, added probe solution and incubated at 37^{o}C overnight. The next day, we first washed embryos 5 X 20 min with probe wash buffer at 37^{o}C and then washed with 5 X SSCT (0.1% Tween20 in 5 X sodium chloride sodium citrate) for 3 X 5 mins at room temperature. From then on, all the experiments are performed at room temperature. We incubated embryos in amplification buffer for 30 mins. During this time, we prepared hairpins. We heated up 30 pmol of hairpin H1 and 30 pmol of hairpin H2 (10 µL of 3 µM stock) separately at 95^{o}C for 90 seconds and cooled down to room temperature in dark for 30 mins. Prepared hairpins are added to 500 µL of amplification buffer. We then removed amplification buffer from embryos and added hairpin solution and incubated the slide in dark overnight. The third day, we washed samples with 5 X SSCT as follows: 2 X 5 mins, 2 X 30 min and 1X 5min. We used Zeiss LSM 800 confocal microscope for imaging. HCR probes, hairpins, hybridization buffer, wash buffer and amplification buffer are purchased from the Molecular Technologies resource in Caltech.

When detecting *Sox10*, *Phox2bb* and *Elavl3* expression, we first performed HCR using anti-*Sox10* probes. After that, we fixed the sample at room temperature for about 15 mins and then washed with PBST for 3 X 5 mins. The samples are then incubated with block buffer for immunohistochemistry using mouse anti-Phox2b IgG1 (Santa Cruz Biotechnology, sc-376997) and mouse anti-HuC/D IgG2b (Thermo Fisher Scientific, A21271) antibodies. We followed whole-mount immunohistochemistry (IHC) staining protocol described previously[41].

For sequential HCR detecting multiple neurotransmitter-related genes, after imaging, we washed off probes and hairpins with in situ hybridization buffer without tRNA (50% formamide, 5 X SSCT, 50 µg/mL heparin, 0.1% Tween20) at 50 ^{o}C for 4 X 20 mins. We checked the fluorescent signals under the confocal microscope again and confirmed all the signal was stripped off. Then, the samples were washed with 5 X SSCT and incubated with HCR probe hybridization for next-round staining.

Analysis of sequential HCR results

We imaged samples with a 20X objective; in each channel, we applied 10-26 slices with 3μm intervals between each two slices in the z-axis and four tiles to cover the whole gut sample. After imaging, we used Fiji[68] to analyze sequential HCR results. We first employed Average intensity projection to project each z-stack to a single image and then concatenate all 9 images into a new stack. We used two plugins Template Matching and Slice Alignment[69] and Image Stabilizer[70] to align the images. After alignment, we merged all 9 images together, and then manually registered each cell in this image. During this process, we referred to the original z-stack to make sure signals in the range of a cell came from a single cell, rather than two or more overlapping cells in the z-axis.

Double fluorescent in situ hybridization

We amplified cDNAs from an 84-hpf cDNA library, purified cDNA with QIAquick Gel Extraction Kit, and performed in vitro transcription using T7 RNA polymerase (Promega, P2075) supplemented with RNasin Ribonuclease Inhibitor (Promega, N2111). We incubated overnight at 37ºC. The next day, we added 1 μL TURBO DNase (Thermo Fisher Scientific, AM2238) per 20 μL system and incubated at 37 ºC for 15-20 mins to terminate the reaction. We then followed MEGAscript Kit User Guide (Thermo Fisher Scientific) to purify RNA probes. Primers used to amplify cDNA templates are as follows: *Ebf1a* (Two probes are used for *Ebf1a* staining. forward-1: 5' - ATGTTCGGGATTCAAGACAGCATTCAAAG and reverse-1: 5' - GCAAAACCGATATGTGTAAAGGATAACG, forward-2: 5' - CTCATAACCCCTCATGCCATCCGAGT and reverse-2: 5' - GATGACTAATACGACTCACTATAGGCTGAAATCAAATGTGCCTCTTCAGC); *Vipb* (first amplified with forward-1: 5' - GGAAACTATTCTTCATCCTAACAGGTG and reverse: 5' - CAAGTCACTAATACGACTCACTATAGGTTTCATTTCAATTATCA AGAATGACTACAG, followed by a second-round PCR with forward-2: AACAGGTGTCAGCGGACAGAGAT and reverse primer); When generating the first probe targeting *Ebf1a*, after amplification, we cloned the cDNA into pGEM-T Easy vector (Promega, A1360). After confirming the correct insertion by plasmid sequencing. We cut the plasmid, purified DNA and then continued to do in vitro transcription.

De-yolking, fixation and dehydration in methanol were performed as described above. After rehydration, we performed double in situ hybridization following a previously published protocol[71] but with changes in the wash step after TSA Plus Cy3 incubation. To further increase signal-to-background ratio, we washed with 25%, 50%, 75% ethanol in PBST for 10 mins each, rehydrated again with 50% and 25% ethanol in PBST and washed with PBST for 3 X 5 mins. Finally, we dissected gut samples and mounted them on slides for imaging.

CRISPR/Cas9-mediated perturbation experiments

We followed a previous publication applying crRNA-tracrRNA and Cas9 complex for efficient gene knockout in the F0 generation[57] by simultaneously injecting 3 guide RNAs, adjusting the protocol for our microinjection device. We first ordered crRNA, tracrRNA and Cas9 from IDT. Next, we tested each crRNA by staining marker genes, like *Adcyap1b* (*Ebf1a*-KO), *Cart2* (*Gata3*-KO) and *Tph1b* (*Satb2*-KO) in both control and experimental groups to evaluate the severity of the phenotypes and determine the crRNA cleavage efficiency. Then we mixed three different crRNA-TracrRNA complexes targeting each gene together with Cas9 for perturbation experiment - *Tyr* (5'-GGACTGGAGGACTTCTGGGG; 5'-GATGCATTATTACGTGTCCC; 5'-GAACCTCTGCCTCTCGGTAG), *Ebf1a* (5'-CGTATAGCGCTAATACGAAG; 5'-GAAAGCGTCGCATGTCTCGT; 5'-GGTAAGCGCTCAGGGTCGCC), *Gata3* (5'-CGT ACTACGGGAACCCGGTT; 5'-GGGAAAGGCCCAAGGTTCCA; 5'-GCATGAGGTCCCAG CTCGTC) and *Satb2* (5'-GAGACTGCTCTCCTCGCCCT; 5'-GGGCGTTGCGTACTGTTGC G; 5'-GGTTGGAGCCGGGCTCTCCA). We used a microinjection device from World Precision Instrument company with minimal injection volume of 2.3nl and decreased the concentration of crRNA-TracrRNA and Cas9 accordingly. We resuspended 2nmol crRNA in 23ul of Duplex buffer, and 5nmol tracrRNA in 57.5ul of Duplex buffer. We then mixed 1ul of crRNA, 1ul of tracrRNA and 1.28ul of Duplex buffer and heated up to 95^{o}C for 5 minutes in the thermocycler. The final concentration of the crRNA-tracrRNA complex (gRNA) was about 26.52uM. Next, we diluted 1ul Cas9 (61uM) in 1.3ul of Duplex buffer to make the concentration of Cas9 equal to the gRNA. Then we added an equal volume of gRNA and diluted Cas9 and incubated

the mixture at 37ºC for 6 minutes. Finally, we mixed three different gRNA/Cas9 complex targeting the same gene at a ratio of 1:1:1 for injection for both control and experimental manipulations.

Before performing perturbation experiments, we let the wild-type male and female fish breed at least two rounds to clean poor-quality eggs and thus diminish individual variation between embryos. We set up 1 adult male and 1 adult female fish in the container and installed a divider between them. Before the injection, we removed the divider and let the fish produce eggs for about 10 minutes. After collecting the embryos, we microinjected the control and experimental (*Ebf1a/Gata3/Satb2*) Cas9/gRNA complex separately into the embryos from the same clutch. After injection, embryos were incubated at 28.5ºC for 6 days. We detected expression of neurotransmitter-related genes in two groups of embryos by HCR. We counted cells manually with the assistance of Fiji. For statistical analysis, we used PRISM (GraphPad) software. We applied the multiple unpaired t test analysis from the Grouped analyses list and error bars represent standard deviation of the mean (Mean with SD).

Analysis of perturbation efficiency by qPCR

To detect the percentage of InDels, we performed qPCR analysis of mutations in genomic regions of *Ebf1a, Gata3* and *Satb2* knockout tissue compared with *Tyr* control. For each gRNA target region, we designed one primer whose center is located close to the putative cleavage site by gRNA/Cas9, and another primer to cooperate with this primer for amplification. If there are large insertions or deletions occurring around the cleavage site, no PCR products would be generated. We also designed primers that target the *Actin beta1* gene as the reference for qPCR analysis. We cut the tails from the control and experimental embryos and then fixed the remaining part for HCR and imaging. We then extracted genomic DNA from the tails. For each control or experimental sample, we first diluted and added 20ul 1X Taq polymerase buffer (Sigma, Catalog number 11146165001), and then heated the sample at 95ºC for 15 mins. We added 2.5 ul 20mg/ml proteinase K and incubated at 50ºC for 3 hours for full digestion. Finally, the samples were incubated at 95ºC for 15 mins to deactivate the proteinase K. The samples were centrifuged at 13000 rpm for 1 min and 20ul of the supernatant was transferred to a new tube for qPCR. We added 80 ul of FastStart

Universal SYBR Green Master (ROX) (Sigma, Catalog number 4913850001) into each sample, mixed well and then distributed 12.5 ul of the reagent each well of a 96-well plate. We added primers for amplifying *Actb1* (reference) and three gRNA targeting regions. There were two replicates for each PCR product. The qPCR program for detecting the efficiency of *Ebf1a*-gRNAs is set as: Step 1, 50ºC for 2 min and 95ºC for 10 min; Step 2, 40 cycles at 95ºC for 15 sec and 57ºC for 1 min; Step 3, melting curve step for detecting the amplification specificity. The only difference of the program for *Gata3* and *Satb2* was the annealing temperature which was set at 58ºC.

For Indels, we first extracted genomic DNAs from embryos injected with 3 combinatorial gRNAs, and then designed primers for each gRNA target region to amplify DNA fragments with the length of 200-700 bp. Next, we purified the PCR products and sent them to the Plasmidsaurus company for sequencing. Different embryos were used for Indel sequencing than for qPCR.

BIBLIOGRAPHY

1. Uribe, R.A. (2024). Genetic regulation of enteric nervous system development in zebrafish. Biochemical Society Transactions *52*, 177–190. 10.1042/BST20230343.

2. Heanue, T.A., Boesmans, W., Bell, D.M., Kawakami, K., Vanden Berghe, P., and Pachnis, V. (2016). A Novel Zebrafish ret Heterozygous Model of Hirschsprung Disease Identifies a Functional Role for mapk10 as a Modifier of Enteric Nervous System Phenotype Severity. PLoS Genet *12*, e1006439. 10.1371/journal.pgen.1006439.

3. Huang, S., Wang, Y., Luo, L., Li, X., Jin, X., Li, S., Yu, X., Yang, M., and Guo, Z. (2019). BMP2 Is Related to Hirschsprung's Disease and Required for Enteric Nervous System Development. Front. Cell. Neurosci. *13*, 523. 10.3389/fncel.2019.00523.

4. Kuil, L.E., Chauhan, R.K., De Graaf, B.M., Cheng, W.W., Kakiailatu, N.J.M., Lasabuda, R., Verhaeghe, C., Windster, J.D., Schriemer, D., Azmani, Z., et al. (2024). ATP5PO levels regulate enteric nervous system development in zebrafish, linking Hirschsprung disease to Down Syndrome. Biochimica et Biophysica Acta (BBA) - Molecular Basis of Disease *1870*, 166991. 10.1016/j.bbadis.2023.166991.

5. Howard, A.G., Baker, P.A., Ibarra-García-Padilla, R., Moore, J.A., Rivas, L.J., Tallman, J.J., Singleton, E.W., Westheimer, J.L., Corteguera, J.A., and Uribe, R.A. (2021). An atlas of neural crest lineages along the posterior developing zebrafish at single-cell resolution. eLife *10*, e60005. 10.7554/eLife.60005.

6. Kuil, L.E., Kakiailatu, N.J.M., Windster, J.D., Bindels, E., Zink, J.T.M., Van Der Zee, G., Hofstra, R.M.W., Shepherd, I.T., Melotte, V., and Alves, M.M. (2023). Unbiased characterization of the larval zebrafish enteric nervous system at a single cell transcriptomic level. iScience *26*, 107070. 10.1016/j.isci.2023.107070.

7. Roy-Carson, S., Natukunda, K., Chou, H., Pal, N., Farris, C., Schneider, S.Q., and Kuhlman, J.A. (2017). Defining the transcriptomic landscape of the developing enteric nervous system and its cellular environment. BMC Genomics *18*, 290. 10.1186/s12864-017-3653-2.

8. Pattyn, A., Morin, X., Cremer, H., Goridis, C., and Brunet, J.F. (1997). Expression and interactions of the two closely related homeobox genes Phox2a and Phox2b during neurogenesis. Development *124*, 4065–4075. 10.1242/dev.124.20.4065.

9. Pattyn, A., Morin, X., Cremer, H., Goridis, C., and Brunet, J.-F. (1999). The homeobox gene Phox2b is essential for the development of autonomic neural crest derivatives. Nature *399*, 366–370. 10.1038/20700.

10. Corpening, J.C., Cantrell, V.A., Deal, K.K., and Southard-Smith, E.M. (2008). A Histone2BCerulean BAC transgene identifies differential expression of *Phox2b* in migrating enteric neural crest derivatives and enteric glia. Dev. Dyn. *237*, 1119–1132. 10.1002/dvdy.21498.

11. Elworthy, S., Pinto, J.P., Pettifer, A., Cancela, M.L., and Kelsh, R.N. (2005). Phox2b function in the enteric nervous system is conserved in zebrafish and is sox10-dependent. Mechanisms of Development *122*, 659–669. 10.1016/j.mod.2004.12.008.

12. Shaner, N.C., Lambert, G.G., Chammas, A., Ni, Y., Cranfill, P.J., Baird, M.A., Sell, B.R., Allen, J.R., Day, R.N., Israelsson, M., et al. (2013). A bright monomeric green fluorescent protein derived from Branchiostoma lanceolatum. Nat Methods *10*, 407–409. 10.1038/nmeth.2413.

13. Hisano, Y., Sakuma, T., Nakade, S., Ohga, R., Ota, S., Okamoto, H., Yamamoto, T., and Kawahara, A. (2015). Precise in-frame integration of exogenous DNA mediated by CRISPR/Cas9 system in zebrafish. Sci Rep *5*, 8841. 10.1038/srep08841.

14. Shepherd, I.T., Beattie, C.E., and Raible, D.W. (2001). Functional Analysis of Zebrafish GDNF. Developmental Biology *231*, 420–435. 10.1006/dbio.2000.0145.

15. Uribe, R.A., and Bronner, M.E. (2015). Meis3 is required for neural crest invasion of the gut during zebrafish enteric nervous system development. MBoC *26*, 3728–3740. 10.1091/mbc.E15-02-0112.

16. Holmberg, A., Schwerte, T., Pelster, B., and Holmgren, S. (2004). Ontogeny of the gut motility control system in zebrafish *Danio rerio* embryos and larvae. Journal of Experimental Biology *207*, 4085–4094. https://doi.org/10.1242/jeb.01260.

17. Young, H.M., Bergner, A.J., and Müller, T. (2003). Acquisition of neuronal and glial markers by neural crest–derived cells in the mouse intestine. J of Comparative Neurology *456*, 1–11. 10.1002/cne.10448.

18. Southard-Smith, E.M., Kos, L., and Pavan, W.J. (1998). SOX10 mutation disrupts neural crest development in Dom Hirschsprung mouse model. Nat Genet *18*, 60–64. 10.1038/ng0198-60.

19. Mundell, N.A., Plank, J.L., LeGrone, A.W., Frist, A.Y., Zhu, L., Shin, M.K., Southard-Smith, E.M., and Labosky, P.A. (2012). Enteric nervous system specific deletion of Foxd3 disrupts glial cell differentiation and activates compensatory enteric progenitors. Developmental Biology *363*, 373–387. 10.1016/j.ydbio.2012.01.003.

20. Van De Putte, T., Francis, A., Nelles, L., Van Grunsven, L.A., and Huylebroeck, D. (2007). Neural crest-specific removal of Zfhx1b in mouse leads to a wide range of neurocristopathies reminiscent of Mowat–Wilson syndrome. Human Molecular Genetics *16*, 1423–1436. 10.1093/hmg/ddm093.

21. Bruno, S., Ghelli Luserna Di Rorà, A., Napolitano, R., Soverini, S., Martinelli, G., and Simonetti, G. (2022). CDC20 in and out of mitosis: a prognostic factor and therapeutic target in hematological malignancies. J Exp Clin Cancer Res *41*, 159. 10.1186/s13046-022-02363-9.

22. Grolmusz, V.K., Karászi, K., Micsik, T., Tóth, E.A., Mészáros, K., Karvaly, G., Barna, G., Szabó, P.M., Baghy, K., Matkó, J., et al. (2016). Cell cycle dependent RRM2 may serve as proliferation marker and pharmaceutical target in adrenocortical cancer. Am J Cancer Res *6*, 2041–2053.

23. Thijssen, P.E., Ito, Y., Grillo, G., Wang, J., Velasco, G., Nitta, H., Unoki, M., Yoshihara, M., Suyama, M., Sun, Y., et al. (2015). Mutations in CDCA7 and HELLS cause immunodeficiency–centromeric instability–facial anomalies syndrome. Nat Commun *6*, 7870. 10.1038/ncomms8870.

24. Duggan, A., Madathany, T., De Castro, S.C.P., Gerrelli, D., Guddati, K., and García-Añoveros, J. (2008). Transient expression of the conserved zinc finger gene INSM1 in progenitors and nascent neurons throughout embryonic and adult neurogenesis. J of Comparative Neurology *507*, 1497–1520. 10.1002/cne.21629.

25. Bouilloux, F., Thireau, J., Ventéo, S., Farah, C., Karam, S., Dauvilliers, Y., Valmier, J., Copeland, N.G., Jenkins, N.A., Richard, S., et al. (2016). Loss of the transcription factor Meis1 prevents sympathetic neurons target-field innervation and increases susceptibility to sudden cardiac death. eLife *5*, e11627. 10.7554/eLife.11627.

26. Ohnishi, T., Shirane, M., and Nakayama, K.I. (2017). SRRM4-dependent neuron-specific alternative splicing of protrudin transcripts regulates neurite outgrowth. Sci Rep *7*, 41130. 10.1038/srep41130.

27. Kobayashi, I., Kobayashi-Sun, J., Kim, A.D., Pouget, C., Fujita, N., Suda, T., and Traver, D. (2014). Jam1a–Jam2a interactions regulate haematopoietic stem cell fate through Notch signalling. Nature *512*, 319–323. 10.1038/nature13623.

28. El Wakil, A., Francius, C., Wolff, A., Pleau-Varet, J., and Nardelli, J. (2006). The GATA2 transcription factor negatively regulates the proliferation of neuronal progenitors. Development *133*, 2155–2165. 10.1242/dev.02377.

29. Saaber, F., Schütz, D., Miess, E., Abe, P., Desikan, S., Ashok Kumar, P., Balk, S., Huang, K., Beaulieu, J.M., Schulz, S., et al. (2019). ACKR3 Regulation of Neuronal Migration Requires ACKR3 Phosphorylation, but Not β-Arrestin. Cell Reports *26*, 1473-1488.e9. 10.1016/j.celrep.2019.01.049.

30. Lins, É.M., Oliveira, N.C.M., Reis, O., Ferrasa, A., Herai, R., Muotri, A.R., Massirer, K.B., and Bengtson, M.H. (2022). Genome-wide translation control analysis of developing human neurons. Mol Brain *15*, 55. 10.1186/s13041-022-00940-9.

31. Paik, J., Ding, Z., Narurkar, R., Ramkissoon, S., Muller, F., Kamoun, W.S., Chae, S.-S., Zheng, H., Ying, H., Mahoney, J., et al. (2009). FoxOs Cooperatively Regulate

Diverse Pathways Governing Neural Stem Cell Homeostasis. Cell Stem Cell *5*, 540–553. 10.1016/j.stem.2009.09.013.

32. Kim, D.-Y., Hwang, I., Muller, F.L., and Paik, J.-H. (2015). Functional regulation of FoxO1 in neural stem cell differentiation. Cell Death Differ *22*, 2034–2045. 10.1038/cdd.2015.123.

33. Leal-Calvo, T., Martins, B.L., Bertoluci, D.F., Rosa, P.S., Camargo, R.M.D., Germano, G.V., Brito De Souza, V.N., Pereira Latini, A.C., and Moraes, M.O. (2021). Large-Scale Gene Expression Signatures Reveal a Microbicidal Pattern of Activation in Mycobacterium leprae-Infected Monocyte-Derived Macrophages With Low iiplicity of Infection. Front. Immunol. *12*, 647832. 10.3389/fimmu.2021.647832.

34. Leiter, O., Zhuo, Z., Rust, R., Wasielewska, J.M., Grönnert, L., Kowal, S., Overall, R.W., Adusumilli, V.S., Blackmore, D.G., Southon, A., et al. (2022). Selenium mediates exercise-induced adult neurogenesis and reverses learning deficits induced by hippocampal injury and aging. Cell Metabolism *34*, 408-423.e8. 10.1016/j.cmet.2022.01.005.

35. Ohtsuka, T., Shimojo, H., Matsunaga, M., Watanabe, N., Kometani, K., Minato, N., and Kageyama, R. (2011). Gene Expression Profiling of Neural Stem Cells and Identification of Regulators of Neural Differentiation During Cortical Development. Stem Cells *29*, 1817–1828. 10.1002/stem.731.

36. Endo, M., Doi, R., Nishita, M., and Minami, Y. (2012). Ror-family receptor tyrosine kinases regulate maintenance of neural progenitor cells in the developing neocortex. Journal of Cell Science, jcs.097782. 10.1242/jcs.097782.

37. Borrett, M.J., Innes, B.T., Tahmasian, N., Bader, G.D., Kaplan, D.R., and Miller, F.D. (2022). A Shared Transcriptional Identity for Forebrain and Dentate Gyrus Neural Stem Cells from Embryogenesis to Adulthood. eNeuro *9*, ENEURO.0271-21.2021. 10.1523/ENEURO.0271-21.2021.

38. Wei, J., Zhou, Y., and Besner, G.E. (2015). Heparin-binding EGF-like growth factor and enteric neural stem cell transplantation in the prevention of experimental necrotizing enterocolitis in mice. Pediatr Res *78*, 29–37. 10.1038/pr.2015.63.

39. Baig, S., Nadaf, J., Allache, R., Le, P.U., Luo, M., Djedid, A., Nkili-Meyong, A., Safisamghabadi, M., Prat, A., Antel, J., et al. (2024). Identity and nature of neural stem cells in the adult human subventricular zone. iScience *27*, 109342. 10.1016/j.isci.2024.109342.

40. Green, S.A., Uy, B.R., and Bronner, M.E. (2017). Ancient evolutionary origin of vertebrate enteric neurons from trunk-derived neural crest. Nature *544*, 88–91. 10.1038/nature21679.

41. El-Nachef, W.N., and Bronner, M.E. (2020). De novo enteric neurogenesis in post-embryonic zebrafish from Schwann cell precursors rather than resident cell types. Development, dev.186619. 10.1242/dev.186619.

42. Espinosa-Medina, I., Jevans, B., Boismoreau, F., Chettouh, Z., Enomoto, H., Müller, T., Birchmeier, C., Burns, A.J., and Brunet, J.-F. (2017). Dual origin of enteric neurons in vagal Schwann cell precursors and the sympathetic neural crest. Proc. Natl. Acad. Sci. U.S.A. *114*, 11980–11985. 10.1073/pnas.1710308114.

43. Uesaka, T., Nagashimada, M., and Enomoto, H. (2015). Neuronal Differentiation in Schwann Cell Lineage Underlies Postnatal Neurogenesis in the Enteric Nervous System. Journal of Neuroscience *35*, 9879–9888. 10.1523/JNEUROSCI.1239-15.2015.

44. Solovieva, T., and Bronner, M. (2021). Schwann cell precursors: Where they come from and where they go. Cells & Development *166*, 203686. 10.1016/j.cdev.2021.203686.

45. Shepherd, I.T., Pietsch, J., Elworthy, S., Kelsh, R.N., and Raible, D.W. (2004). Roles for GFRα1 receptors in zebrafish enteric nervous system development. Development *131*, 241–249. 10.1242/dev.00912.

46. Olden, T., Akhtar, T., Beckman, S.A., and Wallace, K.N. (2008). Differentiation of the zebrafish enteric nervous system and intestinal smooth muscle. genesis *46*, 484–498. 10.1002/dvg.20429.

47. Shepherd, I., and Eisen, J. (2011). Development of the Zebrafish Enteric Nervous System. In Methods in Cell Biology (Elsevier), pp. 143–160. 10.1016/B978-0-12-387036-0.00006-2.

48. Gao, M., Qiao, C., and Huang, Y. (2022). UniTVelo: temporally unified RNA velocity reinforces single-cell trajectory inference. Nat Commun *13*, 6586. 10.1038/s41467-022-34188-7.

49. Faure, L., Soldatov, R., Kharchenko, P.V., and Adameyko, I. 2023. scFates: a scalable python package for advanced pseudotime and bifurcation analysis from single-cell data. *Bioinformatics* 39(1): btac746. 10.1093/bioinformatics/btac746

50. Burbach, J.P.H. (2009). Mammalian Neuropeptide Families. In Encyclopedia of Neuroscience (Elsevier), pp. 635–648. 10.1016/B978-008045046-9.01447-9.

51. Schneider, S., Wright, C.M., and Heuckeroth, R.O. (2019). Unexpected Roles for the Second Brain: Enteric Nervous System as Master Regulator of Bowel Function. Annu. Rev. Physiol. *81*, 235–259. 10.1146/annurev-physiol-021317-121515.

52. Morarach, K., Mikhailova, A., Knoflach, V., Memic, F., Kumar, R., Li, W., Ernfors, P., and Marklund, U. (2021). Diversification of molecularly defined myenteric neuron

classes revealed by single-cell RNA sequencing. Nat Neurosci *24*, 34–46. 10.1038/s41593-020-00736-x.

53. Drokhlyansky, E., Smillie, C.S., Van Wittenberghe, N., Ericsson, M., Griffin, G.K., Eraslan, G., Dionne, D., Cuoco, M.S., Goder-Reiser, M.N., Sharova, T., et al. (2020). The Human and Mouse Enteric Nervous System at Single-Cell Resolution. Cell *182*, 1606-1622.e23. 10.1016/j.cell.2020.08.003.

54. Wang, Z., Du, J., Lam, S.H., Mathavan, S., Matsudaira, P., and Gong, Z. (2010). Morphological and molecular evidence for functional organization along the rostrocaudal axis of the adult zebrafish intestine. BMC Genomics *11*, 392. 10.1186/1471-2164-11-392.

55. Kuil, L.E., Chauhan, R.K., Cheng, W.W., Hofstra, R.M.W., and Alves, M.M. (2021). Zebrafish: A Model Organism for Studying Enteric Nervous System Development and Disease. Front. Cell Dev. Biol. *8*, 629073. 10.3389/fcell.2020.629073.

56. Choi, H.M.T., Schwarzkopf, M., Fornace, M.E., Acharya, A., Artavanis, G., Stegmaier, J., Cunha, A., and Pierce, N.A. (2018). Third-generation *in situ* hybridization chain reaction: multiplexed, quantitative, sensitive, versatile, robust. Development *145*, dev165753. 10.1242/dev.165753.

57. Kroll, F., Powell, G.T., Ghosh, M., Gestri, G., Antinucci, P., Hearn, T.J., Tunbak, H., Lim, S., Dennis, H.W., Fernandez, J.M., et al. (2021). A simple and effective F0 knockout method for rapid screening of behaviour and other complex phenotypes. eLife *10*, e59683. 10.7554/eLife.59683.

58. May-Zhang, A.A., Tycksen, E., Southard-Smith, A.N., Deal, K.K., Benthal, J.T., Buehler, D.P., Adam, M., Simmons, A.J., Monaghan, J.R., Matlock, B.K., et al. (2021). Combinatorial Transcriptional Profiling of Mouse and Human Enteric Neurons Identifies Shared and Disparate Subtypes In Situ. Gastroenterology *160*, 755-770.e26. 10.1053/j.gastro.2020.09.032.

59. Memic, F., Knoflach, V., Morarach, K., Sadler, R., Laranjeira, C., Hjerling-Leffler, J., Sundström, E., Pachnis, V., and Marklund, U. (2018). Transcription and Signaling Regulators in Developing Neuronal Subtypes of Mouse and Human Enteric Nervous System. Gastroenterology *154*, 624–636. 10.1053/j.gastro.2017.10.005.

60. Huber, L., Ferdin, M., Holzmann, J., Stubbusch, J., and Rohrer, H. (2012). HoxB8 in noradrenergic specification and differentiation of the autonomic nervous system. Developmental Biology *363*, 219–233. https://doi.org/10.1016/j.ydbio.2011.12.026.

61. Bray, N.L., Pimentel, H., Melsted, P., and Pachter, L. (2016). Near-optimal probabilistic RNA-seq quantification. Nat Biotechnol *34*, 525–527. 10.1038/nbt.3519.

62. Melsted, P., Booeshaghi, A.S., Liu, L., Gao, F., Lu, L., Min, K.H., Da Veiga Beltrame, E., Hjörleifsson, K.E., Gehring, J., and Pachter, L. (2021). Modular,

efficient and constant-memory single-cell RNA-seq preprocessing. Nat Biotechnol *39*, 813–818. 10.1038/s41587-021-00870-2.

63. Wolf, F.A., Angerer, P., and Theis, F.J. (2018). SCANPY: large-scale single-cell gene expression data analysis. Genome Biol *19*, 15. 10.1186/s159-017-1382-0.

64. Gayoso, A., and Shor, J. (2022). JonathanShor/DoubletDetection: doubletdetection v4.2. Version v4.2 (Zenodo). https://doi.org/10.5281/ZENODO.2678041

65. Zhang, H. (2023). SCP: Single Cell Pipeline. R package version 0.5.6. https://github.com/zhanghao-njmu/SCP

66. Bergen, V., Lange, M., Peidli, S., Wolf, F.A., and Theis, F.J. (2020). Generalizing RNA velocity to transient cell states through dynamical modeling. Nat Biotechnol *38*, 1408–1414. 10.1038/s41587-020-0591-3.

67. Setty, M., Kiseliovas, V., Levine, J., Gayoso, A., Mazutis, L., and Pe'er, D. (2019). Characterization of cell fate probabilities in single-cell data with Palantir. Nat Biotechnol *37*, 451–460. 10.1038/s41587-019-0068-4.

68. Schindelin, J., Arganda-Carreras, I., Frise, E., et al. (2012). Fiji: an open-source platform for biological-image analysis. *Nature Methods* 9: 676–682. 10.1038/nmeth.2019

69. Tseng, Q., Wang, I., Duchemin-Pelletier, E., Azioune, A., Carpi, N., Gao, J., Filhol, O., Piel, M., Théry, M., and Balland, M. (2011). A new micropatterning method of soft substrates reveals that different tumorigenic signals can promote or reduce cell contraction levels. Lab Chip *11*, 2231. 10.1039/c0lc00641f.

70. Li, K. (2008). The image stabilizer plugin for ImageJ. https://www.cs.cmu.edu/~kangli/code/Image_Stabilizer.html

71. Brend, T. and Holley, S.A. (2009). Zebrafish Whole Mount High-Resolution Double Fluorescent In Situ Hybridization. JoVE, 1229. 10.3791/1229.

Chapter 3

SINGLE CELL EPIGENOMIC ANALYSIS UNCOVERS GENE REGULATORY CIRCUITS IN NEURONAL DIFFERENTIATION OF THE ENS

Background

As the largest portion of the peripheral nervous system of vertebrates, the enteric nervous system (ENS) regulates gastrointestinal motility, fluid secretion, vasodilation and the interplay of the gut with immune system, microbiome and central nervous system[1–3]. The ENS is primarily derived from vagal neural crest cells that emerge from the caudal hindbrain, invade the foregut, then migrate caudally to populate the entire length of the gut[4]; in addition, there are contributions from Schwann cell precursors[5,6] as well as the sacral neural crest cells[7–9] in amniotes that contribute to a portion of neurons in the post-umbilical bowel, but the latter population is thought to be absent from zebrafish and anamniotes in general. The recent advent of single-cell technologies holds the promise of elucidating molecular mechanisms underlying progressive neuronal differentiation in the ENS. One reason for this is that the gut is extremely large and therefore most studies of mammalian ENS development have focused on particular subregions of the gut, most commonly the midgut or colon. However, not all region of the ENS contain the same complement of neurons.

ENS development is highly conserved across vertebrates including zebrafish. Given the accessibility of zebrafish to genetic manipulation and imaging together with its much smaller size, this model offers several advantages for tackling important questions in ENS development that are much less tractable in mammalian systems[10]. In particular, the small size of the zebrafish intestinal tract, particularly at embryonic and larval stages, makes it tractable to visual the entire gut *in toto*.

Here, we investigate cell lineage decisions and gene regulatory events underlying ENS differentiation by isolating and analyzing the transcriptome of individual enteric neural crest-derived cells ranging from progenitors to differentiated cell types. From out single cell RNA data, we identified 7 main subtypes of enteric neurons and discovered

multiple transcription factors expressed during the transitioning from neuroblast to mature neurons. To establish the gene regulatory linkages between these transcription factors and thus reveal the molecular mechanism governing neuronal differentiation of the ENS, here we turned to Assays for transposase accessible chromatin with high-throughput sequencing (ATAC-seq). ATAC-seq has been widely used to probe the open chromatins across the genome and infer the potential cis-regulatory elements for a specific gene[11]. The recent advent of single cell ATAC-seq (scATAC-seq) technique[12] and its paired analyses[13,14] have further advanced this exploration at single-cell level, offering deeper insights into gene regulatory network when integrated with scRNA-seq data.

Previous studies applied scATAC-seq in mouse model[15,16] to investigate the neurogenic potential of enteric glia, revealing that the accessibility of cis-regulatory elements associated with neurogenesis were retained in mature glia. Other publications[17,18] focused on the development of human and mouse intestines. However, the neuronal differentiation process from progenitors to mature neurons are largely obscure. In this study, we present scATAC-seq data covering the ENS development from 2 dpf to 5 dpf, integrated with scRNA-seq results, to elucidate the gene regulatory circuits underpinning neuronal differentiation.

Results

Bulk ATAC-seq identifies extensive open chromatic regions across the genome

We used Tg(*Phox2bb:Kaede*) line, a reporter line previously demonstrated to label the ENS lineage[19], to perform bulk ATAC-seq (Figure 15A). We dissected out the gut region from zebrafish embryo at 3 dpf and sorted out Kaede-positive cells as putative ENS cells, as well as the Kaede-negative cells from surrounding tissues (non-ENS) as control. We identified 76,276 high-quality peaks from both ENS and non-ENS cells, demonstrating extensive dynamic regulation across the genome at this stage. Through K-means clustering, we identified approximately 7,000 peaks exhibiting active regulation specifically in ENS cells (Figure 16A). We then isolated these peaks and compared the read counts from these regions between ENS and non-ENS groups. The ENS group displayed significantly higher read abundance, demonstrating that these regions are particularly crucial for ENS development (Figure 16B).

CUT&RUN profiles Phox2bb binding sites

To characterize the molecular regulation in these ENS-specific regions, we applied Cleavage Under Targets & Release Using Nuclease (CUT&RUN) technique[21] to map Phox2bb binding sites across the genome. The CUT&RUN method leverages the high affinity of protein A/G for IgG antibodies, creatively conjugating micrococcal nuclease to protein A/G. This innovative approach enables precise in situ chromatin profiling, allowing us to identify and analyze the binding sites of the specific transcription factor recognized by suitable antibody. We employed the knockin line Tg(*Phox2bb:mNeonGreen*) to isolate ENS cells (Figure 15B) at 3 dpf.

Through CUT&RUN epigenome profiling, we identified more than 10,000 Phox2bb-binding sites. The Homer de novo motif discovery analysis showed that the top-ranked motifs are either the Phox2bb binding motif or highly similar to it (Figure 16C). Since micrococcal nuclease can access and cleave open chromatin regions, we compared the peak regions identified by CUT&RUN with those from bulk ATAC-seq. Both k-means clustering analysis (Figure 16D) and genomic tracks (Figure 15C) revealed that multiple chromatin regions that were actively open in the ATAC-seq data were not detected in the CUT&RUN results. More than 80% of Phox2bb-binding sites were located between 5 and 500 kilobases from the transcription start sites of genes, indicating that these binding sites are situated in distal cis-regulatory domains (Figure 16E). We then used GREAT analysis[23] to associate Phox2bb binding sites with genes and identified 518 candidate target transcription factors (Figure 16F). By integrating CUT&RUN data with previous RNA-seq results, we found that 172 transcription factors were common to both datasets, indicating that these genes are likely reliable downstream targets of Phox2bb.

ATAC-seq results revealed multiple cis-regulatory elements associated with the *Phox2bb* gene, all of which were also detected in the CUT&RUN data, suggesting active autoregulation of *Phox2bb*. Previous reports have indicated that *Phox2bb* represses *Sox10* expression to promote neuronal differentiation[25]. Our CUT&RUN results identified strong binding sites near the *Sox10* gene, supports this finding with molecular evidence. Additionally, we observed *Phox2bb* regulation of *Phox2a* and *Insm1b*, two genes critical for neurogenesis[24,27], as well as *Etv1* and *Hmx3a*, which are expressed in neuronal subtypes as neuroblasts further differentiate, according to our scRNA-seq data. Taken together, these

CUT&RUN results highlight the versatile roles of Phox2bb in neuronal specification and differentiation.

scATAC-seq reveals heterogeneity of ENS cells

We used the Tg(*Phox2bb:mNeonGreen*) line to collect enteric nervous system (ENS) cells at 2, 3, 4, and 5 dpf. Following established protocols[20], we first sorted ENS cells based on mNeonGreen fluorescence, then lysed the cells to enhance transposition by Tn5 (Figure 17A and 18A). Subsequently, we sorted the nuclei into a 384-well plate, with each well containing a unique pair of primers and prepared the libraries for sequencing. Using the analysis tool ArchR[14], we analyzed approximately 3,300 high-quality cells and identified 14 clusters (with the 1st cluster omitted from further analysis due to its small size) (Figure 17 B and C; Figure 18 B and C). The scATAC-seq data revealed patterns consistent with the scRNA-seq results, distinguishing between progenitors (cluster 2, 3, and 5-7), neuroblasts (cluster 4), and various subtypes of neurons (cluster 9-14). To gain deeper insights, we calculated GeneScores, which reflect gene expression by measuring reads in both the gene body and the flanking intergenic regions (Figure 18D). GeneScores were adjusted based on the distance of the regions from the transcription start site; specifically, as the distance from the transcription start site increased, the ratio of reads in these regions was progressively reduced. The GeneScores for several marker genes align with their expression levels observed in the scRNA-seq data. Next, we examined the motif activities for *Sox10*, *Phox2a*, *Ebf1a*, and *Gata3* across the genome (Figure 18E). Our analysis revealed that Sox10 and Phox2a are more active in progenitors and neurons, while Ebf1a and Gata3 exhibited higher activity in inhibitory and excitatory motor neurons, respectively. We were interested in the progenitor groups that emerge at later stages of ENS development, identified as cluster 0 and 15 in the scRNA-seq data and cluster 2 and 3 in the scATAC-seq data, which we referred to as “late progenitors.” We reconstructed the developmental trajectory from the putative original ENS progenitors to these late progenitors (Figure 18F). Our analysis revealed enhanced Foxo1 activity in late progenitors, consistent with the high expression of *Foxo1a* in these cells (Figure 18G). This suggests that transcription factor Foxo1a probably plays a critical role in the specification and maintenance of these late progenitors.

Integrative analysis of scRNA-seq and scATAC-seq

Next, we integrated our previous scRNA-seq and current scATAC-seq data by projecting the gene expression information from scRNA-seq onto the cells with the highest similarity in the scATAC-seq data using the Signac algorithm (Figure 19, A and B). This approach allowed each cell in the scATAC-seq dataset to carry both expression and epigenetic information. We then used ArchR to examine the correlation between gene expression and peak accessibility, finding that higher peak read abundance in the scATAC-seq data correlated with higher gene expression in the scRNA-seq data (Figure 19, C and D). Additionally, we employed the FigR algorithm to infer gene regulatory circuits during neuronal development (Figure 19, E and F). FigR established both positive and negative correlations between peaks and gene expression, indicating activation and repression activities. Using this algorithm, we identified genes and peaks with high statistical significance and visualized the linkages between representative transcription factors and their target genes. In the plot, green lines denote activation, while purple lines indicate repression.

Here, we combine our previous results using scRNA-seq data with ATAC-seq and CUT&RUN to build a gene regulatory network functioning in the developing ENS. With our scRNA-seq data, we identified the expression of *Phox2a*[22,24] and *Insm1b* (zebrafish homolog of *Insm1*)[26,27] in neuroblasts to mature neurons. Our findings agree with previous studies that highlight Phox2a and Insm1b as key transcription factors in neuronal differentiation. Following the activation of *Phox2a* and *Insm1b*, we observed expression of *Etv1* and *Hmx3a* (the zebrafish homolog of Hmx3) in specific neuronal subtypes. *Etv1* was found in both inhibitory and excitatory motor neurons, while *Hmx3a* was primarily expressed in serotonergic neurons and inhibitory motor neurons. Although *Etv1* has long been known to be present in the enteric nervous system[28], recent zebrafish experiments revealed that *Etv1* knockout leads to a significant loss of ENS cells[29]. Conversely, the expression of *Hmx3* (zebrafish homolog *Hmx3a*) in the ENS has not been previously reported. Additionally, we detected *Ebf1a*, *Gata3*, and *Satb2* expression and discovered their functions in inhibitory motor neurons, excitatory motor neurons, and serotonergic neurons, respectively. The increasingly restricted expression patterns of these transcription factors likely reflect the specification and differentiation processes during neurogenesis. CUT&RUN results

discovered the direct regulation of *Phox2bb* to *Phox2a*, *Insm1b*, *Etv1* and *Hmx3a*. Next, we plan to combine computational analysis on scRNA-seq and scATAC-seq, together with perturbation experiments to elucidate the regulatory linkages between these transcription factors and uncover the genetic circuits governing neuronal development.

Methods

Bulk ATAC-seq and analysis

We used the Tg(*Phox2bb:Kaede*) line to perform bulk ATAC-seq. However, in addition to the ENS, this line also exhibited Kaede expression in the head and spinal cord. To isolate putative ENS cells, we meticulously dissected the gut from zebrafish embryos at 3 days post-fertilization (dpf) and followed the cell dissociation procedure described previously. We then adhered to a published protocol omni-ATAC method[30] for low-input cells to conduct bulk ATAC-seq. After using bowtie 2[31] to align the reads to the reference genome (GRCz10 assembly), we employed eaSeq (https://easeq.net) for the advanced analysis.

CUT&RUN and analysis

We followed the previously published protocol to perform CUT&RUN[32], but in the cell lysis step, we adopted the omni-ATAC method[30]. For analysis, we used galaxy platform (https://usegalaxy.org) to align the reads to the genome, utilized MACS[33] to call peaks and finally visualized the tracks with UCSC genome browser. We utilized GREAT algorithm[23] to conduct gene association analysis.

scATAC-seq Experiment and analysis

For scATAC-seq, we use barcoded plate-based scATAC-seq method. We first dissected zebrafish tissues, performed cell dissociation and sorted out ENS cells at 2dpf, 3dpf, 4dpf and 5dpf as described in scRNA-seq part. Sorted cells were undergone nucleus extraction and tagmenation with Tn5 transposase. The reactions were stopped by adding EDTA and cells were sorted again to barcoded 384-well plates. We sorted cells collected at 2dpf, 3dpf, 4dpf and 5dpf into 1, 2, 3 and 3 384-well plates, respectively. After library

preparation, we sequenced the libraries in one lane of a flow cells in Illumina HiSeq 4000 system.

scATAC-seq raw reads were trimmed and demultiplexed with Cutadapt and Bbmap package and aligned to GRCz10 (danRer10) reference genome using Snaptools package. Then, Single-Nucleus Accessibility Profiles hd5 file (snap file) containing cell-by-bin ATAC matrix was created with Snaptools, and the genome bin-size for dimensional reduction was set 5000bp. The downstream scATAC processing was performed by package SnapATAC as demonstrated below: The low-quality cells were flited out with the function "filterCells," and 3099 cells from initial 3456 cells passed the quality control. The dimensional reduction was performed with runDiffusionMaps function, and we chose first 21 PCs as significant components for UMAP analysis. The Graph-based clustering is performed first by constructing a K Nearest Neighbor (KNN) Graph with k=15, and then followed by Louvain clustering. The cluster-specific aggregated bedgraph tracks are generated with the function "runMACSForALL" and MACS2 package. The genome browser track is visualized by the Easeq software.

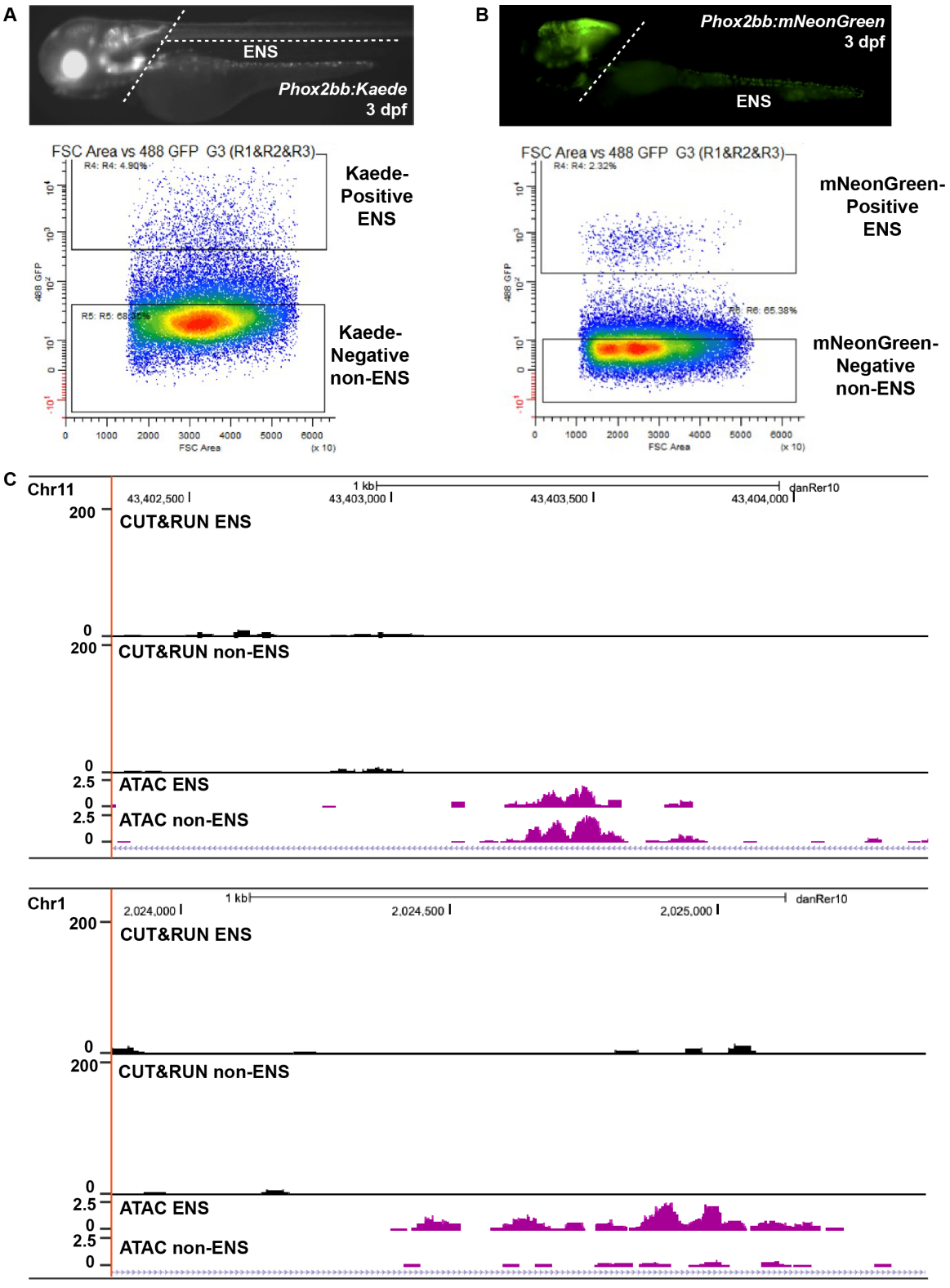

Figure 15. Bulk ATAC-seq and CUT&RUN experiment. (A, B) Tissue dissection and representative fluorescence-activated cell sorting (FACS) records. **(C)** Genomic tracks

showing that CUT&RUN results are distinguishable with ATAC-seq data. Peaks open in ATAC-seq data are not detected in CUT&RUN tracks.

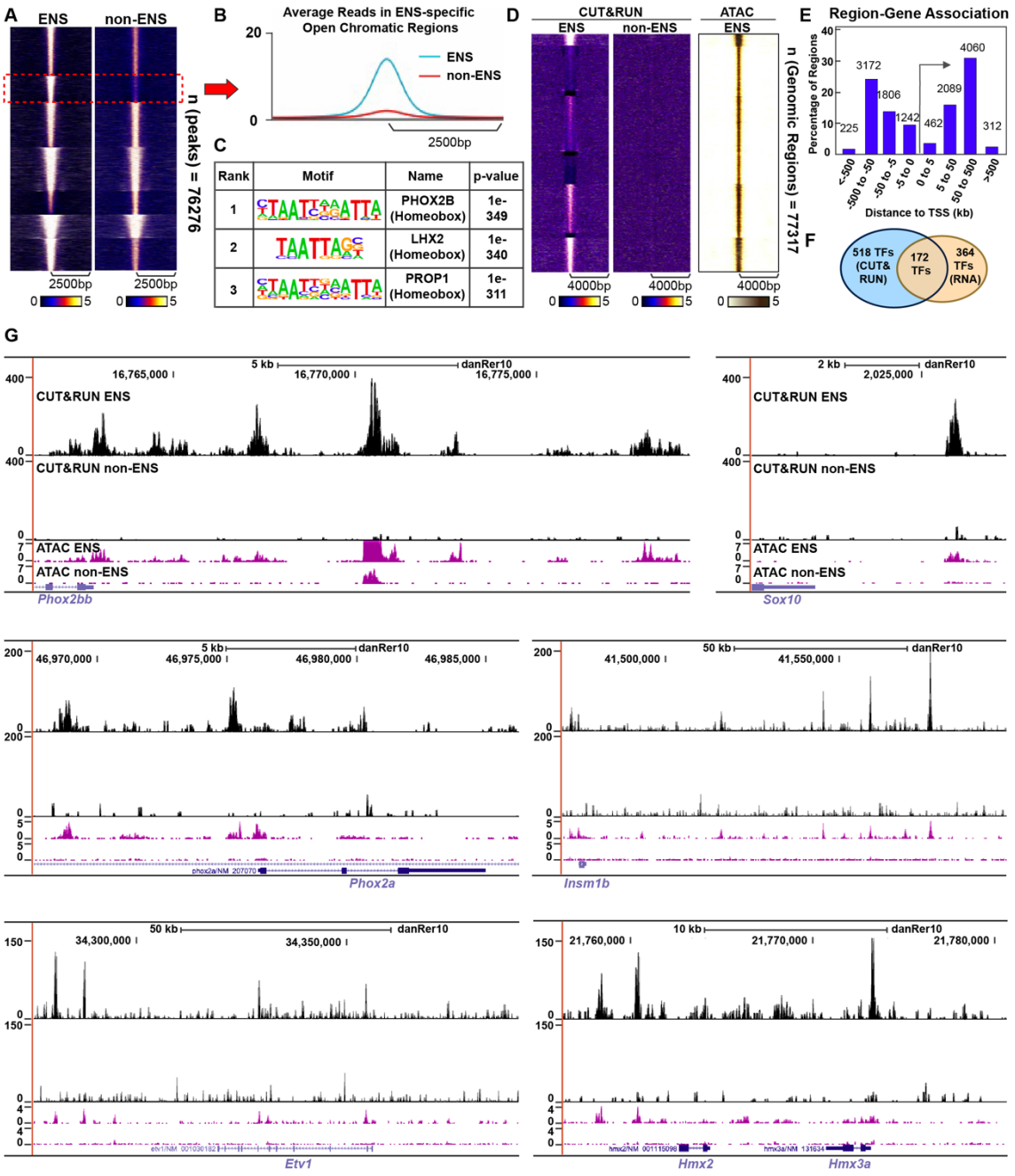

Figure 16. Bulk ATAC-seq and CUT&RUN results demonstrate extensive regulatory activity across the genome in zebrafish ENS at 3 dpf. (A) K-means clustering analysis reveals ENS-specific regulatory regions. **(B)** Histogram of average read counts in peaks identified in ENS-specific regions. **(C)** Homer discovers *Phox2bb* binding motifs and similar sequences in CUT&RUN results. **(D)** K-means clustering of the CUT&RUN results reveals a distinct pattern compared to the ATAC-seq data. **(E)** GREAT analysis displays the distance

of *Phox2bb* binding sites to transcription start sites of candidate target genes. **(F)** Venn diagram shows 172 common transcription factors shared by GREAT analysis of CUT&RUN results and previous RNA-seq results of ENS. **(G)** Genomic tracks manifest autoregulation of *Phox2bb* and its regulation to *Sox10*, *Phox2a*, *Insm1b*, *Etv1* and *Hmx3a*.

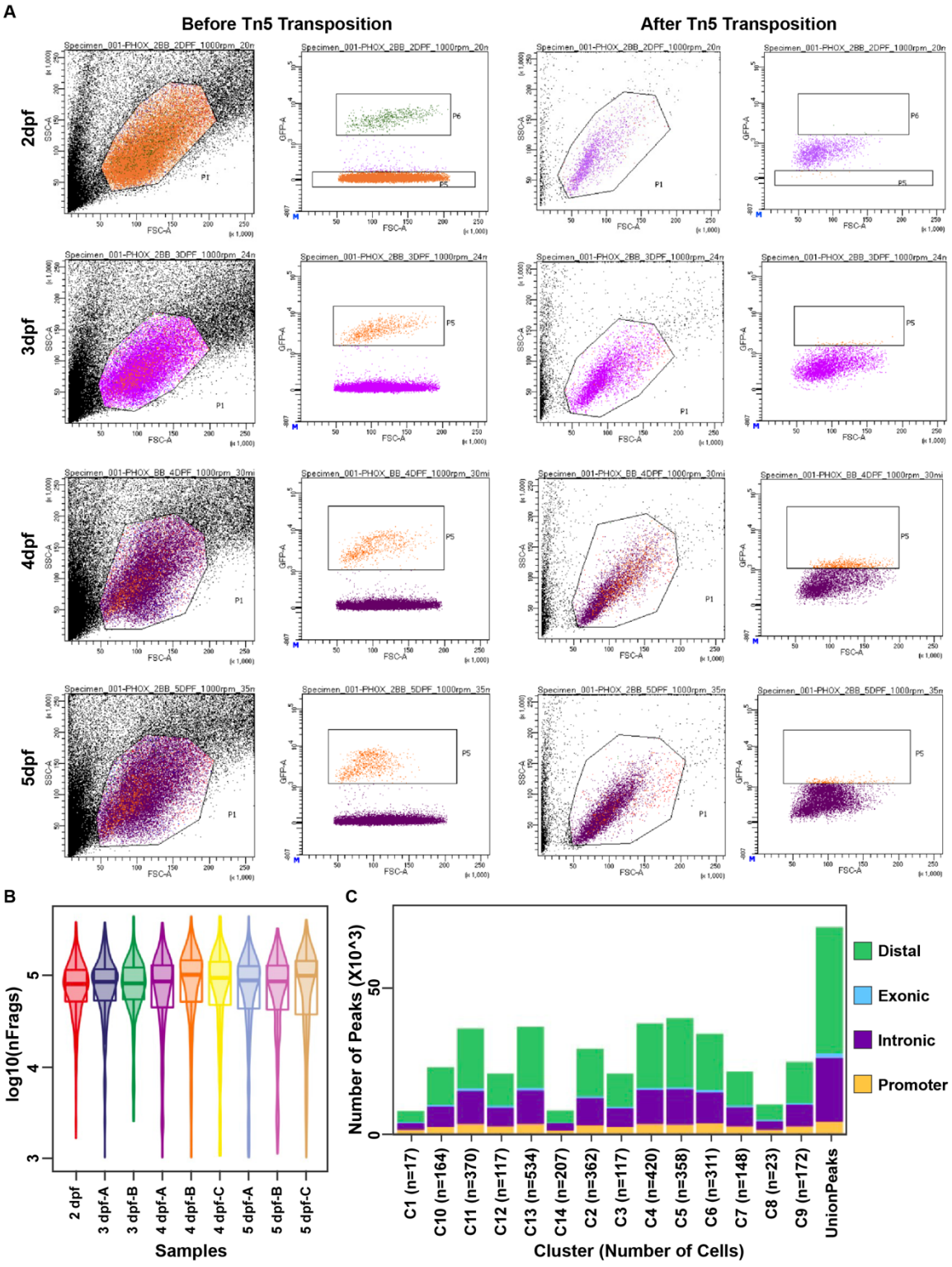

Figure 17. Flow cytometry records and quality examination of scATAC-seq experiments. (A) Representative FACS plots display the single cell and single nucleus

sorting before Tn5 and after transposition step at 2, 3, 4 and 5 dpf, respectively. **(B)** Open fragments identified in scATAC-seq. **(C)** Number of peaks identified in distal, exonic, intronic and promoter regions in each cluster.

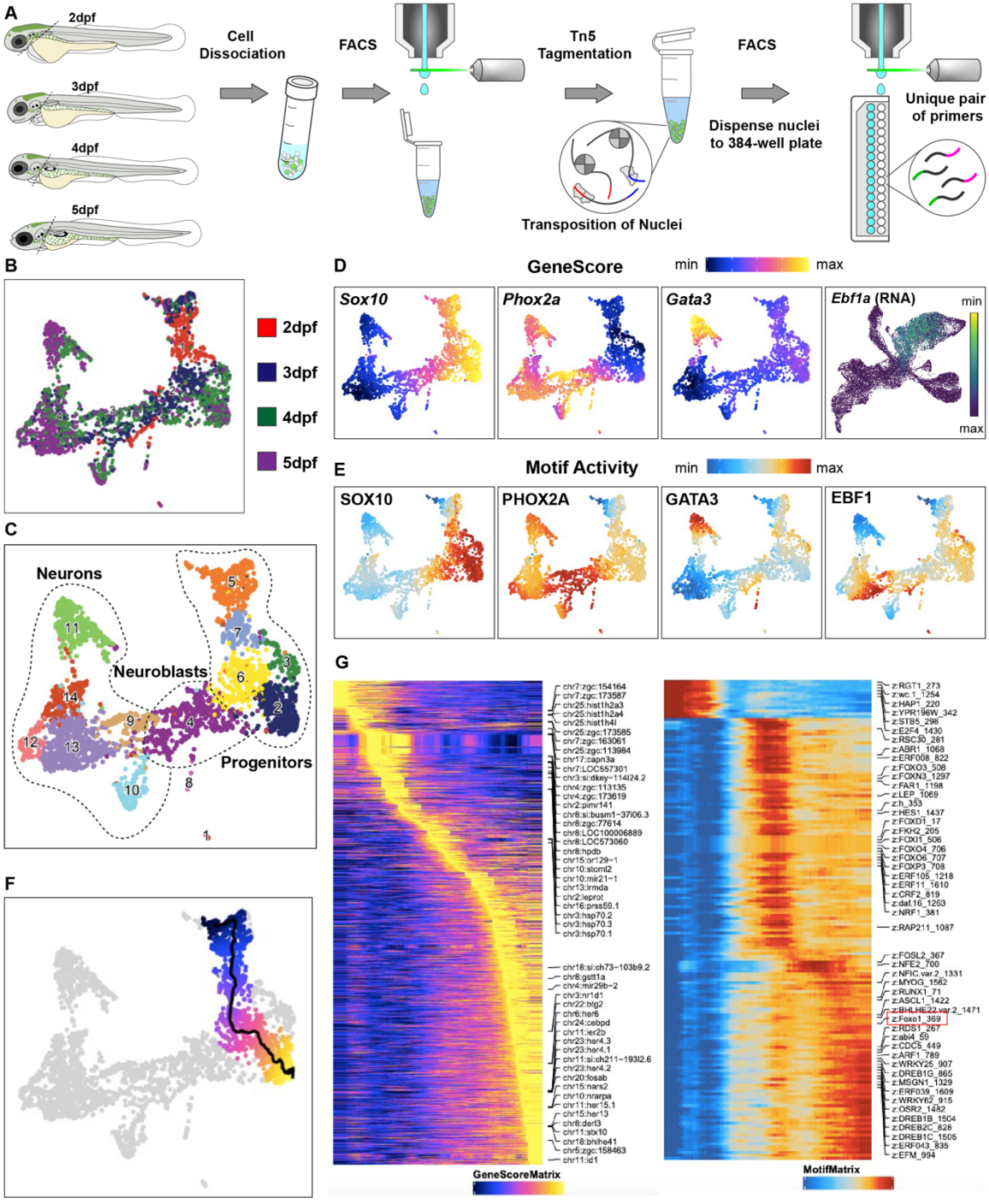

Figure 18. scATAC-seq data manifest heterogeneity and the regulatory activity of ENS cells during embryonic development. (A) Experimental procedure of scATAC-seq experiment. **(B, C)** UMAP plots of ENS cells color-coded by sampling time points and clusters. **(D, E)** GeneScore and motif activity of key transcription factors. **(F)** Developmental

trajectory from enteric neural crest to the late progenitor inferred by ArchR. **(G)** GeneScore and motif activity dynamics along the developmental trajectory **(F)**.

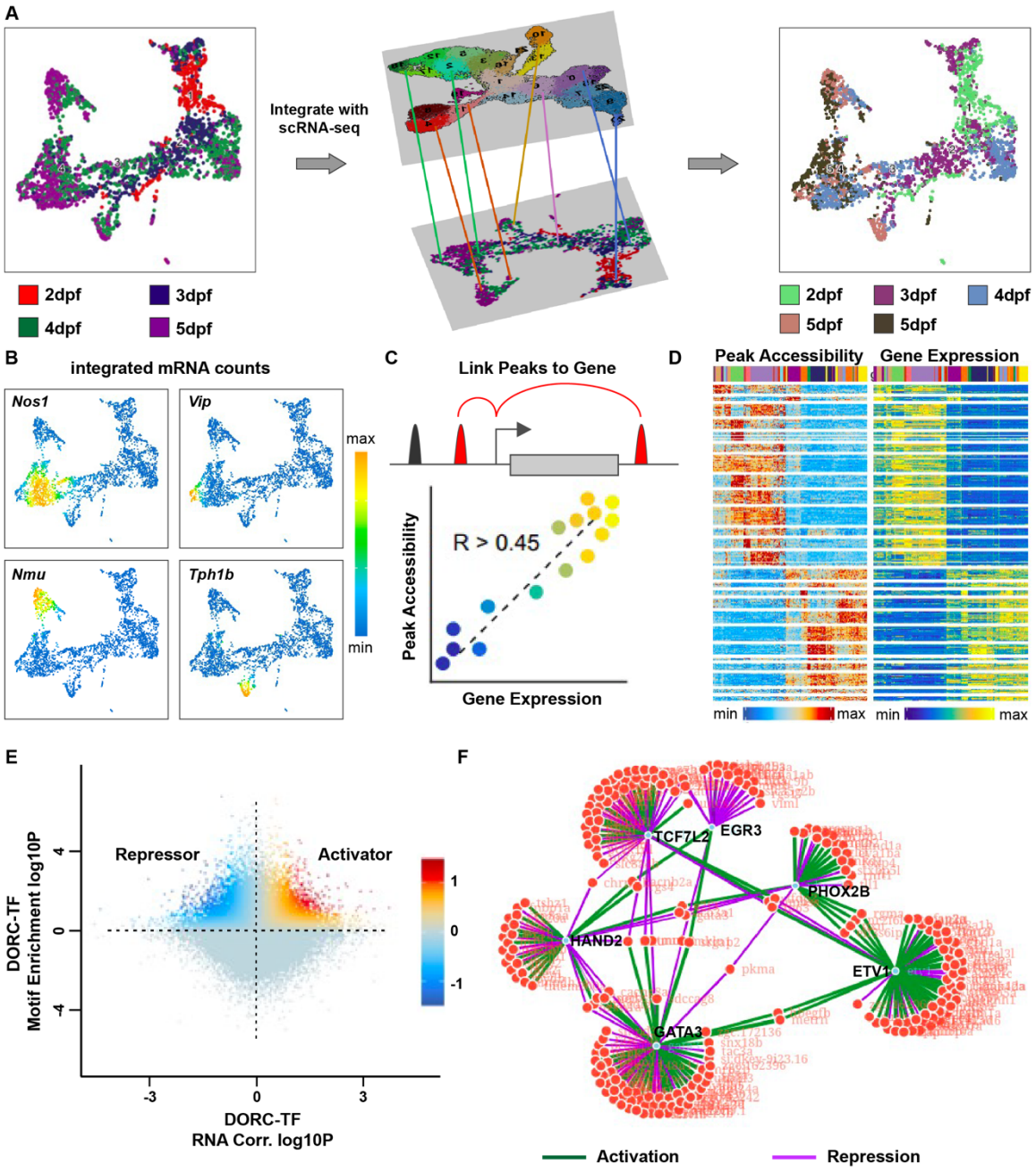

Figure 19. Integration of scRNA and scATAC-seq data unravels the gene regulatory circuit underlying ENS development. (A) Schematic showing the integration of scRNA and scATAC-seq data. **(B)** scRNA-seq data are reflected in the cells analyzed in the scATAC-seq experiment. **(C, D)** Establishment of correlations between peaks and genes by ArchR. **(E, F)** FigR analysis demonstrate complicated gene regulatory circuits during ENS development. **(E)** Plot shows the association between domains of regulatory chromatins

(DORCs) and transcription factors. **(F)** Inferred gene regulatory circuit between transcription factors Phox2b, Etv1, Gata3, Hand2, Tcf7l2 and Egr3.

BIBLIOGRAPHY

1. Gershon, M.D. (1999). The Enteric Nervous System: A Second Brain. Hospital Practice *34*, 31–52. https://doi.org/10.3810/hp.1999.07.153.

2. Yoo, B.B., and Mazmanian, S.K. (2017). The Enteric Network: Interactions between the Immune and Nervous Systems of the Gut. Immunity *46*, 910–926. https://doi.org/10.1016/j.immuni.2017.05.011.

3. Schneider, S., Wright, C.M., and Heuckeroth, R.O. (2019). Unexpected Roles for the Second Brain: Enteric Nervous System as Master Regulator of Bowel Function. Annu. Rev. Physiol. *81*, 235–259. https://doi.org/10.1146/annurev-physiol-021317-121515.

4. Rao, M., and Gershon, M.D. (2018). Enteric nervous system development: what could possibly go wrong? Nat Rev Neurosci *19*, 552–565. https://doi.org/10.1038/s41583-018-0041-0.

5. Solovieva, T., and Bronner, M. (2021). Schwann cell precursors: Where they come from and where they go. Cells & Development *166*, 203686. https://doi.org/10.1016/j.cdev.2021.203686.

6. Uesaka, T., Nagashimada, M., and Enomoto, H. (2015). Neuronal Differentiation in Schwann Cell Lineage Underlies Postnatal Neurogenesis in the Enteric Nervous System. Journal of Neuroscience *35*, 9879–9888. https://doi.org/10.1523/JNEUROSCI.1239-15.2015.

7. Wang, X., Chan, A.K.K., Sham, M.H., Burns, A.J., and Chan, W.Y. (2011). Analysis of the Sacral Neural Crest Cell Contribution to the Hindgut Enteric Nervous System in the Mouse Embryo. Gastroenterology *141*, 992-1002.e6. https://doi.org/10.1053/j.gastro.2011.06.002.

8. Burns, A.J., and Douarin, N.M.L. (1998). The sacral neural crest contributes neurons and glia to the post-umbilical gut: spatiotemporal analysis of the development of the enteric nervous system. Development *125*, 4335–4347. https://doi.org/10.1242/dev.125.21.4335.

9. Pomeranz, H.D., Rothman, T.P., and Gershon, M.D. (1991). Colonization of the post-umbilical bowel by cells derived from the sacral neural crest: direct tracing of cell migration using an intercalating probe and a replication-deficient retrovirus. Development *111*, 647–655. https://doi.org/10.1242/dev.111.3.647.

10. Shepherd, I., and Eisen, J. (2011). Development of the Zebrafish Enteric Nervous System. In Methods in Cell Biology (Elsevier), pp. 143–160. https://doi.org/10.1016/B978-0-12-387036-0.00006-2.

11. Buenrostro, J.D., Giresi, P.G., Zaba, L.C., Chang, H.Y., and Greenleaf, W.J. (2013). Transposition of native chromatin for fast and sensitive epigenomic profiling of open chromatin, DNA-binding proteins and nucleosome position. Nat Methods *10*, 1213–1218. https://doi.org/10.1038/nmeth.2688.

12. Satpathy, A.T., Granja, J.M., Yost, K.E., Qi, Y., Meschi, F., McDermott, G.P., Olsen, B.N., Mumbach, M.R., Pierce, S.E., Corces, M.R., et al. (2019). Massively parallel single-cell chromatin landscapes of human immune cell development and intratumoral T cell exhaustion. Nat Biotechnol *37*, 925–936. https://doi.org/10.1038/s41587-019-0206-z.

13. Stuart, T., Butler, A., Hoffman, P., Hafemeister, C., Papalexi, E., Mauck, W.M., Hao, Y., Stoeckius, M., Smibert, P., and Satija, R. (2019). Comprehensive Integration of Single-Cell Data. Cell *177*, 1888-1902.e21. https://doi.org/10.1016/j.cell.2019.05.031.

14. Granja, J.M., Corces, M.R., Pierce, S.E., Bagdatli, S.T., Choudhry, H., Chang, H.Y., and Greenleaf, W.J. (2021). ArchR is a scalable software package for integrative single-cell chromatin accessibility analysis. Nat Genet *53*, 403–411. https://doi.org/10.1038/s41588-021-00790-6.

15. Laddach, A., Chng, S.H., Lasrado, R., Progatzky, F., Shapiro, M., Erickson, A., Sampedro Castaneda, M., Artemov, A.V., Bon-Frauches, A.C., Amaniti, E.-M., et al. (2023). A branching model of lineage differentiation underpinning the neurogenic potential of enteric glia. Nat Commun *14*, 5904. https://doi.org/10.1038/s41467-023-41492-3.

16. Guyer, R.A., Stavely, R., Robertson, K., Bhave, S., Mueller, J.L., Picard, N.M., Hotta, R., Kaltschmidt, J.A., and Goldstein, A.M. (2023). Single-cell multiome sequencing clarifies enteric glial diversity and identifies an intraganglionic population poised for neurogenesis. Cell Reports *42*, 112194. https://doi.org/10.1016/j.celrep.2023.112194.

17. Hickey, J.W., Becker, W.R., Nevins, S.A., Horning, A., Perez, A.E., Zhu, C., Zhu, B., Wei, B., Chiu, R., Chen, D.C., et al. (2023). Organization of the human intestine at single-cell resolution. Nature *619*, 572–584. https://doi.org/10.1038/s41586-023-05915-x.

18. Smith, R.J., Zhang, H., Hu, S.S., Yung, T., Francis, R., Lee, L., Onaitis, M.W., Dirks, P.B., Zang, C., and Kim, T.-H. (2022). Single-cell chromatin profiling of the primitive gut tube reveals regulatory dynamics underlying lineage fate decisions. Nat Commun *13*, 2965. https://doi.org/10.1038/s41467-022-30624-w.

19. Harrison, C., Wabbersen, T., and Shepherd, I.T. (2014). In vivo visualization of the development of the enteric nervous system using a *Tg(−8.3bphox2b:Kaede)* transgenic zebrafish. Genesis *52*, 985–990. https://doi.org/10.1002/dvg.22826.

20. Chen, X., Miragaia, R.J., Natarajan, K.N., and Teichmann, S.A. (2018). A rapid and robust method for single cell chromatin accessibility profiling. Nat Commun *9*, 5345. https://doi.org/10.1038/s41467-018-07771-0.

21. Skene, P.J., and Henikoff, S. (2017). An efficient targeted nuclease strategy for high-resolution mapping of DNA binding sites. eLife *6*, e21856. https://doi.org/10.7554/eLife.21856.

22. Brunet, J.-F., and Pattyn, A. (2002). Phox2 genes — from patterning to connectivity. Current Opinion in Genetics & Development *12*, 435–440. https://doi.org/10.1016/S0959-437X(02)00322-2.

23. McLean, C.Y., Bristor, D., Hiller, M., Clarke, S.L., Schaar, B.T., Lowe, C.B., Wenger, A.M., and Bejerano, G. (2010). GREAT improves functional interpretation of cis-regulatory regions. Nat Biotechnol *28*, 495–501. https://doi.org/10.1038/nbt.1630.

24. Ernsberger, U., and Rohrer, H. (2005). Phox2a and Phox2b: Essential Transcription Factors for Neuron Specification and Differentiation. In Transcription Factors in the Nervous System, G. Thiel, ed. (Wiley), pp. 53–73. https://doi.org/10.1002/3527608036.ch3.

25. Nagashimada, M., Ohta, H., Li, C., Nakao, K., Uesaka, T., Brunet, J.-F., Amiel, J., Trochet, D., Wakayama, T., and Enomoto, H. (2012). Autonomic neurocristopathy-associated mutations in PHOX2B dysregulate Sox10 expression. J. Clin. Invest. *122*, 3145–3158. https://doi.org/10.1172/JCI63401.

26. Jacob, J., Storm, R., Castro, D.S., Milton, C., Pla, P., Guillemot, F., Birchmeier, C., and Briscoe, J. (2009). Insm1 (IA-1) is an essential component of the regulatory network that specifies monoaminergic neuronal phenotypes in the vertebrate hindbrain. Development *136*, 2477–2485. https://doi.org/10.1242/dev.034546.

27. Lorenzen, S.M., Duggan, A., Osipovich, A.B., Magnuson, M.A., and García-Añoveros, J. (2015). Insm1 promotes neurogenic proliferation in delaminated otic progenitors. Mechanisms of Development *138*, 233–245. https://doi.org/10.1016/j.mod.2015.11.001.

28. Heanue, T.A., and Pachnis, V. (2006). Expression profiling the developing mammalian enteric nervous system identifies marker and candidate Hirschsprung disease genes. Proc. Natl. Acad. Sci. U.S.A. *103*, 6919–6924. https://doi.org/10.1073/pnas.0602152103.

29. Moreno-Campos, R., Singleton, E.W., and Uribe, R.A. (2024). A targeted CRISPR-Cas9 mediated F0 screen identifies genes involved in establishment of the enteric nervous system. PLoS ONE *19*, e0303914. https://doi.org/10.1371/journal.pone.0303914.

30. Corces, M.R., Trevino, A.E., Hamilton, E.G., Greenside, P.G., Sinnott-Armstrong, N.A., Vesuna, S., Satpathy, A.T., Rubin, A.J., Montine, K.S., Wu, B., et al. (2017). An improved ATAC-seq protocol reduces background and enables interrogation of frozen tissues. Nat Methods *14*, 959–962. https://doi.org/10.1038/nmeth.4396.

31. Langmead, B., and Salzberg, S.L. (2012). Fast gapped-read alignment with Bowtie 2. Nat Methods *9*, 357–359. https://doi.org/10.1038/nmeth.1923.

32. Skene, P.J., Henikoff, J.G., and Henikoff, S. (2018). Targeted in situ genome-wide profiling with high efficiency for low cell numbers. Nat Protoc *13*, 1006–1019. https://doi.org/10.1038/nprot.2018.015.

33. Zhang, Y., Liu, T., Meyer, C.A., Eeckhoute, J., Johnson, D.S., Bernstein, B.E., Nusbaum, C., Myers, R.M., Brown, M., Li, W., et al. (2008). Model-based Analysis of ChIP-Seq (MACS). Genome Biol *9*, R137. https://doi.org/10.1186/gb-2008-9-9-r137.

Chapter 4

CONCLUSION

Compared to the murine and human enteric nervous systems which have hundreds of millions of neurons, the zebrafish ENS is much smaller and simpler. This together with the accessibility of zebrafish to genetic manipulation and the ease of imaging offers several advantages for tackling important questions in ENS development at the single cell level. Individual zebrafish larvae have a few hundred neurons; for example, there are ~500 neurons per 6 dpf gut, by which time the zebrafish larvae are feeding. Thus, by sorting *phox2bb*+ cells from different time points, we are able to isolate large numbers of ENS precursors and neurons for single-cell transcriptomics analysis. The small-scale of the zebrafish enteric nervous system enables interrogation of the order of neuronal differentiation and cell lineage decisions throughout the developing gut. Importantly, each developmental time point in our analysis encompasses thousands of neurons or progenitors, which is more than 10-fold the number of ENS cells per embryo and thus covers all neuronal subtypes.

Moreover, the clarity of the zebrafish embryo makes it possible to perform sequential in situ hybridization with multiple probes using hybridization chain reaction. In this way, we can analyze the location of different types of neurons in situ which can be classified by the combinatorial expression of neurotransmitters and neuropeptides in both wild type and experimentally perturbed embryos. This enables assessing ENS differentiation along the entire rostrocaudal extent of the gut at different time points and examining the spatial organization of neuronal subtypes therein. Finally, in this thesis, we were able to predict the developmental trajectories of each neuronal subtype and relate this to gene expression at different developmental stages of maturation, thus providing valuable temporal information.

Proper signaling at specific developmental stages is essential for formation of a functional ENS. Our findings revealed *Ret* expression in the majority of the ENS cells with the except of excitatory motor neurons, which expressed *Ednraa* (zebrafish homolog of *Ednra*), a receptor for endothelin (ET) signaling (Figure 20). Previous publications have

demonstrated that ET-3 inhibited receiving of GDNF signals in avian neural crest cells[1]. Although chicken and mammalian EDNRA are potentially responsive to ET-1 and ET-2[2], similar mechanisms of crosstalk between endothelin and GDNF signals may occur during maturation of ENS neurons in zebrafish. Surprisingly, our data showed that RET partners GFRA1A and GFRA2A had lower expression in ENS progenitors and only were prominently expressed in inhibitory motor neurons (IMN) and 5-HT neurons, respectively, probably because ENS neurons have a greater requirement for GDNF signals compared to progenitors. Our data also revealed that intricate signaling processes including Notch, FGF, and BMP pathways are involved in ENS development (Figure 20). Zebrafish *Notch1* homologs (*Notch1a* and *Notch1b*) displayed conspicuous expression in neuroblasts and progenitors. *Dla* and *Dld* were expressed in Cluster 0 progenitors and neuroblasts at early phases, while *Dlb* and *Dlc* were activated at the neuroblast stage and separately retained in the excitatory motor neurons (EMNs) and IMNs at later stage. Two zebrafish *Fgf13* homologs (*Fgf13a* and *Fgf13b*) were detected in ENS neurons. Three BMP molecules *Bmp4*, *Bmp5*, and *Bmp8a* exhibited distinctive expression in 5-HT neurons, IMNs and subtype of EMNs. Three zebrafish BMP receptors (*Bmpr1aa*, *Bmpr1ab* and *Bmpr1ba*) were expressed in cluster 0 progenitors, neuroblasts and neurons, with higher expression in 5-HT and IMN groups. These complex and extensive signaling interactions highlight the intricate nature of ENS development.

Gene regulatory analysis coupled with loss of function experiments have provided clues to some of the transcriptional regulators that are critical for early ENS development. In enteric neural crest cells, *Sox10* and *Ascl1* have been shown to function together with *Pax3* to mediate expression of *Ret* and *Ednrb* that are required for their migration and differentiation[3,4]. *Sox10* also is required for maintenance of progenitors[5,6] and *Ascl1* is required for neurogenic lineage specification[7]. *Sox10* and *Tfap2b* are major drivers of early enteric development in vagal neural crest cells, followed by *SoxB* and *Hbox* genes driving neuronal differentiation[8]. Loss of *Tbx3* reduces NOS1-expressing myenteric neurons[9], loss of *Sox6* reduces gastric dopamine neurons[10], and loss of *Pbx3* affects differentiation into Calbindin+ neurons[11]. Previous studies proved that *Tlx2*, *Hoxb5b* (zebrafish Hoxb5 homolog) and *Tbx2a/b* (zebrafish Tbx2 homolog) are crucial for ENS development[12–14]. Our data revealed widespread expression of these genes in the ENS, supporting previous

conclusions. Mouse *Hand2* was shown to be closely related to the neurogenesis of Vip+ neurons, but not ACh+ neuron[15]. Our data indicated that Hand2 expression was confined to 5HT and IMNs (including Vip+/Vipb+ neurons) and absent from EMNs (mainly ACh+ neurons). Our results are consistent with findings from mouse models and suggested an evolutionally conserved function of *Hand2*.

Here, we extend the list of known transcriptional regulators involved in enteric nervous system development by using CRISPR mediated perturbation in zebrafish. Our results reveal novel functions for *Ebf1a*, *Satb2* and *Gata3* in inhibitory motor neurons, serotonergic neurons and excitatory motor neurons in the ENS. *Ebf1* has been associated with lineage branch points in the developing mammalian ENS[18], but their functions have not been tested. Using CRISPR/Cas9 mediated knock-down, we find that loss of *Ebf1a* specifically affects expression of the PACAP peptide, characteristic of inhibitory motor neurons, suggesting that it is critical for their development. Whereas *Gata3* and *Satb2* expression were not previously noted in the ENS, we find that loss of *Gata3* leads to expansion of *Cart2* expression throughout the gut and loss of cholinergic neurons, suggestive of a cell fate switch in excitatory neurons, and knock-out of *Satb2* selectively diminishes serotonin expression, without affecting markers characteristic of other lineages. As each of these three factors is expressed in and differentially affects a different cluster, this analysis expands understanding of transcriptional inputs into ENS sublineages. While all of our loss-of-function results relied upon crispants rather than mutant lines due to lethality of the genes of interest, qPCR analysis revealed more than 90% loss of the target genes after using multiple guide RNAs per target[16].

There are several single cell RNA-seq studies that characterize the cell types and developmental trajectory of the ENS in the mouse and human[9,17–21]. Due to the large size of these organisms, these studies have been confined to discrete parts of the intestines. Despite the size and complexity differences between the zebrafish and mammalian enteric nervous system, our data align well with previous results from single cell analyses of the mammalian ENS. In both mouse and human ENS, scRNA-seq data have suggested that cell lineage decisions occur via binary decisions that lead to differentiation of different neuronal subtypes. First, there is a proposed bifurcation between inhibitory and excitatory neurons followed by diversification into distinct neuronal subtypes [98,104].

Importantly, this initial branching correlates with *Etv1/Ebf1* in one branch (branch A) and *Bnc2/Satb1/Casz1* in another (branch B). The present data nicely support this model and suggest that the zebrafish ENS develops in a similar fashion, with an initial binary branch between excitatory and other neuronal subtypes followed by subsequent branching bifurcations (Fig 7F). This suggests that there may be deep evolutionary conservation of ENS lineage decisions. Moreover, the fact that we find that *Ebf1a* is critical for formation of EN2 neurons, which have neurotransmitters characteristic of inhibitory motor neurons, nicely fits with its proposed association with neuronal subtype differentiation in the mammalian ENS (branch A). Analogously, we show that *Satb2* has a critical function in zebrafish serotonergic neurons, like its proposed function in mammals.

Based on these discoveries, our future goal is to integrate CUT&RUN results and functional analysis of specific transcription factors, such as *Phox2a*, *Insm1b*, *Etv1/4*, *Hmx3a*, *Ebf1a*, *Gata3* and *Satb2* to reconstruct the gene regulatory circuits regulating the neuronal differentiation. A second goal is to elucidate the interactions between EN2 and progenitors. Our findings showed that the EN2 (Adcyap1b+/Nos1+/Vipb+) lineage emerged early with the expression of Dll4, and its receptors Notch1a/b were present in progenitors and neuroblasts. Expression of multiple Notch target genes like *Her2*, *Her4.1*, *Her6*, *Her9*, *Her12*, *Her15.1*, *Hey1* and *Hey2* indicated activation of Notch pathway. We plan to validate the expression of Dll4 and Notch1a/b in the gut and perform perturbation experiments using conditional knockout lines *Phox2bb*:*Cas9* together with U6: gRNAs (targeting *Dll4* or *Notch1a/b*) to observe the number and distribution pattern of neuronal subtypes. Next, we will use CUT&RUN to explore downstream genes of Notch effectors in the Her/Hey family. With these results, we aim to validate one of two hypotheses: either the neuronal subtypes are predetermined prior to migration of progenitors into the gut, or neuronal subtypes are induced via interactions between progenitors and early differentiating neurons. Third, we plan to extend our research to investigate ENS development in larvae and adults. The embryonic ENS is comprised of approximately 500 cells. As the fish develop, this number increases to potentially tens of thousands, and the diversity of neuronal types also becomes more complex. We aim to utilize single-cell multi-omics technologies to delve into the dynamic changes in transcriptomics and

epigenomics of neuronal subtypes, as well as the underlying gene regulatory networks driving this development.

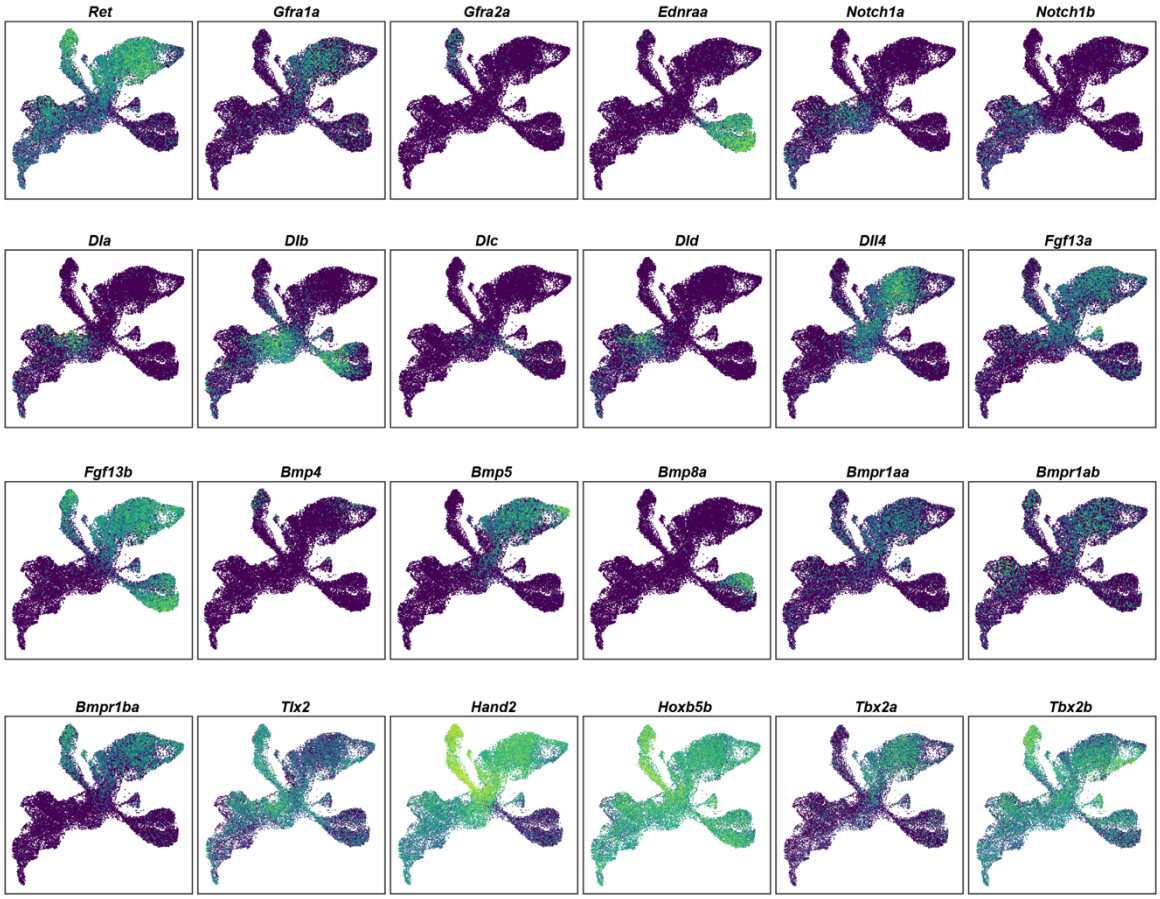

Figure 20: UMAP plots displaying the expression of genes encoding signaling molecules and transcription factors.

BIBLIOGRAPHY

1. Nagy, N., and Goldstein, A.M. (2006). Endothelin-3 regulates neural crest cell proliferation and differentiation in the hindgut enteric nervous system. Developmental Biology *293*, 203–217. https://doi.org/10.1016/j.ydbio.2006.01.032.

2. Michinaga, S., Hishinuma, S., and Koyama, Y. (2023). Roles of Astrocytic Endothelin ETB Receptor in Traumatic Brain Injury. Cells *12*, 719. https://doi.org/10.3390/cells12050719.

3. Chatterjee, S., and Chakravarti, A. (2019). A gene regulatory network explains RET–EDNRB epistasis in Hirschsprung disease. Human Molecular Genetics *28*, 3137–3147. https://doi.org/10.1093/hmg/ddz149.

4. Fujiwara, N., Miyahara, K., Nakazawa-Tanaka, N., Akazawa, C., and Yamataka, A. (2016). Altered differentiation of enteric neural crest-derived cells from endothelin receptor-B null mouse model of Hirschsprung's disease. Pediatr Surg Int *32*, 1095–1101. https://doi.org/10.1007/s00383-016-3964-4.

5. Cantrell, V.A. (2004). Interactions between Sox10 and EdnrB modulate penetrance and severity of aganglionosis in the Sox10Dom mouse model of Hirschsprung disease. Human Molecular Genetics *13*, 2289–2301. https://doi.org/10.1093/hmg/ddh243.

6. Paratore, C., Goerich, D.E., Suter, U., Wegner, M., and Sommer, L. (2001). Survival and glial fate acquisition of neural crest cells are regulated by an interplay between the transcription factor Sox10 and extrinsic combinatorial signaling. Development *128*, 3949–3961. https://doi.org/10.1242/dev.128.20.3949.

7. Memic, F., Knoflach, V., Sadler, R., Tegerstedt, G., Sundström, E., Guillemot, F., Pachnis, V., and Marklund, U. (2016). Ascl1 Is Required for the Development of Specific Neuronal Subtypes in the Enteric Nervous System. J. Neurosci. *36*, 4339–4350. https://doi.org/10.1523/JNEUROSCI.0202-16.2016.

8. Ling, I.T.C., and Sauka-Spengler, T. (2019). Early chromatin shaping predetermines multipotent vagal neural crest into neural, neuronal and mesenchymal lineages. Nat Cell Biol *21*, 1504–1517. https://doi.org/10.1038/s41556-019-0428-9.

9. Wright, C.M., Schneider, S., Smith-Edwards, K.M., Mafra, F., Leembruggen, A.J.L., Gonzalez, M.V., Kothakapa, D.R., Anderson, J.B., Maguire, B.A., Gao, T., et al. (2021). scRNA-Seq Reveals New Enteric Nervous System Roles for GDNF, NRTN, and TBX3. Cellular and Molecular Gastroenterology and Hepatology *11*, 1548-1592.e1. https://doi.org/10.1016/j.jcmgh.2020.12.014.

10. Memic, F., Knoflach, V., Morarach, K., Sadler, R., Laranjeira, C., Hjerling-Leffler, J., Sundström, E., Pachnis, V., and Marklund, U. (2018). Transcription and Signaling Regulators in Developing Neuronal Subtypes of Mouse and Human Enteric Nervous System. Gastroenterology *154*, 624–636. https://doi.org/10.1053/j.gastro.2017.10.005.

11. Morarach, K., Mikhailova, A., Knoflach, V., Memic, F., Kumar, R., Li, W., Ernfors, P., and Marklund, U. (2021). Diversification of molecularly defined myenteric neuron classes revealed by single-cell RNA sequencing. Nat Neurosci *24*, 34–46. https://doi.org/10.1038/s41593-020-00736-x.

12. Borghini, S., Di Duca, M., Santamaria, G., Vargiolu, M., Bachetti, T., Cargnin, F., Pini Prato, A., De Giorgio, R., Lerone, M., Stanghellini, V., et al. (2007). Transcriptional regulation of TLX2 and impaired intestinal innervation: possible role of the PHOX2A and PHOX2B genes. Eur J Hum Genet *15*, 848–855. https://doi.org/10.1038/sj.ejhg.5201852.

13. Howard, A.G.A., Nguyen, A.C., Tworig, J., Ravisankar, P., Singleton, E.W., Li, C., Kotzur, G., Waxman, J.S., and Uribe, R.A. (2022). Elevated Hoxb5b Expands Vagal Neural Crest Pool and Blocks Enteric Neuronal Development in Zebrafish. Front. Cell Dev. Biol. *9*, 803370. https://doi.org/10.3389/fcell.2021.803370.

14. Kuil, L.E., MacKenzie, K.C., Tang, C.S., Windster, J.D., Le, T.L., Karim, A., De Graaf, B.M., Van Der Helm, R., Van Bever, Y., Sloots, C.E.J., et al. (2021). Size matters: Large copy number losses in Hirschsprung disease patients reveal genes involved in enteric nervous system development. PLoS Genet *17*, e1009698. https://doi.org/10.1371/journal.pgen.1009698.

15. Hendershot, T.J., Liu, H., Sarkar, A.A., Giovannucci, D.R., Clouthier, D.E., Abe, M., and Howard, M.J. (2007). Expression of Hand2 is sufficient for neurogenesis and cell type–specific gene expression in the enteric nervous system. Developmental Dynamics *236*, 93–105. https://doi.org/10.1002/dvdy.20989.

16. Kroll, F., Powell, G.T., Ghosh, M., Gestri, G., Antinucci, P., Hearn, T.J., Tunbak, H., Lim, S., Dennis, H.W., Fernandez, J.M., et al. (2021). A simple and effective F0 knockout method for rapid screening of behaviour and other complex phenotypes. eLife *10*, e59683. https://doi.org/10.7554/eLife.59683.

17. May-Zhang, A.A., Tycksen, E., Southard-Smith, A.N., Deal, K.K., Benthal, J.T., Buehler, D.P., Adam, M., Simmons, A.J., Monaghan, J.R., Matlock, B.K., et al. (2021). Combinatorial Transcriptional Profiling of Mouse and Human Enteric Neurons Identifies Shared and Disparate Subtypes In Situ. Gastroenterology *160*, 755-770.e26. https://doi.org/10.1053/j.gastro.2020.09.032.

18. Morarach, K., Mikhailova, A., Knoflach, V., Memic, F., Kumar, R., Li, W., Ernfors, P., and Marklund, U. (2021). Diversification of molecularly defined myenteric neuron

classes revealed by single-cell RNA sequencing. Nat Neurosci *24*, 34–46. https://doi.org/10.1038/s41593-020-00736-x.

19. Hockley, J.R.F., Taylor, T.S., Callejo, G., Wilbrey, A.L., Gutteridge, A., Bach, K., Winchester, W.J., Bulmer, D.C., McMurray, G., and Smith, E.S.J. (2019). Single-cell RNAseq reveals seven classes of colonic sensory neuron. Gut *68*, 633–644. https://doi.org/10.1136/gutjnl-2017-315631.

20. Drokhlyansky, E., Smillie, C.S., Van Wittenberghe, N., Ericsson, M., Griffin, G.K., Eraslan, G., Dionne, D., Cuoco, M.S., Goder-Reiser, M.N., Sharova, T., et al. (2020). The Human and Mouse Enteric Nervous System at Single-Cell Resolution. Cell *182*, 1606-1622.e23. https://doi.org/10.1016/j.cell.2020.08.003.

21. Lasrado, R., Boesmans, W., Kleinjung, J., Pin, C., Bell, D., Bhaw, L., McCallum, S., Zong, H., Luo, L., Clevers, H., et al. (2017). Lineage-dependent spatial and functional organization of the mammalian enteric nervous system. Science *356*, 722–726. https://doi.org/10.1126/science.aam7511.

22. Elmentaite, R., Kumasaka, N., Roberts, K., Fleming, A., Dann, E., King, H.W., Kleshchevnikov, V., Dabrowska, M., Pritchard, S., Bolt, L., et al. (2021). Cells of the human intestinal tract mapped across space and time. Nature *597*, 250–255. https://doi.org/10.1038/s41586-021-03852-1

INDEX

C
CRISPR/Cas9, 23, 91, 105
CUT&RUN, 117, 120

H
Hirschsprung's disease, 5

I
Intrinsic primary afferent neurons (IPANs), 2
Irritable bowel syndrome, 5

K
Kallisto and Bustools workflow, 100

M
Myenteric plexus, 1

N
Neural crest cells (NCCs), 3

P
Pseudo-obstruction syndrome, 5

S
scFates, 19, 101
Sequential hybridization chain reaction, 20, 104
Single cell RNA-sequencing, 17, 100, 119
Single cell ATAC-sequencing, 118, 119, 121
Submucosal plexus, 1

U
UniTVelo, 19, 101